Compound Inelastic Nucleon and Gamma-Ray Angular Distributions for Even- and Odd-Mass Nuclei

ERIC SHELDON

Laboratorium für Kernphysik, Eidgenössische Technische Hochschule, 8049 Zürich, Switzerland

DOUGLAS M. VAN PATTER

Bartol Research Foundation, Swarthmore, Pennsylvania

The current theoretical and experimental status of angular distributions of inelastically scattered nucleons and succeeding γ radiations on the basis of a compound-nucleus mechanism is reviewed, with special reference to symmetry, isotropy, and identity characteristics. Results of investigations using a fast computer to ascertain the influence of higher partial waves, multipole mixing, unobserved intermediate transitions, and the presence of additional exit channels are presented, together with an over-all survey of distribution systematics and tabulations of numerical parameters to assist in evaluation of differential cross sections by hand. The predictions for both proton and neutron inelastic scattering are discussed in detail and illustrated by analyses of experimental data for many nuclear spin sequences. In particular, it is shown for γ distributions that the effect of cascades from higher levels upon the distribution structure and magnitude can be very appreciable. Also, the examination of the predicted behavior of $(n, n'\gamma)$ distributions near threshold has disclosed features deserving of further experimental and theoretical study. A set of recently measured $(n, n'\gamma)$ distributions for several heavy nuclei involving transitions between nuclear states of relatively high integer or half-integer spin is shown to compare well with the theoretical predictions when suitable account is taken of cascade and exit-channel contributions. It is concluded that there is a wide range of application of this theoretical approach to energy-averaged distributions, much of which remains yet to be exploited.

CONTENTS

1. INTRODUCTION

Availability of fast computers conjoined with improvements in experimental techniques has opened the way to increasingly wide-ranging studies of the angular distributions of reaction products from such processes as inelastic scattering of nucleons and heavier particles.

In the case of compound inelastic scattering of relatively low-energy nucleons, the means are now at hand to measure and analyze absolute nucleon and γ distributions for odd- as well as even-mass target nuclei and thereby to extend greatly the variety of nuclear spin sequences beyond those involving a ground-state spin-parity of 0^+. The numerical analysis can take cognizance of spin–orbit interaction, the presence of competing exit channels in decay of the compound nucleus (CN), *mixed* multipolarity in the γ transitions, and the existence of intermediate unobserved (mixed) transitions.

Except that it does not take CN fluctuations into account, as has been done in the recent Moldauer formalism,[1] the familiar theory due to Wolfenstein,[2] Hauser and Feshbach,[3] and Satchler[4] (with emendations) continues to furnish an appropriate basis for distribution analyses of the type presented here. The fundamental expressions have been embodied in a very general computer program (described in Sec. 4D),

[1] P. A. Moldauer, Phys. Rev. **123**, 968 (1961); and **129**, 754 (1963); Rev. Mod. Phys. **36**, 1079 (1964); Phys. Rev. **135**, B642 (1964). An automatic code for the evaluation of total cross sections from Moldauer's formulae has been described by P. A. Moldauer, C. A. Engelbrecht, and G. J. Duffy, "NEARREX, A Computer Code for Nuclear Reaction Calculations," Argonne National Laboratory Report ANL-6978, 1964 (unpublished). Other programs which take account of level width fluctuations have been compiled by R. S. Caswell at the National Bureau of Standards [J. Res. Natl. Bur. Std. (U.S.) **A66**, 389 (1962) and Bull. Am. Phys. Soc. **10**, 12 (1965)], and by L. Cranberg and T. A. Oliphant at Los Alamos.

[2] L. Wolfenstein, Phys. Rev. **82**, 690 (1951).

[3] W. Hauser and H. Feshbach, Phys. Rev. **87**, 366 (1952).

[4] G. R. Satchler, Phys. Rev. **94**, 1304 (1954); and **104**, 1198 (1956); erratum, Phys. Rev. **111**, 1747 (1958).

which goes somewhat beyond the capabilities of other[5] commensurate codes and makes possible the evaluation of differential cross sections for a number of recently measured inelastic-scattering processes, as well as permitting an over-all survey of distribution behavior for an extensive range of nuclear spin sequences. The calculations can include arbitrarily many partial waves in nucleon entrance and exit channels.

2. UNDERLYING THEORY

In order to pave the way for a description of the computer program and calculations, we commence with an outline of the familiar statistical continuum approach.

The general expression for a differential cross section[6] as a Legendre-polynomial expansion of even order,

$$d\sigma/d\Omega = \sum a_\nu P_\nu(\cos\theta), \qquad (1)$$

in which the summation extends over angular momenta entering into the over-all process and over the index ν ($\nu = 0, 2, 4, \cdots$) whose range is prescribed by vector momentum coupling conditions, contains coefficients a_ν that weight the angular-dependent Legendre terms and that can be decomposed into a product of energy-dependent and of momentum-dependent terms. The latter are just appropriate "transition parameters," one for each constituent step of the over-all process. Their values are dictated by the nature and angular momentum of the particle effecting the transition, as well as by the initial and final nuclear spins involved; for example, in the case of a γ transition of pure multipolarity L linking nuclear levels of spin J_i and J_f, the appropriate parameter, as tabulated by Ferentz and Rosenzweig,[7] is[8]

$$F_\nu(LLJ_fJ_i) \equiv (-)^{J_f-J_i-1} \hat{J}_i(\hat{L})^2$$
$$\times \langle \nu 0 \mid LL1-1 \rangle W(LLJ_iJ_i; \nu J_f). \quad (2a)$$

F_ν must be written with the *intermediate* state J_i at the end of its argument.

For mixed multipolarity L, L' having a mixing ratio[9]

$$\delta \equiv \langle J_f \| L' \| J_i \rangle / \langle J_f \| L \| J_i \rangle, \qquad (3)$$

the requisite γ-transition parameter expressed in terms of generalized F_ν as defined by Biedenharn,[10]

$$F_\nu(LL'J_fJ_i) \equiv (-)^{J_f-J_i-1} \hat{J}_i \hat{L}\hat{L}'$$
$$\times \langle \nu 0 \mid LL'1-1 \rangle W(LL'J_iJ_i; \nu J_f) \quad (2b)$$

is

$$A_\nu(LL'J_fJ_i) = (1+\delta^2)^{-1}$$
$$\times [F_\nu(LLJ_fJ_i) + 2\delta F_\nu(LL'J_fJ_i) + \delta^2 F_\nu(L'L'J_fJ_i)]. \quad (4)$$

When the transition is effected by particles other than photons, the appropriate linking term results on multiplying the commensurate γ-transition parameter by a "particle parameter" b_ν $(ij'; x)$ for particles x of total angular momentum j, j'. The b_ν have been defined by Biedenharn and Rose [following Eq. (41d) and Eq. (79) of Ref. 11] and later, more explicitly, by Devons and Goldfarb [Eqs. (15.9), (13.10), (13.11), (13.12), (14.12), (14.13), (14.14) of Ref. 12.]. A nucleon transition from J_i to J_f is accordingly represented by a term of the form

$$\eta_\nu(jj'J_fJ_i) \equiv b_\nu(jj'; N) F_\nu(LL'J_fJ_i)$$
$$= (-)^{J_f-J_i-\frac{1}{2}} \hat{J}_i \hat{j}\hat{j}' \langle \nu 0 \mid jj'\tfrac{1}{2}-\tfrac{1}{2} \rangle$$
$$\times W(jj'J_iJ_i; \nu J_f), \quad (5)$$

some principal values of which have been tabulated by Satchler.[13] Since $(\hat{s})^2/2 = 1$ for nucleons, the η_ν are the same for emission as for absorption of nucleons.

In the case of one or more *unobserved* transitions intervening between the observed steps, the linking parameter for radiation of total angular momentum L, L' is

$$U_\nu(LL'J_iJ_f) = (1+\delta^2)^{-1} [\hat{J}_i \hat{J}_f(-)^{J_i+J_f}]$$
$$\times [(-)^L W(J_iJ_iJ_fJ_f; \nu L)$$
$$+ \delta^2(-)^{L'} W(J_iJ_iJ_fJ_f; \nu L')] \quad (6)$$

for each unobserved transition $J_i \rightarrow J_f$.[14] This expression is independent of the nature of the unobserved radiation $(\gamma, N, d, \alpha, \cdots)$ and is an *incoherent* sum for nonzero values of the mixing ratio δ. The normalization is

$$F_0 = A_0 = \eta_0 = U_0 = b_0 = 1. \qquad (7)$$

An alternative formalism used by Satchler[4] employs a parameter I_ν such that[15]

$$I_\nu \equiv (\hat{J}_i / \hat{J}_f) U_\nu \qquad (8)$$

---

[5] Commensurate Hauser–Feshbach programs have been compiled in FORTRAN by several groups. For a listing of the code assembled by J. G. Wills we are indebted to G. R. Satchler, and for a more recent modified, extended version in use at Los Alamos, to L. Cranberg and T. A. Oliphant. Control calculations comparing results of our program with these two codes yielded perfect numerical agreement. Also recently made available to us is the ABACUS code of E. H. Auerbach, which performs compatible calculations and supplies substantially the same results.

[6] We make a distinction between a cross section $d\sigma/d\Omega$, expressed in absolute units (mb sr^{-1}), and a distribution $W(\theta)$, expressed in arbitrary units, which in general is normalized to $W(90°) = 1$, or alternatively to $a_0 = 1$.

[7] M. Ferentz and N. Rosenzweig, Argonne National Laboratory Report ANL-5324, 1955 (unpublished).

[8] For brevity, we employ the notation $\hat{k} \equiv (2k+1)^{\frac{1}{2}}$.

[9] M. Sakai and T. Yamazaki, Institute for Nuclear Study, Tokyo, Report INSJ-66, 1964 (unpublished).

[10] L. C. Biedenharn, in *Nuclear Spectroscopy*, edited by F. Ajzenberg-Selove (Academic Press Inc., New York, 1960), Part B, p. 732.

[11] L. C. Biedenharn and M. E. Rose, Rev. Mod. Phys. 25, 729 (1953).

[12] S. Devons and L. J. B. Goldfarb, in *Handbuch der Physik*, edited by S. Flügge (Springer-Verlag, Berlin, 1957), Vol. 42, p. 362.

[13] G. R. Satchler, Proc. Roy. Soc. (London) 66A, 1081 (1953).

[14] The phase factor has been corrected from that quoted by Satchler (Ref. 4).

[15] The argument of the phase factor should read $(J_1'+J_2-j-\nu)$.

for an unobserved transition from J_i to J_f. This Racah function has the disadvantage of not being normalized to unity when $\nu=0$.

For inelastic nucleon scattering $(N, N'\gamma)$ involving the spin sequence [Fig. 1(a)]

$$J_0(\,j_1=l_1\pm\tfrac{1}{2})\,J_1(\,j_2=l_2\pm\tfrac{1}{2})\,J_2(L, L')\,J_3,$$

the set of transition parameters appropriate to the N' distribution is, accordingly,

$$\eta_\nu(\,j_1j_1J_0J_1)\cdot\eta_\nu(\,j_2j_2J_2J_1), \qquad (9)$$

wherein mixed-j interferences of the type j_1, j_1' and j_2, j_2' are absent. For the γ distributions, the parameter product is

$$\eta_\nu(\,j_1j_1J_0J_1)\,U_\nu(\,j_2j_2J_2J_1)\,A_\nu(LL'J_3J_2), \qquad (10)$$

since the scattered nucleons are not observed.

This can readily be extended to include additional unobserved intermediate transitions, as in $(N, N'\gamma-\gamma)$ processes characterized by the spin sequence [Fig. 1(b)]

$$J_0(\,j_1=l_1\pm\tfrac{1}{2})\,J_1(\,j_2=l_2\pm\tfrac{1}{2})$$
$$\rightarrow J_2(L_2+\delta_2{}^2L_2')\,J_3(L_3+\delta_3{}^2L_3')\,J_4,$$

where the radiation L_2, L_2' is unobserved and L_3, L_3' observed. The product of transition parameters now becomes

$$\eta_\nu(\,j_1j_1J_0J_1)\,U_\nu(\,j_2j_2J_2J_1)\,U_\nu(L_2L_2'J_2J_3)$$
$$\times A_\nu(L_3L_3'J_4J_3). \qquad (11)$$

To arrive at the over-all distribution coefficients a_ν that weight the Legendre polynomials, the respective transition-parameter product must be multiplied by a statistical spin factor

$$g=\hat{J}_1{}^2/(\hat{s}\cdot\hat{J}_0)^2, \qquad (12)$$

which takes account of the probability that the incident particles of spin s have the right orientation for resonance capture,[16] and by a Hauser–Feshbach penetra-
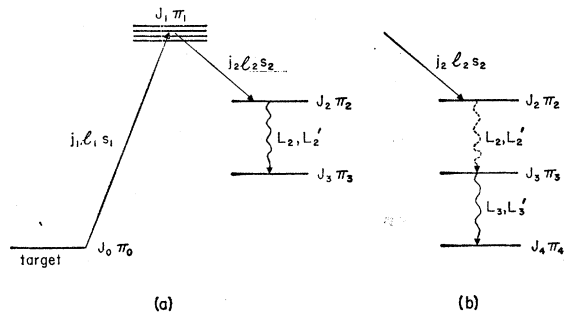

FIG. 1. Spin and angular momentum nomenclature employed for various types of transition sequences.

[16] E. Fermi, *Nuclear Physics*, notes compiled by J. Orear, A. H. Rosenfeld, and R. A. Schluter (University of Chicago Press, Chicago, 1950), revised ed., p. 157.

bility term

$$\tau\equiv T_{l_1}(E_1)\cdot T_{l_2}(E_2)\Big/\sum_{ljE}T_l(E), \qquad (13)$$

which takes account of CN barrier penetrabilities for incident particles of energy E_1 and emergent particles of energy E_2 in the c.m. system. The summation in the denominator runs over all possible decay channels of the compound nucleus. If, for simplicity, this is confined to just the elastic channels to J_0 and inelastic channels to J_2 it is termed the "two-channel approximation." In general, however, additional exit channels are open, which should be taken into account, since they can exert a radical influence upon the magnitude of the angular distribution.

The theoretical expressions can be extended to take account of spin–orbit interaction by using "generalized" transmission coefficients[17] $T_l^{(\pm)}$, wherein the superscript $(\pm)$ refers to the vector composition of spin and orbital angular momenta to a resultant $j=l\pm\tfrac{1}{2}$. The relationship between generalized and normal transmission coefficients is simply[17]

$$T_l=[(l+1)\,T_l^{(+)}+lT_l^{(-)}]/(2l+1). \qquad (14)$$

In absolute magnitude (e.g., mb sr^{-1}) the differential cross section ensues on multiplying the above terms by $\tfrac{1}{4}\lambda^2$, where λ is the rationalized wavelength of the incident particle in the center-of-mass system [for low energies, $\lambda^2=\hbar^2/(2ME_1)=207.3963/E_1^{(\mathrm{MeV})}$ mb].

For the *nucleon distribution* we obtain

$$d\sigma/d\Omega_1=\tfrac{1}{4}\lambda^2\sum g\eta_\nu(\,j_1j_1J_0J_1)\eta_\nu(\,j_2j_2J_2J_1)\tau P_\nu(\cos\theta_1)$$
$$(15)$$

as a function of the scattering angle θ_1 referred to the incident beam direction. Substitution of the requisite Racah functions reduces this to

$$d\sigma/d\Omega_1=\tfrac{1}{8}\lambda^2\sum NCW\tau P_\nu(\cos\theta_1), \qquad (16)$$

with summation over j_1, j_2, ν and with

$$N\equiv(-)^{J_0-2J_1+J_2-1}(\hat{J}_1)^4(\hat{j}_1)^2(\hat{j}_2)^2/(\hat{J}_0)^2, \qquad (17)$$

$$C\equiv\langle\nu0\mid j_1j_1\tfrac{1}{2}-\tfrac{1}{2}\rangle\langle\nu0\mid j_2j_2\tfrac{1}{2}-\tfrac{1}{2}\rangle, \qquad (18)$$

$$W\equiv W(J_1J_1j_1j_1;\nu J_0)W(J_1J_1j_2j_2;\nu J_2). \qquad (19)$$

The Racah coefficients vanish unless ν is restricted to the range $0\leq\nu\leq2j_1, 2J_1, 2j_2$.

For the $(N, N'\gamma)$ process, the γ distribution is[18]

$$d\sigma/d\Omega_2=\tfrac{1}{4}\lambda^2\sum g\eta_\nu(\,j_1j_1J_0J_1)\,U_\nu(\,j_2j_2J_1J_2)$$
$$\times A_\nu(LL'J_3J_2)\tau P_\nu(\cos\theta_2) \qquad (20)$$

[17] E. Sheldon, Rev. Mod. Phys. **35**, 795 (1963).
[18] As mentioned by R. B. Day and M. Walt [Phys. Rev. **117**, 1330 (1960)], Satchler's expression in Ref. 4 for the γ distribution $W(\theta)$ should be multiplied by $\hat{J}_2/\hat{J}_1$. In the numerical formula that follows for $J_0=0$, $J_2=2$, $J_3=0$, the coefficient of the third term should read $[4+P_2(\cos\theta)]$, that of the fourth term, $[5+2.714\,P_2(\cos\theta)-1.714\,P_4(\cos\theta)]$, and that of the final term, $[10-0.714P_2(\cos\theta)+0.857P_4(\cos\theta)]$.

in terms of the angle of emergence θ_2 referred to the incident beam direction. This in turn reduces to

$$d\sigma/d\Omega_2 = \tfrac{1}{8}\lambda^2 \sum N'C'W'M(\delta)\tau P_\nu(\cos\theta_2),\quad (21)$$

with summation over j_1, j_2, and ν (now restricted to $0 \leq \nu \leq 2j_1, 2J_1, 2J_2, 2L'$),

and

$$N' \equiv (-)^{J_0+J_3-j_2+\frac{1}{2}}(\hat{J}_1)^4(\hat{j}_1)^2(\hat{J}_2)^2/(\hat{J}_0)^2,\quad (22)$$

$$C' \equiv \langle\nu 0 \mid j_1 j_1 \tfrac{1}{2}-\tfrac{1}{2}\rangle,\quad (23)$$

$$W' \equiv W(J_1J_1j_1j_1; \nu J_0)W(J_1J_1J_2J_2; \nu j_2),\quad (24)$$

$$M(\delta) \equiv (1+\delta^2)^{-1}[M(LL)+2\delta M(LL')+\delta^2 M(L'L')],\quad (25)$$

where

$$M(LL') \equiv \hat{L}\hat{L}'\langle\nu 0 \mid LL'1-1\rangle W(J_2J_2LL'; \nu J_3).\quad (26)$$

For an $(N, N'\gamma-\gamma)$ process in which the second gamma transition (from J_3 to J_4) is observed, its distribution is given by

$$d\sigma/d\Omega_{2'} = \tfrac{1}{4}\lambda^2 \sum g\eta_\nu(j_1 j_1 J_0 J_1) U_\nu(j_2 j_2 J_1 J_2)$$
$$\times U_\nu(L_2L_2'J_2J_3) A_\nu(L_3L_3'J_4J_3)\tau P_\nu(\cos\theta_{2'}),\quad (27)$$

or, in reduced form, by

$$d\sigma/d\Omega_{2'} = \tfrac{1}{8}\lambda^2 \sum N''C'W'U(\delta_2)M'(\delta_3)\tau P_\nu(\cos\theta_{2'}),\quad (28)$$

where the summation extends over j_1, j_2, ν (with $0 \leq \nu \leq 2j_1, 2J_1, 2J_2, 2J_3, 2L_3'$) and

$$N'' \equiv (-)^{J_0-J_4-j_2+\frac{1}{2}}(\hat{J}_1)^4(\hat{J}_2)^2(\hat{J}_3)^2(\hat{j}_1)^2/(\hat{J}_0)^2,\quad (29)$$

$$U(\delta_2) \equiv (1+\delta_2^2)^{-1}[U(L_2L_2)+\delta_2^2 U(L_2'L_2')],\quad (30)$$

$$U(L_2L_2) = (-)^{L_2}W(J_2J_2J_3J_3; \nu L_2),\quad (31)$$

$$M'(\delta_3) \equiv (1+\delta_3^2)^{-1}$$
$$\times[M(L_3L_3)+2\delta_3 M(L_3L_3')+\delta_3^2 M(L_3'L_3')],\quad (32)$$

$$M(L_3L_3') \equiv \hat{L}_3\hat{L}_3'\langle\nu 0 \mid L_3L_3'1-1\rangle$$
$$\times W(J_3J_3L_3L_3'; \nu J_4).\quad (33)$$

When $\delta_2 = \delta_3 = 0$, we arrive at the simpler form

$$d\sigma/d\Omega_{2'} = \tfrac{1}{8}\lambda^2 \sum N'''C'''W'''\tau P_\nu(\cos\theta_{2'}),\quad (34)$$

where

$$N''' \equiv (-)^{J_0-J_4-j_2+L_2+\frac{1}{2}}(\hat{J}_1)^4(\hat{J}_2)^2$$
$$\times(\hat{J}_3)^2(\hat{j}_1)^2(\hat{L}_3)^2/(\hat{J}_0)^2,\quad (35)$$

$$C''' \equiv \langle\nu 0 \mid j_1 j_1 \tfrac{1}{2}-\tfrac{1}{2}\rangle\langle\nu 0 \mid L_3L_31-1\rangle,\quad (36)$$

$$W''' \equiv W(J_1J_1j_1j_1; \nu J_0)W(J_1J_1J_2J_2; \nu j_2)$$
$$\times W(J_2J_2J_3J_3; \nu L_2)W(J_3J_3L_3L_3; \nu J_4).\quad (37)$$

It is a characteristic of the angular distributions in all the above cases that they are exactly symmetrical

about 90°. In the mathematical formalism, this is expressed by the fact that throughout, the angular dependence is given by Legendre polynomial expansions of *even* order (P_0, P_2, P_4, $\cdots$, each of which is symmetrical about 90°). A brief discussion of the factors underlying this symmetry property is given in Appendix B, where it is shown that unless there is a preferred spin direction, as in the case of aligned nuclei or polarized particles, the angular distributions of the products of reactions proceeding by way of CN formation display this basic symmetry exactly. For a direct interaction this is not the case with particle distributions—though it must be stressed that, contrary to widespread belief, DI particle distributions *can* in particular instances evince a form indistinguishable from that of a symmetrical CN distribution (the respective absolute magnitudes differ appreciably, however, and the peak-to-valley ratios appear to be considerably higher than those for CN distributions)—the subsequent γ transitions have, of course, symmetrical distributions.

We relegate discussion of these points to Appendix B, and proceed to a consideration of conditions which bring about isotropy or identity of γ distributions.

3. ISOTROPY AND IDENTITY OF γ DISTRIBUTIONS

When the summation index is restricted to the single value $\nu = 0$, the distribution is isotropic, as is well known, and has the value

$$(d\sigma/d\Omega_1)_{\nu=0} = (d\sigma/d\Omega_2)_{\nu=0} = \sigma/(4\pi) = \tfrac{1}{8}\lambda^2 \sum(\hat{J}_1/\hat{J}_0)^2\tau.$$
$$(38)$$

Thus the γ distribution from an $(N, N'\gamma)$ process is isotropic when $J_2 = 0$ or $\tfrac{1}{2}$, and that from an $(N, N'\gamma-\gamma)$ process is isotropic when J_2 or $J_3 = 0$ or $\tfrac{1}{2}$. Apart from this trivial instance of equality of γ distributions in a cascade, more general conditions leading to distribution identity can be established. Of various possibilities, all involving *pure* multipolarity (or alternatively the same values of mixing ratios δ for corresponding γ transitions), the first is familiar, viz., (a) in an $(N, N'\gamma_1-\gamma_2)$ process, the distribution of γ_1 is in magnitude and structure identical with that of γ_2 when

$$L_2 = L_2' = L_3 = L_3'(=L)\quad \text{and}\quad J_4 = 0.\quad (39)$$

This follows immediately on substitution in the appropriate condition for identity,

$$N'M(0) = N''U(0)M'(0),\quad (40)$$

derived from the expressions (21) and (28).

We note that the above depends only on J_2, J_3, J_4, and L, and hence on the nature of the transitions preceding the γ decay. If, however, more than a single unobserved γ transition precedes the observed γ decay

to a spin-zero level, as in an $(N, N'\gamma_1-\gamma_2-\gamma_3)$ process, the distributions of γ_1 and γ_3 are not in general identical even if the γ radiations are of the same pure multipolarity. Only in the special case of a regular monotonic level sequence (e.g., $0^+, 2^+, 4^+, 6^+$) does equality obtain.

For the consideration of basic γ transitions[19] cascading through nuclear levels whose spins form a regular monotonic sequence, it is useful[20] to invoke an identity which can readily be verified from first principles:

$$\frac{W(J-L, J-L, L, L; \nu J)}{W(J-L, J-L, J, J; \nu L)}$$
$$\equiv (-)^{2J}(\hat{J})^2 W(JJLL; \nu, J+L). \quad (41)$$

The condition (40) can upon substitution and use of the Racah identity (41) be shown to be satisfied in the more general situation when (b)

$$L_2 = L_2' = L_3 = L_3' \ (=L)$$
and
$$L = |J_2 - J_3| = |J_3 - J_4|. \quad (42)$$

This situation is encountered not only in the case of a rotational band of levels with spins 0^+, 2^+, 4^+, but in several odd-mass nuclei having half-integer spins which would appear to be amenable to experimental investigation (e.g., P^{31}, Tb^{159}, Lu^{175}, Hf^{177}, $Tl^{203,205}$).

In point of fact, an even less restrictive condition than this has been formulated by Raboy and Krohn[21] who extended the work of Weneser and Hamilton[22] and Biedenharn, Arfken, and Rose,[23] considering multiple γ cascades. The decay scheme is symbolized in Fig. 2. Raboy and Krohn showed that with respect to a transition (A) between levels of arbitrary spin (irrespective of the multipolarity, mixing ratio or, indeed, the particle nature of the radiation effecting the transition), the individual distributions of either of two preceding or following transitions (B, C) are equal when they entail pure, basic decay between levels whose spins form a regular monotonic sequence. No restrictions on L, δ,
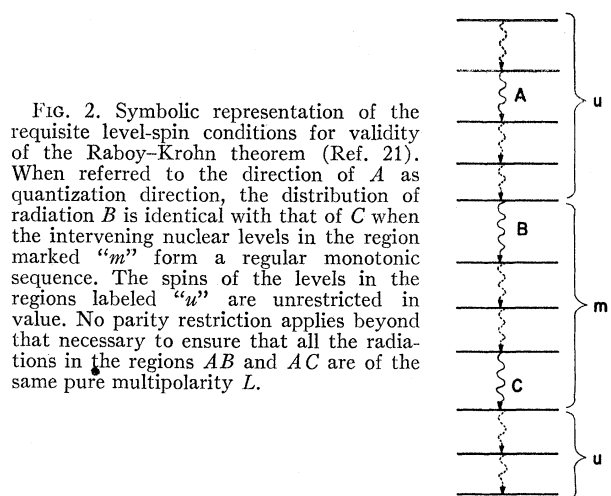

Fig. 2. Symbolic representation of the requisite level-spin conditions for validity of the Raboy–Krohn theorem (Ref. 21). When referred to the direction of A as quantization direction, the distribution of radiation B is identical with that of C when the intervening nuclear levels in the region marked "m" form a regular monotonic sequence. The spins of the levels in the regions labeled "u" are unrestricted in value. No parity restriction applies beyond that necessary to ensure that all the radiations in the regions AB and AC are of the same pure multipolarity L.

and J obtain for unobserved transitions common to both the AB, AC sequences, but any unobserved transitions intervening between B and C must be basic as well as of pure multipolarity, and at the same time involve a monotonic sequence of nuclear spins which join regularly to those for the transitions B and C.

A subsidiary remark in the first sentence of the paper by Weneser and Hamilton[22] to the effect that the distributions are unaltered on adding a constant to all the level spins has to be qualified, however. Only when the constant is a multiple of the basic pure multipolarity L is this statement valid (for example, increasing the level spins by $\frac{1}{2}$ throughout drastically changes the distributions from their previous form and magnitude; similarly for unit spin increase throughout when $L=2$).

4. NUMERICAL EVALUATION OF ANGULAR DISTRIBUTIONS

A. Introduction

The expressions (15), (21), (28), and (34) furnish differential cross sections for such processes as $(n, n'\gamma)$, $(p, p'\gamma)$, $(n, p\gamma)$, $(p, n\gamma)$, $(t, p\gamma)$, $(He^3, p\gamma)$, etc., of the type $(N, N'\gamma)$ or $(N, N'\gamma-\gamma)$, but can involve lengthy summations which render hand calculations both tedious and liable to error.

In the present section, we define and discuss weighting coefficients $\alpha_{i\nu}$ in the expansion

$$d\sigma/d\Omega = \tfrac{1}{8}\lambda^2 \sum_{i,\nu} \alpha_{i\nu}\tau_i P_\nu(\cos\theta) \equiv \tfrac{1}{8}\lambda^2 \sum_\nu a_\nu P_\nu(\cos\theta). \quad (43)$$

Numerical values of the $\alpha_{i\nu}$ for some commonly occurring spin sequences have been tabulated in Appendix A. Next, we present expressions for the coefficients c_ν and C_ν used in converting given numerical expansions for a certain nuclear spin transition sequence to those for other spin sequences. Finally, details of the flexible

[19] Unmixed radiation of pure multipolarity L between levels J_i and J_f such that $L = |J_i - J_f|$.

[20] Also useful for effecting the reduction is the sum rule due to G. Racah [Phys. Rev. **62**, 438 (1942)], which is most conveniently represented as

$$W(abcd; ef) = \sum_g (-)^{a+b+c+d+e+f+g}(\hat{g})^2 W(adbc; ge)W(adcb; gf).$$

Although the alternative form given by A. Simon, J. H. Vander Sluis, and L. C. Biedenharn [Oak Ridge National Laboratory Report ORNL-1679, 1954 (unpublished)] is correct, there are erroneous versions in other publications, e.g., the argument of the phase in Eq. (16) of the paper by L. C. Biedenharn [J. Math. Phys. **31**, 287 (1952-3)] should read $(j_1+j_2-J_a)$ and the recursion relation (28) in the above paper should be emended to $W(avcd; ad)W(a\bar{v}cd; ad) = \cdots$. In the paper of L. C. Biedenharn, J. M. Blatt, and M. E. Rose [Rev. Mod. Phys. **24**, 249 (1952)], the left-hand side of Eq. (16) should read $W(afgb; cd)$.

[21] S. Raboy and V. E. Krohn, Phys. Rev. **98**, 24 (1955).

[22] J. Weneser and D. R. Hamilton, Phys. Rev. **92**, 321 (1953).

[23] L. C. Biedenharn, G. B. Arfken, and M. E. Rose, Phys. Rev. **83**, 586 (1951).

distribution code "MANDY," written in ALGOL for a CDC 1604-A computer, are outlined.

B. Restricted Legendre Expansion Coefficients $\alpha_{i\nu}$

The evaluation of CN angular distributions follows from building products of requisite numerical and Racah functions for each permitted permutation of the momentum ensemble l_1, j_1, J_1, l_2, j_2 and for each even value of ν, to obtain the respective restricted expansion coefficients $\alpha_{i\nu}$, where i is a running index characterizing the permutation. The permutation range is restricted by setting a limit to the orbital momenta l_1, l_2 taken into consideration; under present physical conditions a reasonable limit is $l_{\max}=4$, as discussed in Sec. 5. The ensuing $\alpha_{i\nu}$ refer to a given sequence of nuclear spins and to observation of radiation in a given transition step (e.g., N', γ_1, γ_2, or γ_3, etc.), but can in many instances be converted from those for a certain "basic" sequence to those for related spin sequences, as discussed later. The $\alpha_{i\nu}$ for N' distributions, dictated essentially only by the nuclear spins J_0 and J_2, can readily be transformed from those for a J_0/J_2 sequence to those for a J_0/J_2' combination involving a new value J_2' of the residual nuclear spin. For γ-transitions, the $\alpha_{i\nu}$ are governed additionally by further spins, such as J_3, J_4, etc. and by multipole mixing ratios, which renders conversion more difficult and tabulation more involved. The policy adopted has been to choose a set of "basic" spin sequences and list the $\alpha_{i\nu}$ together with respective momenta l_1, j_1, $J_1\pi_1$, l_2, j_2.

C. Conversion Factors c_ν and C_ν

It is possible to define simple numerical conversion coefficients that generate the $\alpha_{i\nu}$ for a new transition sequence from known α's for a different given sequence. These conversion factors eliminate the labor of evaluating the $\alpha_{i\nu}$ afresh from first principles. They can be applied to nucleon transitions wherever the total particle angular momenta j_1 or j_2 are the same in the new as in the old transition. From the $\alpha_{i\nu}$ for observed N' radiation in a $J_0\pi_0{\rightarrow}J_1\pi_1{\rightarrow}J_2\pi_2$ reaction sequence, those for a new sequence in which J_2 is replaced by J_2' (but π_2 unchanged, and the new j_2 numerically equal to the old) are obtained by multiplying by

$$c_{i\nu}=\eta_\nu(j_2j_2J_2'J_1)/\eta_\nu(j_2j_2J_2J_1) \tag{44}$$

$$= (-)^{J_2'-J_2}W(j_2j_2J_1J_1;\nu J_2')/W(j_2j_2J_1J_1;\nu J_2), \tag{45}$$

where $c_{i0}\equiv1$ for all i. Alternatively, the $\alpha_{i\nu}$ for a sequence in which J_0 is replaced by J_0' (but π_0 and j_1 unchanged), are generated by the similarly normalized

conversion factor

$$c_{i\nu}=\eta_\nu(j_1j_1J_0'J_1)/\eta_\nu(j_1j_1J_0J_1) \tag{46}$$

$$= (-)^{J_0'-J_0}W(j_1j_1J_1J_1;\nu J_0')/W(j_1j_1J_1J_1;\nu J_0). \tag{47}$$

Any additional terms in the basic tabulation where j_2 or j_1 do not coincide with the old values have to be evaluated afresh or alternatively necessitate construction of an appropriately modified numerical conversion factor.

In the case of observed γ distributions, the factors C_ν represent a more powerful approach in that the basic tabulation now involves no new combination of momenta and $\alpha_{i\nu}$. Accordingly, instead of using $c_{i\nu}$'s to convert individual $\alpha_{i\nu}$'s, it suffices to multiply the summed coefficients $a_\nu\equiv\sum_i\alpha_{i\nu}\tau_i$ by an over-all factor C_ν. (These factors are identical with those employed in β–γ and γ–γ angular-correlation calculations.) From the a_ν determined for a standard sequence, $J_0\pi_0{\rightarrow}J_1\pi_1{\cdots\rightarrow}J_2\pi_2{\rightarrow}J_3\pi_3$, those for a sequence (i) $J_0\pi_0{\rightarrow}J_1\pi_1{\cdots\rightarrow}J_2\pi_2{\rightarrow}J_3'\pi_3'$ and others involving unobserved intermediate γ transitions ($\cdots\rightarrow$), such as (ii) $J_0\pi_0{\rightarrow}J_1\pi_1{\cdots\rightarrow}J_2\pi_2{\cdots\rightarrow}J_3\pi_3{\rightarrow}J_4\pi_4$, or (iii) $\cdots\cdots\rightarrow J_3\pi_3{\cdots\rightarrow}J_4\pi_4{\rightarrow}J_5\pi_5$, etc. can be generated by use of the Cj. The situation is, however, complicated if γ transitions involve mixed multipolarity. For simplicity, the standard sequence should involve pure γ radiation of multipolarity $L_2=L_2'$ effecting the transition from J_2 to J_3. The appropriate γ transition parameter then reduces from $A_\nu(L_2L_2'J_3J_2)$ to $F_\nu(L_2L_2J_3J_2)$, so that the conversion factor for case (i) above becomes

$$C_\nu = A_\nu(L_2{}^{\text{new}}L_2'{}^{\text{new}}J_3'J_2)/F_\nu(L_2L_2J_3J_2), \tag{48}$$

and if $L_2{}^{\text{new}}=L_2'{}^{\text{new}}$, this reduces further to

$$C_\nu = F_\nu(L_2{}^{\text{new}}L_2{}^{\text{new}}J_3'J_2)/F_\nu(L_2L_2J_3J_2) \tag{49}$$

$$= (-)^{J_3'-J_3}\left(\frac{\hat{L}_2{}^{\text{new}}}{\hat{L}_2}\right)^2\frac{\langle\nu0\mid L_2{}^{\text{new}}L_2{}^{\text{new}}1-1\rangle}{\langle\nu0\mid L_2L_21-1\rangle}$$

$$\times\frac{W(L_2{}^{\text{new}}L_2{}^{\text{new}}J_2J_2;\nu J_3')}{W(L_2L_2J_2J_2;\nu J_3)}, \tag{50}$$

which becomes particularly simple if $L_2{}^{\text{new}}=L_2$.

For case (ii), in which one unobserved intermediate γ transition is involved, the general expression for the conversion factor is

$$C_\nu = U_\nu(L_2L_2'J_2J_3)A_\nu(L_3L_3'J_4J_3)/A_\nu(L_2L_2'J_3J_2), \tag{51}$$

and if the standard transition is of pure multipolarity

$L_2 = L_2'$ then

$$C_\nu = U_\nu(L_2 L_2' J_2 J_3) A_\nu(L_3 L_3' J_4 J_3)/F_\nu(L_2 L_2 J_3 J_2) \quad (52)$$

$$= N'' U(\delta_2) M'(\delta_3)/N' M(0), \quad (53)$$

allowing for the unobserved new transition to be of mixed multipolarity L_2, L_2' and the observed radiation to be of multipolarity L_3, L_3'.

Analogously, for case (iii), which involves two unobserved intermediate steps, the conversion factor is

$$C_\nu = U_\nu(L_2 L_2' J_2 J_3) U_\nu(L_3 L_3' J_3 J_4)$$

$$\times A_\nu(L_4 L_4' J_5 J_4)/A_\nu(L_2 L_2' J_3 J_2), \quad (54)$$

and so on for higher numbers of successive intervening transition steps involving unobserved cascade radiation. Numerical results for cases (i), (ii), and (iii) have been given by Benjamin,[24] and also by Mathur and Tucker.[25]

The above expressions can be combined when it is, for example, desired to establish conversion factors taking the a_ν for the standard sequence $J_0\pi_0 \rightarrow J_1\pi_1 \cdots \rightarrow J_2\pi_2 \rightarrow J_3\pi_3$ into those for a sequence such as $J_0\pi_0 \rightarrow J_1\pi_1 \cdots \rightarrow J_2\pi_2 \cdots \rightarrow J_3'\pi_3' \rightarrow J_4\pi_4$, where we have an intermediate unobserved step leading to a new level of spin–parity $J_3'\pi_3'$. In this instance, the conversion factor ensues from combination of (48) and (51):

$$C_\nu = U_\nu(L_2^{\text{new}} L_2'^{\text{new}} J_2 J_3')$$

$$\times A_\nu(L_3 L_3' J_4 J_3')/A_\nu(L_2 L_2' J_3 J_2). \quad (55)$$

A similar approach applied to an observed γ transition of pure multipolarity leads to conversion factors of the type C_ν which transform the a_ν from those for a given spin sequence involving pure multipolarity L to those for the same sequence but different pure multipolarity L'. Such factors, which we distinguish from the normal C_ν by the superscript $(L \rightarrow L')$, take the form

$$C_\nu^{(L \rightarrow L')} = \frac{F_\nu(L'L'J_f J_i)}{F_\nu(LLJ_f J_i)} = \frac{M(L'L')}{M(LL)}$$

$$= \frac{(\hat{L}')^2}{(\hat{L})^2} \cdot \frac{\langle \nu 0 \mid L'L'1-1 \rangle}{\langle \nu 0 \mid LL1-1 \rangle} \cdot \frac{W(L'L'J_i J_i; \nu J_f)}{W(LL J_i J_i; \nu J_f)}. \quad (56)$$

These $C_\nu^{(L \rightarrow L')}$ do not depend upon the spins of levels other than those between which the transition is observed. However, the range of ν is dictated by selection rules which involve extraneous spins. The $C_\nu^{(L \rightarrow L')}$ are normalized to unity for $\nu = 0$; when $\nu > 0$, they can take on numerically simple values. An instance is furnished by the spin sequence $\frac{1}{2}^+ \rightarrow J_1\pi_1 \cdots \rightarrow \frac{3}{2}^+ \rightarrow \frac{1}{2}^+$, for which

---

[24] R. W. Benjamin, Ph.D. thesis, University of Texas, 1965 (unpublished), and private communication.

[25] I. L. Morgan, J. B. Ashe, D. O. Nellis, R. W. Benjamin, S. C. Mathur, W. E. Tucker, O. M. Hudson, and P. S. Buchanan, Annual Progress Report, Nuclear Physics Laboratory, Texas Nuclear Corporation, August 1964 (unpublished).

the $\alpha_{i\nu}$ are listed in Table X of Appendix A. The values of the latter are given for pure $M1$ multipolarity, since those for $E2$ γ radiation are numerically the same: with ν curbed to $\nu = 0, 2$ we find that

$$C_0^{(M1 \rightarrow E2)} = 1; \qquad C_2^{(M1 \rightarrow E2)} = \frac{F_2(22\frac{1}{2}\frac{3}{2})}{F_2(11\frac{1}{2}\frac{3}{2})} = -1. \quad (57)$$

Thus the $E2$ distribution has identically the same form as the $M1$ except that it is inverted about the line $d\sigma/d\Omega_2 = a_0$. On the other hand, for an observed $\frac{3}{2}^+ \rightarrow \frac{3}{2}^+$ γ transition, with the same restriction upon the range of ν, we obtain multipole conversion factors from $M1$ to $E2$ radiation which have the values $C_0^{(M1 \rightarrow E2)} = 1$, $C_2^{(M1 \rightarrow E2)} = 0$. It accordingly follows that the distribution of pure $E2$ radiation effecting the transition $\frac{3}{2}^+ \rightarrow \frac{3}{2}^+$ or $\frac{3}{2}^- \rightarrow \frac{3}{2}^-$ is isotropic. However, for an observed $\frac{5}{2}^+ \rightarrow \frac{3}{2}^+$ γ transition, the appropriate $M1 \rightarrow E2$ multipole conversion factors are $C_0^{(M1 \rightarrow E2)} = 1$, $C_2^{(M1 \rightarrow E2)} = -0.51020$ and terms with $\nu = 4$ now have to be evaluated. Similarly, for an observed $3^+ \rightarrow 2^+$ transition, we have $C_0^{(M1 \rightarrow E2)} = 1$, $C_2^{(M1 \rightarrow E2)} = -0.35714$ and new $\nu = 4$ terms.

In the case of multipolarity conversion $L \rightarrow L'$ in an *unobserved* transition (followed by a given observed γ transition), the factors are

$$C_\nu^{(L \rightarrow L')} = \frac{U_\nu(L'L'J_i J_i')}{U_\nu(LLJ_i J_i')} = \frac{U(L'L')}{U(LL)}$$

$$= (-)^{L-L'} \frac{W(J_i J_i J_i' J_i'; \nu L')}{W(J_i J_i J_i' J_i'; \nu L)}, \quad (58)$$

with $C_0^{(L \rightarrow L')} = 1$ again.

D. Automatic Computation of Angular Distributions

The ALGOL code "MANDY" for a fast computer (e.g., CDC 1604-A) was compiled independently of existing Hauser–Feshbach programs (such as that of Wills, and its modifications[5]) to attain the widest degree of flexibility in application and to serve thereafter as a basis for a general CN *correlation* code "BARBARA" of greater complexity, going beyond the confines of the present publication. Both programs are designed to handle arbitrarily high angular momenta, arbitrary values of nuclear spin (integer and half-integer), and γ radiation (at will, preceded by an unobserved mixed transition) of mixed multipolarity. Results are automatically furnished not only for a specified multipole mixture (using δ from input data) but also for $\delta = 0$.

The input data for "MANDY," apart from specification of various options which steer the course of calculation, is in the simplest instance confined to statement of nuclear spins and parities, $J_0\pi_0$, $J_2\pi_2$, $J_3\pi_3$ (and $J_4\pi_4$ if relevant), the γ multipolarities L_2, L_2' with requisite mixing ratio δ_2 (and L_3, L_3', δ_3 if needed), and the nucleon orbital momentum cutoff limits $l_{1\,\text{max}}$, $l_{2\,\text{max}}$. In this instance the code will effect automatic tabulation
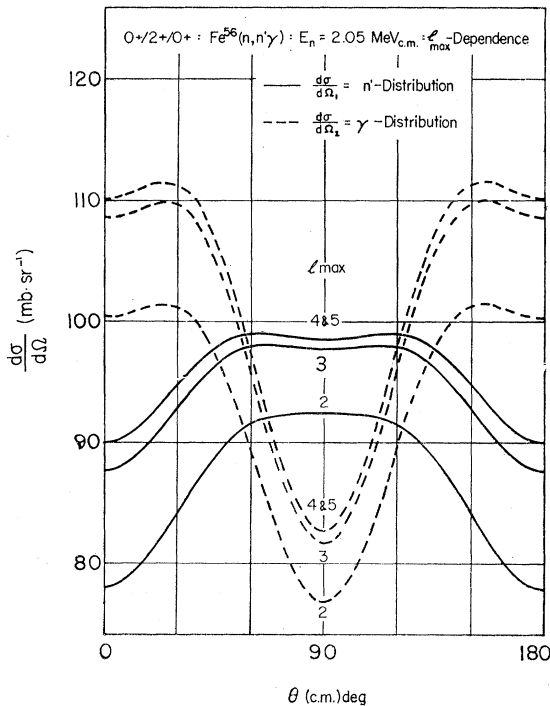
FIG. 3. Dependence of the absolute nucleon and γ distributions upon the orbital momentum cutoff l_{max}, illustrated by inelastic neutron scattering on Fe^{56} at 2.05 MeV. In this case, the distribution *structure* experiences no appreciable change as the number of partial waves is increased, and the magnitude attains its ultimum value at $l_{max}=4$.

(bearing in mind Racah and conservation restrictions) and evaluation of the Legendre polynomial series restricted expansion coefficients $\alpha_{i\nu}$, as relevant to the species of distribution under consideration (viz., N', γ, $\gamma-\gamma$ or, at will, both nucleon *and* γ distributions consecutively). In each instance the Racah functions which make up the appropriate distribution expressions are evaluated in subroutines.

The above is usually extended to proceed further to numerical evaluation of absolute and normalized angular distributions, together with print-out of absolute and normalized expansion coefficients a_ν and $a_\nu^* \equiv a_\nu/a_0$, respectively. Since $a_\nu = \sum_i \alpha_{i\nu}\tau_i$, the latter Legendre expansion coefficients depend through the τ_i upon the transmission coefficients $T_l^{(\pm)}$ and thus upon the choice of optical potential, unlike the potential-independent restricted coefficients $\alpha_{i\nu}$. Apart from necessary changes in options, additional input data has to be supplied for subroutine automatic evaluation of the τ_i and thence of the differential cross sections $d\sigma/d\Omega_1$ or $d\sigma/d\Omega_2$ (or both) in mb sr^{-1}, and normalized distributions $W(\theta_1)$ or $W(\theta_2)$ (or both) such that $W(90°) = 1$. These additional input data comprise incident and emergent particle energies E_1 and E_2 in the center-of-mass system, the angular interval $\Delta\theta$ for which the distribution is to be evaluated [because of symmetry about 90°, the CN

distribution is evaluated over the range $0°(\Delta\theta)90°$] and four sets of transmission coefficients, the first pair of sets, T_0, $\cdots$, $T_{l_1max}^{(-)}$, T_0, $\cdots$, $T_{l_1max}^{(+)}$ referring to the incident channel $J_0 \rightarrow J_1$ and the second pair, T_0', $\cdots$, $T_{l_2max}^{(-)'}$, T_0', $\cdots$, $T_{l_2max}^{(+)'}$ to the emergent channel $J_1 \rightarrow J_2$. If spin–orbit interaction is neglected, the $T_l^{(-)}$ and $T_l^{(+)}$ are mutually identical. If the possibility of CN decay through additional exit channels is to be taken into account (resulting in a marked influence upon the τ_i values and thence upon the cross section), the number of extra channels has to be specified through a final option, and the relevant sets of transmission coefficients appended to the input data.

5. INFLUENCE OF HIGHER PARTIAL WAVES UPON ANGULAR DISTRIBUTIONS

Computer calculations in which the orbital momentum limit l_{max} was increased stepwise have confirmed that the partial-wave cutoff at $l_{max}=2$ adopted by some authors in order to curb the complexity of their hand calculations represents too restrictive a condition. Incorporation of the influence of higher partial waves not only results in an increase in the magnitude of the differential cross section, as illustrated in Fig. 3, but can perceptibly change the distribution structure.

Figure 3 shows results[26] for the Fe^{56} $(n, n'\gamma)$ reaction at 2.05 $MeV_{c.m.}$ using a partial wave cutoff l_{max}, which ranges from 2 to 5. Each curve, as computed using generalized Perey–Buck transmission coefficients $T_l^{(\pm)}$, is indistinguishable from that for the averaged coefficients T_l. The figure indicates that at low energies, partial waves having momenta $l>4$ exert no appreciable influence upon the magnitude or structure of angular distributions. The slight dip in the neutron distribution around 90°, as occasioned by the influence of the a_4 Legendre expansion coefficient, becomes evident only when orbital momenta higher than $l=2$ are taken into account.

This effect is illustrated still more vividly in the proton distributions to the first 2^+ level of Ni^{60} in Fig. 4. Here the higher partial waves induce relative augmentation of the a_4 with the result that the dip around 90° becomes progressively more apparent.

6. INFLUENCE OF MULTIPOLE MIXING RATIOS

Quantitative evaluation of the effect upon the γ distribution on varying the mixing ratio δ for various different spin sequences, using the code "MANDY," has indicated that marked sensitiveness may be found

---

[26] In Ref. 17, the left-hand scale of Fig. 43 is numerically wrong; it should be multiplied by 25. The curve for $l \leq 4$ in the figure should be displaced to tally with that for $l \leq 5$. An unfortunate error in Fig. 18 of Ref. 17 has also come to light: the experimental points for $\theta_2 = 30°$ should be interchanged with those for $\theta_2 = 90°$, thereby yielding somewhat better agreement with the theoretical correlation curves, which have been correctly drawn and captioned. Also, in Eq. (153), the factor $(8\pi)^{\frac{1}{2}}\sigma^3$ should be deleted.

among odd-mass as well as even-mass nuclei. Figure 5 depicts the case of a

$$\tfrac{1}{2}^+ \to J_1\pi_1 \to \tfrac{3}{2}^+ \underset{M1+E2}{\longrightarrow} \tfrac{1}{2}^+$$

transition sequence as evaluated for the inelastic scattering of 2-MeV neutrons on Si^{29}. The striking inversion of structure for $\delta = +3.4$ (a value taken from Ref. 27) is immediately evident upon comparison with curves for alternative values proposed in the past. The intersection of all γ distributions around $\theta_2 = 55°$ and $125°$ is a consequence of their structure being of the form

$$d\sigma/d\Omega_2 = a_0 + a_2 P_2(\cos\theta_2), \qquad (59)$$

since higher orders in ν are ruled out by the condition $\nu \leq 2J_2 = 2 \times \tfrac{3}{2}$. The δ-dependence, which thus reposes solely in the coefficient a_2 (the term a_0 is simply a constant), is rendered ineffective at the two angles for which the second-order Legendre polynomial P_2 is zero. In the case of comparison with relative, rather than absolute, measurements these special angles would represent suitable points for normalization. That the *neu-*
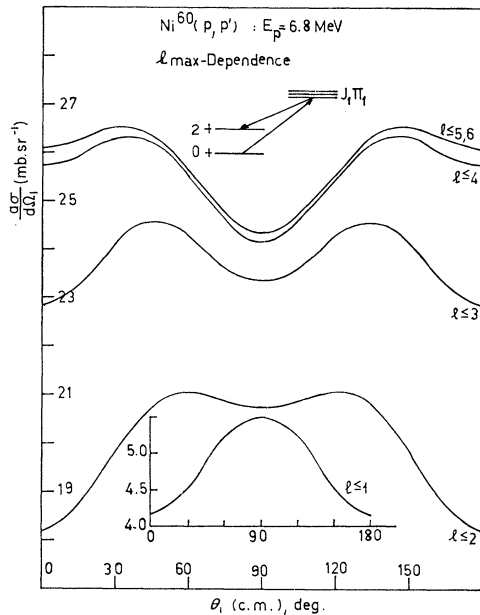

FIG. 4. An analogous orbital momentum dependence to that of Fig. 3, and for the same spin sequence, but for inelastic proton scattering on Ni^{60} at 6.8 MeV. Attention is drawn to the change in structure as higher partial waves are taken into consideration, causing the dip at 90° to become progressively more pronounced. The figure in the insert shows that the distribution for the unrealistically low momentum cutoff at $l_{max}=1$ displays no indication of a dip, since terms with ν higher than 2 are absent.

27 D. A. Bromley, H. E. Gove, E. B. Paul, A. E. Litherland, and E. Almqvist, Can. J. Phys. 35, 1042 (1957); G. J. McCallum and A. E. Litherland, Bull. Am. Phys. Soc. 5, 56 (1960).
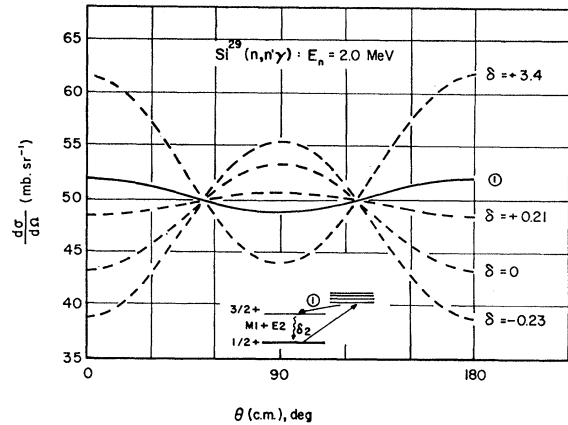
FIG. 5. Different distributions associated with different values of the mixing ratio δ in the case of de-excitation radiation of mixed $M1+E2$ multipolarity following inelastic scattering of 2-MeV neutrons on Si^{29}. The curves intersect around 55° and 125° because the δ dependence in the weighting coefficient a_2 of the second-order Legendre polynomial $P_2(\cos\theta)$ is suppressed by the vanishing of P_2 at the above angles. The intersection of the neutron distribution ① also approximately coincides with these angles because the value of a_4 is here too small to exert any appreciable influence. Of the numerical values of δ depicted in the figure, which were taken from various publications, the most likely are -0.23 or $+3.4$ (Ref. 27).

tron distribution, whose form is given by

$$d\sigma/d\Omega_1 = a_0 + a_2 P_2(\cos\theta_1) + a_4 P_4(\cos\theta_1), \quad (60)$$

also appears to pass through the points of coincidence is because of the negligibly small value of a_4 which obtains in this case and the equality of the terms a_0 for nucleon and γ distributions in the same spin sequence.

Radioactive decay processes have provided the main basis for experimental elucidation of a γ transition's multipole character through studies of γ–γ angular correlations, whose sensitivity to the multipole mixing ratio generally enables the latter to be established within fairly narrow limits. Since statistical reaction theory makes definite predictions for an $(N, N'\gamma)$ angular distribution as a function of δ, comparison of experimental least-squares-fit values of a_2^* and a_4^* (where $a_\nu^* \equiv a_\nu/a_0$) with the range of values given by theory enables δ to be established together with its (fairly narrow) error limits. For an $(N, N'\gamma)$ process in which no unobserved γ transitions intervene before the observed γ distribution, the locus of points associated with δ's ranging from 0 to ∞ and of positive or negative phase is an ellipse in which points for δ's of the same magnitude but opposite sign have the same ordinate. The zone within this representation described by the values and error limits of a_2^* and a_4^* which give the least-squares fit to the experimental γ distribution defines the value of δ for the observed transition.

It has recently been shown that γ distributions from inelastic nucleon scattering can also be utilized. Sen Gupta and Van Patter have investigated $(p, p'\gamma)$

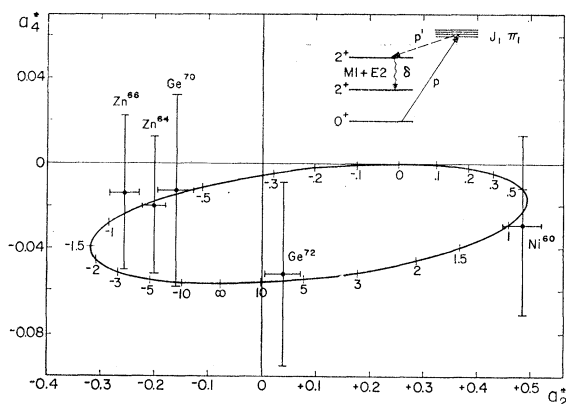FIG. 6. Experimental results for $(p, p'\gamma)$ angular distributions of $2_2{}^+{\rightarrow}2_1{}^+$ transitions compared with the theoretical δ ellipse plotted in $a_4{}^*$ vs $a_2{}^*$ space. The theoretical predictions for the various nuclei do not differ by more than 3% from the average δ ellipse shown. The points for Ni^{60}, Zn^{66}, and Zn^{68} are the average of four measurements with $E_p=4.42$ to 5.42 MeV (Ref. 28), while the points for Ge^{70} and Ge^{72} are the averages of two measurements at 5 and 6 MeV (Ref. 29).

reactions on Ni^{60}, Zn^{64}, and Zn^{66} involving the $2_2{}^+(M1+E2)2_1{}^+(E2)0_1{}^+$ transitions.[28] Their results, together with more recent measurements[29] for Ge^{70} and Ge^{72}, are summarized in Fig. 6. Each point represents the average of two or more angular distributions, which have been averaged to reduce effects due to level density fluctuations.

In Fig. 6, the $a_4{}^*$ scale is expanded by a factor of 4 relative to the $a_2{}^*$ scale in order to separate the two branches $(\pm)$ of δ values. The present accuracy of the experimental measurements is not sufficient to distinguish between these branches, since these $a_4{}^*$ values have a typical uncertainty of about ± 0.04, which is comparable with the separation of the two branches of the ellipse. In fact, the precision of these present measurements may well be limited by the presence of fluctuations in level densities.

From presently available knowledge of measured δ values for $2_2{}^+{\rightarrow}2_1{}^+$ transitions in medium-weight nuclei, values roughly within the region $-3<\delta<3$ are expected. Accordingly, it is assumed that values of δ from the lower side of the δ-ellipse should be taken in accord with the experimental limits for $a_2{}^*$. This procedure yields δ values for Zn^{66} and Ge^{72} in reasonable agreement with those measured in radioactivity studies,[30] while in the case of Zn^{64} and Ge^{70}, no previous determinations have been made. The Ni^{60} value indi-

cates an anomalously large $M1$ component, in distinct disagreement with one earlier radioactivity measurement, but probably in good agreement with new preliminary results[31] for the Cu^{60} decay.

At higher proton bombarding energies, the possibility arises that the second 2^+ level may be fed by transitions from higher levels: e.g., in the case of Ni^{60}, there is a feeding from the 2.63-MeV $3_1{}^+$ state to the 2.16-MeV $2_2{}^+$ state. Unless an appropriate correction is applied, this could cause a systematic error in the δ determination by this method. If the $2_2{}^+{\rightarrow}0_1{}^+$ transition is sufficiently prominent to permit an accurate angular distribution measurement, then a second procedure may be employed. This involves the measurement of the ratio $a_2{}^*(2_2{}^+{\rightarrow}2_1{}^+)/a_2{}^*(2_2{}^+{\rightarrow}0_1{}^+)$, which is independent of the magnetic substate populations for this $2_2{}^+$ state, and hence avoids our usual assumption of compound nucleus formation. This method is equivalent to taking the ratio of $a_2{}^*$ values from two γ–γ angular correlations in a radioactive decay, which is ordinarily not necessary since in this case each correlation may be used independently. Using this second procedure, Mohindra and Van Patter[29] have recently determined δ values for Ni^{60}, Ge^{70} and Ge^{72}. This procedure was implied in the discussion of ellipse II in the paper of Sen Gupta and Van Patter.[28]

Figure 7 shows new theoretical results for inelastic neutron scattering, as evaluated using Perey–Buck transmission coefficients. The top ellipse is that for a

$$0^+{\rightarrow}J_1\pi_1{\rightarrow}2^+\underset{M1+E2}{\xrightarrow{\hspace{1.5cm}}}2^+$$

sequence, wherein 2.37-MeV neutrons are inelastically scattered from Zn^{66}. Its form is practically identical with that for 4.82-MeV protons scattered under the same conditions.

When, however, the above mixed transition is unobserved and the following de-excitation step of pure $E2$ multipolarity is observed, the measured distribution of the latter depends on the magnitude (but not the sign) of the mixing ratio for the unobserved decay. Thus for the spin sequence

$$0^+{\rightarrow}J_1\pi_1{\rightarrow}2^+\underset{M1+E2}{\xrightarrow{\hspace{1.5cm}}}2^+\underset{E2}{\rightarrow}0^+$$

under the above conditions, the multipole mixing of the penultimate step can be determined to within a phase factor from measurements of the distribution of the final $E2$ γ radiation. Results for different δ's now lie on a line in the $a_2{}^*/a_4{}^*$ representation, points for δ's of equal magnitude but opposite sign being coincident since the U_ν term for the unobserved step involves only δ^2 [see Eq. (30)]. For a process in which not only the intermediate (unobserved) step but also the final

[28] A. K. Sen Gupta and D. M. Van Patter, Phys. Letters **3**, 355 (1963); Nucl. Phys. **50**, 17 (1964); A. K. Sen Gupta, P. N. Trehan, and D. M. Van Patter, Bull. Am. Phys. Soc. **7**, 81 (1962).

[29] R. K. Mohindra and D. M. Van Patter, Bull. Am. Phys. Soc. **10**, 38 (1965); Phys. Rev. **139**, B274 (1965).

[30] A. Schwarzschild and L Grodzins, Phys. Rev. **119**, 276 (1960); R. B. Arns and M. L. Wiedenbeck, Phys. Rev. **112**, 229 (1958).

[31] G. T. Wood and S. M. Shafroth, Topical Conference on *Bases for Nuclear Spin Parity Assignments*, Gatlinburg, abstract B10 (1965).

(observed) transition are of mixed multipolarity, the locus of points for different values of δ_3 but a fixed value of δ_2 again becomes an ellipse.

Though the δ ellipse representation offers a large amount of information in compact form, particularly when ellipses (and point "ellipses") for several sequences are depicted conjointly for comparison, as has been done by Van Patter and Mohindra,[32] certain features are brought out more clearly by the alternative representation of $|\delta|$ separately against a_2^* and a_4^* (a representation employed in studies of radioactive γ decay). By way of contrast with the preceding, direct
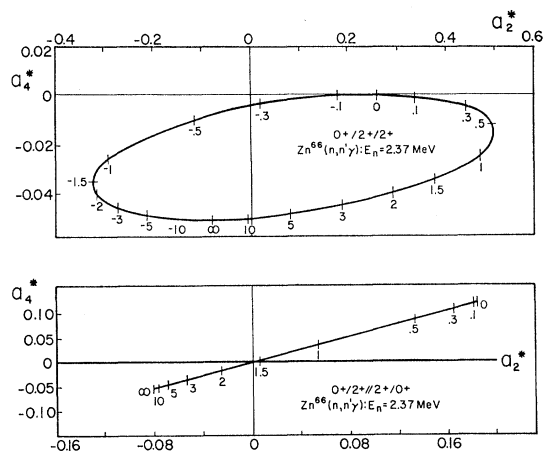
FIG. 7. Theoretical predictions for the variation of a_4^* vs a_2^* for the entire range of values of multipole mixing ratio δ in the case of inelastic scattering of 2.37-MeV neutrons to the second level (2^+) of Zn^{66}. The loci of points for different values of δ form an ellipse for the spin sequence

$$0^+ \longrightarrow J_1\pi_1 ---\to 2_2{}^+ \underset{M1+E2}{\longrightarrow} 2_1{}^+,$$

but a straight line for the sequence

$$0^+ \longrightarrow J_1\pi_1 ---\to 2_2{}^+ \underset{M1+E2}{---\to} 2_1{}^+ \underset{E2}{\longrightarrow} 0^+,$$

since in the latter instance only even-powered terms in ν enter into the calculation which also causes points for positive and negative δ phases to coincide. The symbol $---\to$ denotes an unobserved transition.

plots of the latter type for the above transitions are given in Figs. 8 and 9.

Figure 8 depicts the plot of $|\delta|$ vs a_2^* for an observed mixed transition (curves No. 1) from the second to the first level, contrasted with the curve (No. 2) for the same transition, but now unobserved, followed by a pure observed ground-state transition. The latter curve is of altogether different character, symmetric about the δ origin, where a_2^* is maximal (positive). The symmetry ensues from the fact that the second transition is pure quadrupole, and δ for the first transition is of even order in the distribution expression. In the plots of $|\delta|$ vs a_4^*, as depicted in Fig. 9, this symmetry about

[32] D. M. Van Patter and R. K. Mohindra, Phys. Letters **12**, 223 (1964).
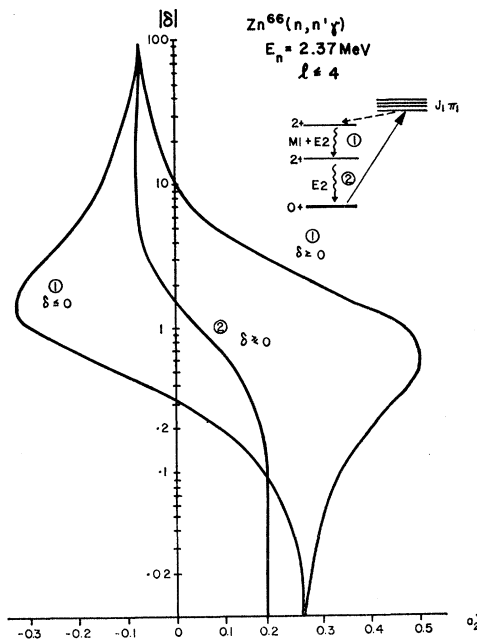
FIG. 8. The same data as contained in Fig. 7, but depicted in the alternative representation of δ vs a_2^*, showing characteristic symmetry with respect to positive and negative phases of δ.
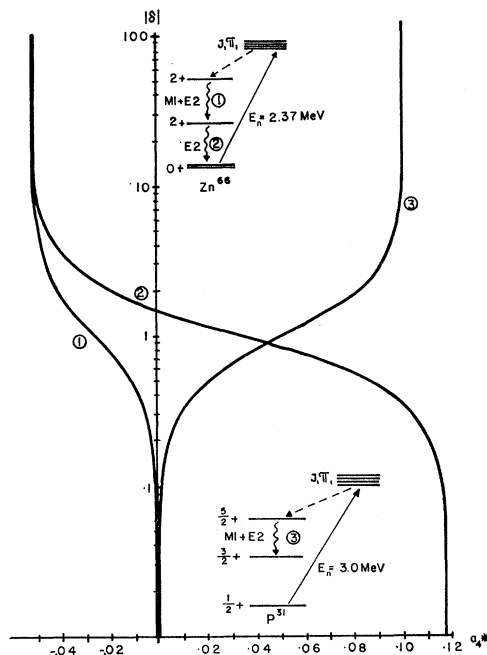
FIG. 9. The data of Fig. 7, but in the representation of δ vs a_4^*, which complements Fig. 8. Also shown is the theoretical result for the half-integer spin sequence

$$\tfrac{1}{2}{}^+ \longrightarrow J_1\pi_1 ---\to \tfrac{5}{2}{}^+ \underset{M1+E2}{\longrightarrow} \tfrac{3}{2}{}^+$$

as exemplified by inelastic scattering of 3-MeV neutrons on P^{31}.
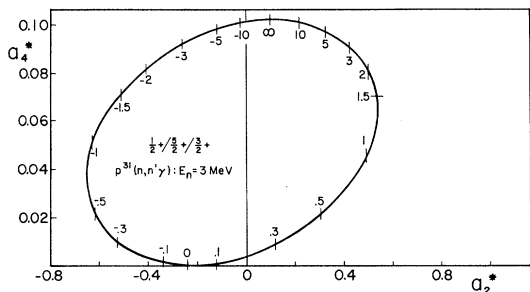
FIG. 10. The δ dependence of the mixed $M1+E2$ γ radiation from the $\frac{5}{2}^+$ to the $\frac{3}{2}^+$ level of P^{31}, following inelastic scattering of 3-MeV neutrons, depicted in the δ-ellipse representation.

the δ origin occurs, for the particular cases considered, as a consequence of the fact that only terms of *even* order in δ enter into the respective distributions when $\nu=4$ [the $M1$-$E2$ interference term of *first* order in δ_2 vanishes for $\nu=4$ (but not for $\nu=2$) in consequence of the Racah triangle restriction $\Delta(LL'\nu)$]. For mixed transitions of higher order, however, such as $M2+E3$, this symmetry would not obtain.

Figure 9 also displays results for the odd-mass nucleus P^{31}, which involves the half-integer spin sequence

$$\tfrac{1}{2}^+ \longrightarrow J_1\pi_1 \longrightarrow \tfrac{5}{2}^+ \underset{M1+E2}{\longrightarrow} \tfrac{3}{2}^+.$$

This differs from that above by being confined to *positive* values of a_4^* whose magnitudes are appreciably larger than those for the $0^+/2^+/2^+$ sequence. Again, as
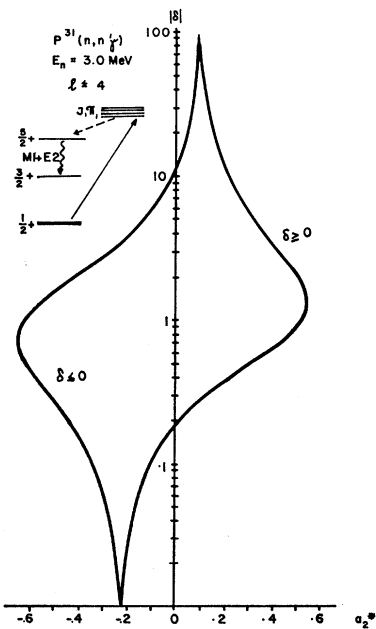
FIG. 11. Plot of δ vs a_2^* for a mixed $M1+E2$ γ transition from the second level ($\frac{5}{2}^+$) to the first level ($\frac{3}{2}^+$) of P^{31} at $E_n=3.0$ MeV. This complements curve No. 3 shown in Fig. 9 and presents the data of Fig. 10 in alternative form.

follows from symmetry considerations, the points for $\delta=0$ and ∞ correspond with extremal values of a_4^*. Figure 10 shows the δ dependence for this half-integral spin sequence in the elliptical representation, while Fig. 11 depicts the same data plotted directly against a_2^*, for comparison with Fig. 8.

In the case of a sequence such as $\tfrac{1}{2}^+ \longrightarrow J_1\pi_1 \cdots \longrightarrow \tfrac{3}{2}^+ \longrightarrow \tfrac{1}{2}^+$, for which $a_4^*=0$, the δ ellipse representation cannot be employed. Hence direct plots of δ vs a_2^* for Si^{29} are shown in Fig. 12.

This latter representation truly comes into its own when nuclear states of spin 1 or $\frac{3}{2}$ experience mixed-multipole γ decay. The slightly asymmetric structure appears to be characteristic of δ vs a_2^* plots (even for
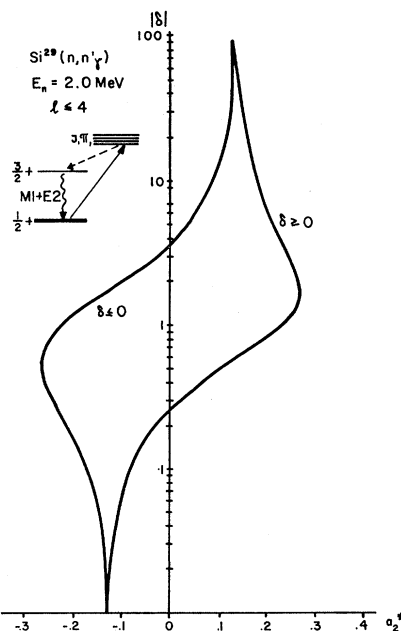
FIG. 12. Plot of δ vs a_2^* for a $\frac{3}{2}^+\to\frac{1}{2}^+$ γ transition of mixed $M1+E2$ multipolarity following inelastic scattering of 2-MeV neutrons to the first level of Si^{29}.

sequences when the a_4^* are nonzero), as follows from comparison with Figs. 8 and 11, and a further common feature is revealed on examining the δ values for which a_2^* is maximal, a situation which corresponds with the distributions essentially having maximal amplitude. Throughout, one finds maximal positive a_2^* when $\delta\approx1.4$, indicating distributions to have maximal amplitude (forming a dip at 90°) when the $E2$ intensity admixture in mixed radiation is double that of $M1$ (with the relative phase positive). Maximal *negative* values of a_2^* (distributions peaking at 90°) occur at negative δ's varying between -0.56 and -1.45, and accordingly do not display so striking a uniformity as that for positive $(a_2^*)_{max}$. Whereas Fig. 12 refers to de-excitation of the first level, Figs. 8 and 11 are concerned with transitions from the second to the first level.

In general, levels of even nuclei with $J_2 \leq 4$ have a substantial decay to the first 2^+ state. Recent calculations have revealed that in such instances transitions of the type $3(D, Q)2$ have the largest sensitivity to the $E2/M1$ mixing ratio.[32] In the case of (p, p') excitation of a 2.63-MeV state in Ni^{60} with 5.92-MeV protons, the calculated $3^+(E2)2^+$ angular distribution is given by

$$W(\theta_2) = 1 + 0.092 P_2(\cos \theta_2) + 0.225 P_4(\cos \theta_2). \quad (61)$$

A substantial contribution (43%) still originates from the $l_1=2$, $l_2=0$ term. The δ ellipse for a $3^+(M1, E2)2^+$ transition is generated by the conversion factors:

$$C_2 = (-2.8 + 15.336\delta + \delta^2)/(1+\delta^2); \qquad C_4 = \delta^2/(1+\delta^2). \quad (62)$$

This ellipse is shown in Fig. 13, together with the averaged experimental results which are also listed in Table I. The extreme sensitivity of the $3^+(M1, E2)2^+$ ellipse compared with other transition types is very striking, and in fact a conservative limit of $|\delta| > 30$ may now be given[29] for this particular transition in Ni^{60}. In Table I, predictions for other transition types are also given, with some of them illustrated in Fig. 13. The predictions for $3(D)2$ or $3(Q)2$ transitions for this $(p, p'\gamma)$ reaction are nearly independent of parity, so that the $3^-(E1, M2)2^+$ δ ellipse is nearly identical with the $3^+(M1, E2)2^+$ ellipse shown. The angular distributions for $1(D, Q)2$ transitions are confined to a small region on the a_2^* axis, all corresponding to near isotropy. It may thus be very difficult to identify transitions of this type by this method. Fortunately, as Day and Walt[18] have pointed out, spin-1 levels can be recognized on the basis of angular distributions of their $1(D)0$ ground-state transitions, which differ markedly from those for levels of spins 2 or 3. Transitions of this $1(D)0$ type have been recently identified in Fe^{56} (3.45

FIG. 13. Theoretical predictions for various transition types for the $(p, p'\gamma)$ angular distribution of a 2.63→2.16-MeV transition in Ni^{60}. The average result of three angular distribution measurements (Ref. 32) is represented by the cross-hatched area.

TABLE I. Theoretical predictions for the $(p, p'\gamma)$ angular distribution of a 2.63→2.16-MeV transition in Ni^{60} at $\bar{E}_p = 5.92$ MeV, assuming different transition types.

J_2	Transition	J_3	a_2^*	a_4^*
0^+	$E2$	2^+	0	0
1^+	$M1$	2^+	-0.013	0
1^+	$E2$	2^+	-0.063	0
1^-	$E1$	2^+	-0.010	0
2^+	$M1$	2^+	$+0.245$	0
2^+	$E2$	2^+	-0.075	-0.052
2^-	$E1$	2^+	$+0.201$	0
2^-	$M2$	2^+	-0.062	-0.008
3^+	$M1$	2^+	-0.257	0
3^+	$E2$	2^+	$+0.092$	$+0.225$
3^-	$E1$	2^+	-0.246	0
3^-	$M2$	2^+	$+0.088$	$+0.183$
4^+	$E2$	2^+	$+0.366$	-0.120
Experimental weighted average			$+0.084$ ± 0.024	$+0.191$ ± 0.036

MeV) on the basis of $(n, n'\gamma)$ angular-distribution data of Benjamin[24] and in Ni^{60} (3.19 MeV) from $(p, p'\gamma)$ angular-distribution data.[29]

7. LIMITING ANGULAR DISTRIBUTIONS

It is possible to make some general predictions regarding the behavior of $(n, n'\gamma)$ angular distributions near the threshold for excitation of a particular level. These are based on the expectation that for incident neutron energies sufficiently close to threshold, the (n, n') cross section for that level will be dominated by terms involving penetrabilities for s-wave outgoing neutrons.

a. Transitions from 2^+ Levels

A particularly simple example of a limiting angular distribution involves the $2^+(E2)0^+$ transition from the first 2^+ state of an even nucleus. We shall focus attention on the properties of terms of the type τ [Eq. (13)], which involve dominant partial-wave combinations. In this case, the two τ terms with $l_2=0$ (s wave) also have $l_1=2$, and correspond to d-wave excitation of $\frac{3}{2}^+$ and $\frac{5}{2}^+$ compound states. From Table VI of Appendix A, the contributions of these compound states to the overall angular distribution are given by $[4+2P_2(\cos \theta)]$ and $[6+3.428 P_2(\cos \theta) - 3.428 P_4(\cos \theta)]$, respectively. Near threshold, the denominators of these τ terms [which are the Hauser–Feshbach sums $\sum_{ljE} T_l(E)$] are also equal, which means that the predicted angular distributions become effectively independent of the optical-model parameters. The sum of these two contributions yields a limiting angular distribution given by

$$W(\theta_2) = 1 + 0.5428 P_2(\cos \theta_2) - 0.3428 P_4(\cos \theta_2), \quad (63)$$

which has an angular asymmetry $W(0°)/W(90°)$ of 2, as shown on the right of Fig. 14. We therefore expect experimental $(n, n'\gamma)$ angular distributions to approach this model-independent limit near threshold,
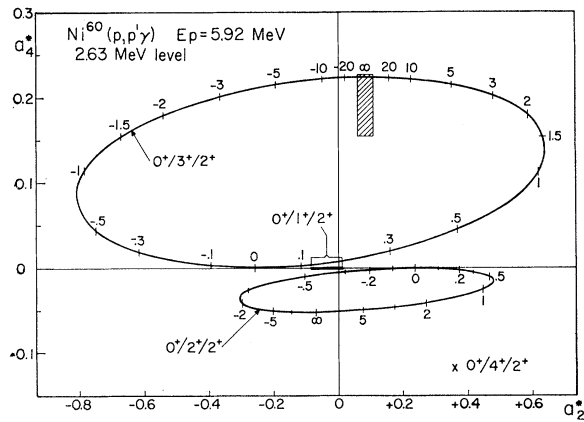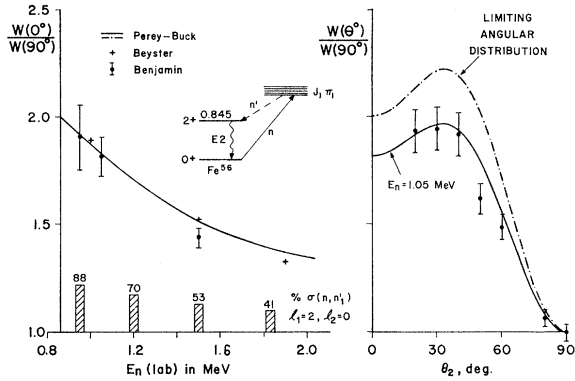
FIG. 14. Variation of the asymmetry in the distributions of γ rays following scattering of neutrons to the first level (2^+) of Fe^{56} as the incident neutron energy is increased from the threshold value of 0.85 to 2 MeV. Results of calculations employing Perey–Buck and Beyster penetrabilities are compared with recent measurements by Benjamin (Refs. 24, 25). On the lower left, the percentage contribution to the (n, n_1') cross section is shown for the partial wave combination which dominates at threshold. On the right, Benjamin's angular distribution data is shown to be slightly less anisotropic than the predicted limit, in accord with calculation for an energy slightly above threshold.

Despite the present paucity of relevant experimental data, this prediction has now been clearly verified by recent measurements of Benjamin[24],[25] which included some (n, $n'\gamma$) angular distributions near the threshold for the 0.845-MeV first 2^+ state of Fe^{56}. The experimental conditions (neutron energy spread of 70 keV) were evidently satisfactory for adequate statistical averaging. The observed distributions for E_n(lab) $= 0.95$ and 1.05 MeV were nearly identical to the limiting case (63), with asymmetries only slightly less than 2. The experimental asymmetries shown on the left of Fig. 14 have been estimated by extrapolating the forward angle data ($\theta \leq 40°$) to $0°$ in a manner consistent with theory. An alternative procedure would be to employ least-squares analyses, which should yield asymmetries lying within the range of the indicated error bars.

Calculations using Perey–Buck penetrabilities predict a rapid decrease in the angular asymmetry above threshold, despite the fact that the percentage contribution to the inelastic cross section of the two $T_2 \cdot T_0'$ terms decreases rather slowly. (For brevity, we add a prime to penetrabilities that refer to outgoing channels.) This dropoff is primarily caused by the increased influence of τ terms of the types $T_1 \cdot T_1'$ and $T_2 \cdot T_2'$, both of which are associated with much smaller asymmetries. The form of this dropoff is very nearly model-independent for Fe^{56}, as revealed in Fig. 14 by the similarity in predicted asymmetries using Beyster penetrabilities, and therefore should be insensitive to effects due to fluctuations of level widths. At $E_n = 1.05$ MeV (roughly 0.2 MeV above threshold), the extent of this dropoff is clearly revealed by the angular distribution data shown on the right of Fig. 14, which is less anisotropic than the limiting case. At higher energies, the asymmetry is

expected to level off gradually, in agreement with Benjamin's data for $E_n = 1.5$ MeV, as well as with the earlier results of Day and Walt[18] at 2.56 MeV, in which an asymmetry close to 1.3 was observed.

This limiting angular distribution (63) has in fact a wider application. It should also be approached near threshold for ground-state transitions from second 2^+ states, since the denominators of the $J_1 = \frac{3}{2}^+$ and $\frac{5}{2}^+$ τ terms will still remain equal (if terms involving $l_2 = 4$ to the first 2^+ state are negligible). A lower-lying 4^+ state should not appreciably influence this equality. For higher 2^+ states, one expects in general that contributions from final states with different J, π will effect an inequality in the denominators of these two τ terms, thereby altering the limiting angular distribution to some extent. However, the limiting angular asymmetry *will remain* 2, since each of the angular contributions from $J_1 = \frac{3}{2}^+$ or $\frac{5}{2}^+$ has $W(0°)/W(90°) = 2$. This statement applies equally well to the two contributions from $J_1 = \frac{3}{2}^-$ or $\frac{5}{2}^-$ for a 2^- level. One therefore expects that every spin-2 level will exhibit a similar behavior of the $2^+(E2)0^+$ angular asymmetry near threshold, which should approach a limiting value of 2, and decrease rapidly above, the rate being accentuated for nuclei near a p-wave resonance of the optical model.

Another transition of general interest is the $2^+(M1, E2)2^+$ γ decay, particularly from the second 2^+ level. By application of the appropriate conversion factor C_ν as given by Eq. (48), the limiting angular distribution for this mixed transition is

$$W(\theta_2) = 1 + (1+\delta^2)^{-1}(0.38 + 1.112\delta - 0.1163\delta^2)P_2(\cos\theta_2)$$
$$- (1+\delta^2)^{-1} \times 0.0979 P_4(\cos\theta_2). \quad (64)$$

As indicated in Fig. 15, this limiting expression yields an elongated ellipse with a narrow range of negative a_4^*
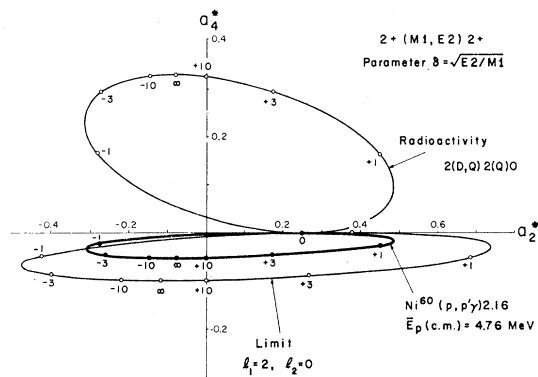
FIG. 15. Theoretical results in δ-ellipse representation of a_4^* vs a_2^* for the $2_2^+ \rightarrow 2_1^+$ γ transition in Ni^{60} following scattering of 4.76-MeV protons. The potential-independent limiting δ ellipse, obtained on the assumption that at low energy the contribution of the $l_1 = 2$ incoming and $l_2 = 0$ outgoing partial waves dominates that of all the other partial wave components, is contrasted with the δ ellipse calculated for the full ensemble of partial waves and that for radioactive decay of the 2.16-MeV second 2^+ level of Ni^{60}.

values. This limiting ellipse should be approached near threshold for an $(n, n'\gamma)$ reaction under the same conditions as has been outlined above for $2^+(E2)0^+$ transitions. By way of contrast, the familiar $2(D, Q)2(Q)0$ ellipse for a $\gamma-\gamma$ angular correlation in radioactivity has a much wider range of $a_4{}^*$ values (positive), together with a slightly reduced range of $a_2{}^*$ values. Because the mixed transition occurs first in this radioactivity decay, the sign of δ measured will be opposite to that determined from an $(N, N'\gamma)$ angular distribution measurement. As is illustrated in Fig. 15 for a typical case in Ni^{60}, the predicted ellipse for a $(p, p'\gamma)$ reaction is substantially smaller than the limit (64). This diminution is mainly caused by the presence of dominating τ terms involving $l_1=1$, $l_2=1$. In the case of inelastic proton scattering, the basic condition for the limit is not fulfilled, i.e., one does not have

$$T_2(E_1)\,T_0{}'(E_2)\gg T_1(E_1)\,T_1{}'(E_2),\ \text{etc.} \quad (65)$$

b. Ground-State Transitions from Spin-3 Levels

A study of the behavior of theoretical $(n, n'\gamma)$ angular patterns for octupole $(3\rightarrow0)$ transitions has revealed some unexpected facets near threshold. First let us consider the rare but interesting case where the first excited state has $J^\pi=3^-$. Near threshold, the two dominating τ terms [Eq. (13)] have $l_1=3$, $l_2=0$, corresponding to f-wave excitation of $\frac{5}{2}^-$ and $\frac{7}{2}^-$ compound states, whose contributions to the overall angular distribution are proportional to $[6+5.143P_2(\cos\ \theta)+0.857P_4(\cos\ \theta)]$ and $[8+7.143P_2(\cos\ \theta)+1.403P_4(\cos\ \theta)-4.545P_6(\cos\ \theta)]$, respectively. In this instance, since the denominators of these τ terms are equal, the sum of their contributions yields a model-independent limit

$$W(\theta_2)=1+0.8776P_2(\cos\ \theta_2)+0.1614P_4(\cos\ \theta_2)$$
$$-0.3247P_6(\cos\ \theta_2), \quad (66)$$

which has an angular asymmetry of 2.37, as indicated in Fig. 16.

Above threshold, the percentage contribution of these $T_3 \cdot T_0{}'$ terms diminishes slowly in a fashion similar to the $T_2 \cdot T_0{}'$ terms shown in Fig. 14 for a $2^+(E2)0^+$ transition. Nevertheless, the predicted behavior of the $3^-(E3)0^+$ asymmetry differs strikingly, for instead of dropping rapidly, it should remain roughly constant (about 2.3 to 2.5) for a substantial range of energies above threshold. In fact, as shown in the inset of Fig. 16, a small initial increase is expected due to the increasing influence of τ terms of the type $T_2 \cdot T_1{}'$ and $T_4 \cdot T_1{}'$, which have angular asymmetries of 2.44 and 2.73, respectively.

The presence of other open exit channels (excepting 0^+ states) will generally cause some minor changes in these predictions. Figure 16 illustrates the effect of open (n, p) channels on the angular asymmetry of the
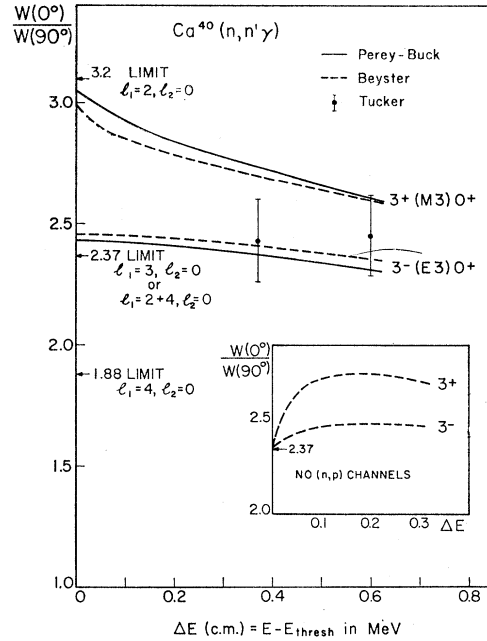
FIG. 16. Plot of the asymmetry for the distribution of de-excitation γ radiation from the second level of Ca^{40} against the energy above threshold of incident neutrons inelastically scattered to the second level. For spin–parity assignments of $3^\pm$ for this level, the theoretical curves evaluated from Perey–Buck and Beyster transmission coefficients are compared with the values derived from the experimental results of Tucker (Refs. 25, 33, 37). Also shown are the potential-independent limiting values of the asymmetry at threshold for different dominant partial-wave combinations. The calculations, which take account of four neutron and four proton exit channels for decay of the compound nucleus, show the transition multipolarity to be $E3$, and the parity of the spin-3 level to be negative. The inset shows the theoretical curves of asymmetry vs energy above threshold when no account is taken of proton decay channels.

3.73-MeV $3^-(E3)0^+$ transition in the Ca^{40} $(n, n'\gamma)$ reaction. For these calculations, we have adopted proton transmission coefficients corresponding to a Woods–Saxon potential with a surface-derivative absorptive term having the same parameters as used previously.[28],[29] These open (n, p) channels go to low-lying negative-parity states in K^{40}, and their inclusion causes the denominator of the $J_1=\frac{7}{2}^-$ τ term to become larger than the $J_1=\frac{5}{2}^-$ τ term. The net result is a slightly increased asymmetry limit, which is no longer model-independent, together with a gradually decreasing asymmetry above threshold (Fig. 16). For the more general case of an $(n, n'\gamma)$ reaction for a 3^- state lying above one or more 2^+ states, the denominator of the $J_1=\frac{5}{2}^-$ τ term will be larger than that of the $\frac{7}{2}^-$ term, causing the limiting asymmetry to be less than 2.37. Nevertheless, the presence of other τ terms with larger asymmetries should still maintain the overall asymmetry for such a 3^- state to a value near 2.5 for a considerable energy range above threshold. Any influence due to fluctuations in level widths on the asymmetry should be relatively unimportant in this instance, since

a large asymmetry will still result even if the relative contributions of such terms are affected.

The calculated behavior of a $3^+(M3)0^+$ angular asymmetry turned out to be surprising near threshold for an $(n, n'\gamma)$ reaction. In this instance, the two τ-terms for outgoing s-wave neutrons involve $l_1=2$ and 4, respectively. At first glance, one expects the $l_1=2$ term to dominate,[32] with an asymmetry limit of 3.2. While this is true in general when there are many open channels, it is not correct if there are no states (except 0^+ states) below the 3^+ level. (Admittedly, this is of no practical interest for even–even nuclei.) For incident energies sufficiently close to threshold to satisfy the condition that T_2, $T_4 \gg T_0'$, these two τ-terms become equally effective, *irrespective of how much the value of T_2 exceeds that of T_4* for the incoming neutrons. In this situation, the $3^+(M3)0^+$ asymmetry limit is also 2.37. However when other channels are open, the $l_1=2$ τ term does dominate, and an asymmetry limit slightly less than 3.2 should result (see the uppermost curves of Fig. 16). The amount of the departure from 3.2 depends on how much these other exit channels contribute to the reaction cross section. It is therefore slightly model-dependent, as illustrated by the small difference in the predicted limits using either Perey–Buck or Beyster neutron T_l values.

The net outcome of this theoretical study is the discovery of an appreciable parity dependence for the angular distributions of $(3\rightarrow0)$ transitions near threshold of an $(n, n'\gamma)$ reaction. It is of interest to compare these predictions with Tucker's recent Ca^{40} $(n, n'\gamma)$ results for $E_n=4.20$ and 4.43 MeV.[25,33] We have extrapolated his forward-angle data $(\theta=30°, 40°)$ to $0°$ in accord with the expected theoretical shape in order to extract values for the angular asymmetry. This procedure seems to be reasonable since his data fit the theoretical shapes very well, as is described at the end of Sec. 8. Although his measurements do not begin as close to threshold as might be desired, they appear to favor the known $3^-(E3)0^+$ assignment for this 3.73-MeV transition in Ca^{40}. If the $(n, n'\gamma)$ angular distributions of ground-state transitions from other spin-3 levels could be measured with comparable accuracy near threshold, it is likely that they could be uniquely identified.

8. EFFECT OF EXTRA CN EXIT CHANNELS

Further physical factors influence markedly the magnitude of the differential cross section, and thus need to be taken into account in comparison of absolute experimental results with theoretical data, even though the distribution *structure* may hardly be affected. Having already dealt with the *increase* in the cross section that ensues upon including higher partial waves in

the reaction channels, we now examine the *decrease* in the cross section that results from taking additional CN decay channels into account. The "two-channel approximation," in which the exit channels are confined solely to those leading to the ground state (elastic channel) and a single excited state (inelastic channel) of the target nucleus, represents an approach which is not meaningful under most experimental conditions. A valid treatment must take into account each of the additional open exit channels by which the CN can decay—this involves simply a modification of the transmission term τ in evaluation of the numerical cross section. The presence of appropriate additional transmission coefficients in the denominator of the τ term occasioned by each extra open decay channel results in a reduction of the overall cross section by an amount which depends upon the channel spin and energy but is of the order of 20% per extra channel. The reduction affects nucleon and γ distributions alike, as is evident from examples in this section and in Sec. 10.

As examples, we have chosen instances of spin sequences that yield distributions characterized by particularly large anisotropy, since these are of especial interest in their own right. It is fortunate that absolute experimental results have recently become available for comparison with theoretical predictions, since a purely structural comparison would be relatively insensitive to the influence of extra decay channels.

To illustrate the quantitative effect upon a *neutron distribution*, measurements taken by Cranberg et al.[34] are especially well suited. Inelastic scattering distributions for 2.5-MeV neutrons on Pb^{206} were measured by the Los Alamos group absolutely for seven low-lying states of the target nucleus. Of this data, the differential cross section for scattering to the first 0^+ level at 1.18-MeV excitation is particularly striking because of the large anisotropy associated with a $0^+\rightarrow J_1\pi_1\rightarrow0^+$ spin sequence. The theoretical distribution also features this pronounced structure, but is in marked quantitative disagreement with experimental absolute cross sections unless adequate provision is made for the many open decay channels of the compound nucleus Pb^{207*}. Use of the two-channel approximation furnishes a theoretical cross section whose magnitude is more than 10-fold that measured experimentally, and even incorporation of all the eight levels (comprising the ground state and seven excited levels) for which data are shown by the authors does not suffice to bring the calculated cross sections down to the observed values. However, when 13 levels lying below an excitation energy of 2.5 MeV are considered (in some instances, by allocating tentative spin assignments) excellent numerical agreement

[33] W. E. Tucker, Ph.D. thesis, University of Texas, 1964 (unpublished).

[34] L. Cranberg, C. D. Zafiratos, J. S. Levin, and T. A. Oliphant, Phys. Rev. Letters **11**, 341 (1963); L. Cranberg, in *Progress in Fast Neutron Physics*, edited by G. C. Phillips, J. B. Marion, and J. R. Risser (University of Chicago Press, Chicago, 1963), p. 89.

ensues on using transmission coefficients derived by the authors from an optical potential of the derivative Woods–Saxon type which had been found to give good fits to elastic and inelastic scattering data for bismuth. These transmission coefficients, which are appreciably lower than corresponding tabulated values[35] for a Perey–Buck or a Bjorklund–Fernbach potential, yield com-

Table II. Computed values of the differential cross section for scattering of 2.5-MeV neutrons to the 1.18-MeV (0^+) level of Pb^{206}.

Potential	l_{max}	No. of exit channels	$d\sigma(0°)$ (mb sr^{-1})	$d\sigma(90°)$ (mb sr^{-1})
Perey–Buck	3	2	184	49
Perey–Buck	4	2	191	50
Cranberg	6	2	89	22
Cranberg	6	8	17	5
Perey–Buck	4	8	31	10
Perey–Buck	2	13	15	7
Perey–Buck	4	13	25	8
Cranberg	6	13[a]	15	4

[a] Also computed by Cranberg *et al.* (Refs. 34, 36), who obtained identically the same results.
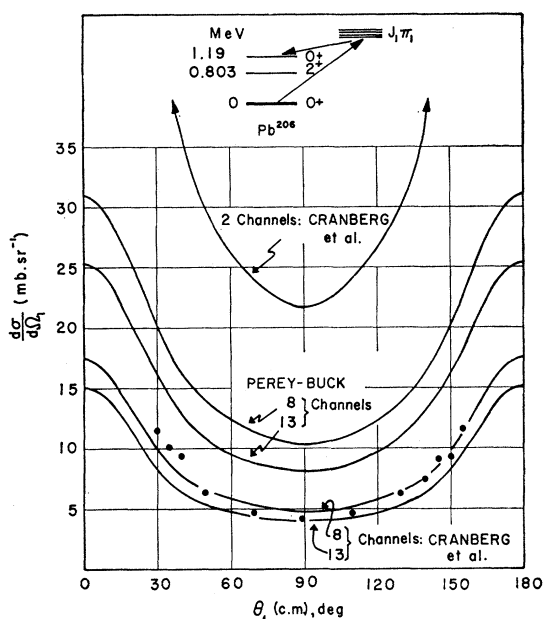

Fig. 17. Comparison of the experimentally determined differential cross sections for scattering of 2.5-MeV neutrons to the second 0^+ level of Pb^{206} (Ref. 34) with theoretical curves evaluated for various numbers of open neutron channels for decay of the compound nucleus. The calculations have been based upon two distinct, but formally similar, optical potentials, namely the nonlocal "global" potential of Perey and Buck, and a local derivative potential of Woods–Saxon type derived by Cranberg *et al.* from analysis of elastic and inelastic neutron distributions at 2.5 MeV on Bi^{209}. The parameters of the equivalent local Perey–Buck potential applicable to this case, namely $V = 47.25$ MeV, $W' = 10$ MeV, $r_0 = 1.25$ F, $a = 0.65$ F, $V_{so} = 8$ MeV, may be compared with those for the potential of Cranberg *et al.* when expressed in the same nomenclature: $V = 41.9$ MeV, $W' = 14.4$ MeV, $r_0 = 1.32$ F, $a = 0.635$ F, $V_{so} = 6$ MeV. The higher transmission coefficients furnished by the potential of Perey and Buck account for the higher differential cross sections derived therefrom. The curve in the two-channel approximation for a Perey–Buck potential dips from 191 mb sr^{-1} at $0°$ to 50 mb sr^{-1} at $90°$, whereas that for the potential of Cranberg *et al.* drops from 89 mb sr^{-1} at $0°$ to the values indicated in the figure (which shows only the lower values for reasons of space). The eight levels employed in the next order of approximation are those which feature in the papers of Cranberg *et al.* (Ref. 34): 0 (0^+), 0.803 (2^+), 1.175 (0^+), 1.341 (3^+), 1.462 (2^+), 1.720 (4^+), 1.762 (2^+), and 1.998 MeV (4^+). The thirteen levels in the highest order are those actually used in the calculations of Cranberg *et al.* (see footnote 36); in addition to the above, they comprise the following levels (with tentative spin assignments): 1.720 (1^+), 2.155 (2^+), 2.20 (2^+), 2.20 (7^-), and 2.384 MeV (6^-). A still closer fit to the experimental points can be achieved when level-width fluctuations are taken into account (Ref. 36).

mensurately lower cross sections, even when the number of partial waves (corresponding to $l \leq 6$) exceeds that ($l \leq 4$) for which Perey–Buck penetrabilities are listed.

Calculations have been effected using not only the transmission coefficients ($T_l^{(\pm)}$ up to $l \leq 6$) and spin assignments of Cranberg *et al.* for 13 decay channels of the compound nucleus,[36] but also for the 8 channels mentioned above, and for simply 2 channels in order to elucidate the effect of open exit channels. The results have in Fig. 17 been compared with those derived using penetrabilities ($T_l^{(\pm)}$ up to $l \leq 4$) for a Perey–Buck nonlocal potential. In all cases the distribution *structure* was found to be essentially the same, but the magnitudes differ markedly with change in the number of channels, as shown in Table II. We add two remarks concerning the above results. Firstly, the computations with the code "MANDY" were throughout in perfect numerical agreement with those obtained from the *correlation* code "BARBARA" (since de-excitation γ radiation from a 0^+ state has an isotropic distribution, the N'–γ correlation is basically the same as the N' distribution, albeit lower by a factor 4π), and with those undertaken by Cranberg *et al.* using a completely independent program. Secondly, additional (as yet unpublished) calculations by Cranberg, Oliphant, and Levin that take level-width fluctuations into account evidently yield a still closer measure of agreement with the experimental data as regards structure and magnitude [the improvement applies not only to the scattering distribution of neutrons to the second (0^+) level, but of those to other levels, especially to the first (2^+) level].

The dependence of theoretical *proton distributions* on the number of open CN channels is essentially similar. For example, consider the theoretical calculations shown in Fig. 18 for the Ni^{58} (p, p') reaction at $E_p = 9.35$ MeV. These were obtained using an optical potential of the

[35] E. H. Auerbach and F. G. J. Perey, Brookhaven National Laboratory Report No. 765 (T-286), July 1962 (unpublished).

[36] We are indebted to T. A. Oliphant of Los Alamos for several private communications on this subject, as also to L. Cranberg for stimulating discussions on the most recent aspects of this work, now being prepared for publication.
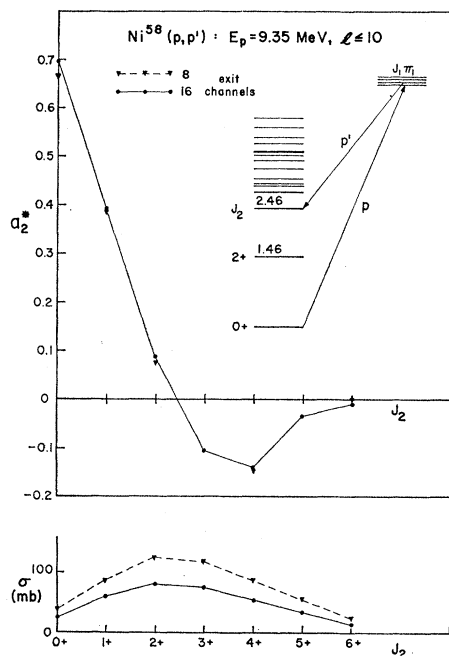
FIG. 18. Systematic variation of the values of $a_2{}^*$ and inelastic cross section with the spin assignment J_2 of the 2.46-MeV level of Ni⁵⁸ populated by scattering of 9.35-MeV protons. The calculations have included the effect of either 8 or 16 exit channels and orbital momenta with $l \leq 10$, and have been based upon an optical potential of the derivative Woods–Saxon type (see text).

derivative Woods–Saxon type:

$$V = -V_0/(e^x+1) + iW'(d/dx')\{1/(e^{x'}+1)\}, \quad (67)$$

where $x = (r-r_0 A^{\frac{1}{3}})/a$ and $x' = (r-r_0'A^{\frac{1}{3}})/a'$. The same parametric choices were made as for earlier comparisons with $(p, p'\gamma)$ cross sections,[28,29] i.e., $V_0 = 52$ MeV, $W' = 44$ MeV, $r_0 = r_0' = 1.25$ F, $a = 0.65$ F, and $a' = 0.47$ F.

Figure 18 shows the predicted $a_2{}^*$ variation of the distribution structure with spin J_2 (2.46-MeV level), taking 16 exit channels (with tentative spin choices) into account. (A similar variation of differential cross sections is shown in Fig. 36, Sec. 12, for the 2.78-MeV level of Ni⁵⁸.) Halving this number of exit channels does not affect appreciably either the structure of these distributions, or the relative cross sections for different spin-value assignments to a particular level. Nevertheless, each calculated (p, p') cross section is increased by roughly 50% with this reduction of exit channels, as illustrated at the bottom of Fig. 18.

Such an effect is not only important for reliable estimates of CN cross sections for inelastic proton channels, but cannot be disregarded in calculations of elastic scattering from a zero-spin target, particularly at back angles where the compound elastic-scattering contribution becomes comparable to the shape elastic cross section. Even for nuclei where reliable spin determinations for most of the low-lying levels are not yet available, it is better to include many exit channels

using reasonable spin choices rather than to omit them entirely. At lower proton bombarding energies (≈ 5 MeV), the number of effective exit channels is considerably reduced, and in the case of a nucleus such as Ni⁵⁸, only levels with excitation energies $\lesssim 3$ MeV need to be considered. The systematic variations of (p, p') distributions and their comparison with experimental data are discussed in Sec. 12.

Already in the previous section, the effect of extra exit channels upon γ *distributions* has been taken into account, and in some of the sections that follow the effect is presented in some detail. Particularly relevant in this connection are the results depicted in Fig. 30, referring to γ transitions in Pb²⁰⁶ following inelastic scattering of 4.1-MeV neutrons, and hence closely related to the above analysis of the Los Alamos data at 2.5 MeV. Since, however, the calculations underlying the distributions in Fig. 30 involved consideration not only of extra decay channels, but also of contributions from unobserved γ cascades (for which the treatment is outlined in Sec. 9), this set of results is relegated to Sec. 11, where results for other lead isotopes are also given, and instead as illustrative examples for this section, the distributions of de-excitation γ radiation following inelastic scattering of 4.20-, 4.43- and 5.00-MeV neutrons on Ca⁴⁰ have been presented. No cascade contributions needed to be taken into account in these cases.

Figure 19 shows the very markedly anisotropic distributions of the γ radiation effecting the ground-state transition from the second level of Ca⁴⁰ (3⁻→0⁺, pure $E3$). The γ-distributions for de-excitation of the 0⁺ first level are, of course, isotropic. The experimental data is that of Tucker,[25,33,37] to which reference has already been made in Sec. 7.2 (see Fig. 16). The calculations that yielded the curves in Fig. 19 differ from those of Tucker in that they solely employed Perey–Buck penetrabilities for the neutron transitions (whereas Tucker used Perey–Buck, Bjorklund–Fernbach, and Beyster penetrabilities, of which the last-named were found to provide the best fits to experimental data, since there was an appreciable progressive decrease in the cross sections furnished by the above sequence of potentials) and included higher partial waves ($l \leq 5$ as against Tucker's limits $l_1 \leq 3$, $l_2 \leq 2$). The proton penetrabilities (up to $l \leq 3$) for the extra CN decay channels to K⁴⁰ were the same as those used by Tucker (derived from "black nucleus" parameters of Feshbach, Shapiro, and Weisskopf[38]). Although Tucker further took account of an extra α-decay channel

[37] I. L. Morgan, J. B. Ashe, R. W. Benjamin, O. M. Hudson, S. C. Mathur, D. O. Nellis, C. V. Parker, and W. E. Tucker, Annual Progress Report, Nuclear Physics Division, Texas Nuclear Corporation, Sept. 1963 and Status Report, June 1964 (unpublished).

[38] H. Feshbach, M. M. Shapiro, and V. F. Weisskopf, New York Operations Office, U. S. Atomic Energy Commission, NYO-3077, 1953 (unpublished).

to the ground state of Ar^{37} in his hand calculations, using penetrabilities derived from the formulae of Feshbach, Shapiro, and Weisskopf, this has been omitted from the present computations because, firstly, the spin assignment is ambiguous; secondly, the code "MANDY" treats spin-$\frac{1}{2}$ particles only; and thirdly, the use of the above penetrabilities is open to criticism in the present case. The large numerical discrepancy between theoretical and experimental absolute cross sections in the two-channel approximation is greatly diminished on inclusion of the additional open neutron and proton decay channels, but nevertheless remains appreciable even when full provision is made (the considerable reduction brought about by the four proton channels is indicated in the 5-MeV data of Fig. 19). Such an overestimate of the inelastic cross section for a low-
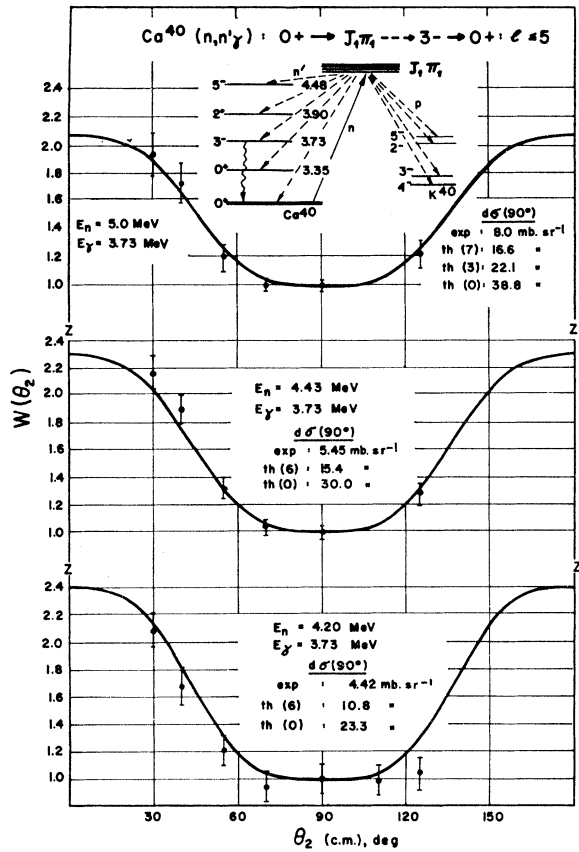
FIG. 19. Angular distribution data of Tucker (Refs. 25, 33, 37) for $E3$ de-excitation γ radiation from the $Ca^{40}(n, n'\gamma)$ reaction at three incident energies, compared with theoretical curves based on Perey–Buck penetrabilities, as in Fig. 16. The absolute cross sections show discrepancies which may be ascribed to level-width fluctuations near threshold. The calculated numerical results are labelled according to the number of *extra* exit channels taken into consideration, so that $th(0)$ denotes the value derived in the two-channel approximation. Even with 7 extra channels at the highest incident energy, theoretical values derived from Perey–Buck penetrabilities appreciably exceed those determined experimentally, but with a Beyster potential the agreement is much closer.
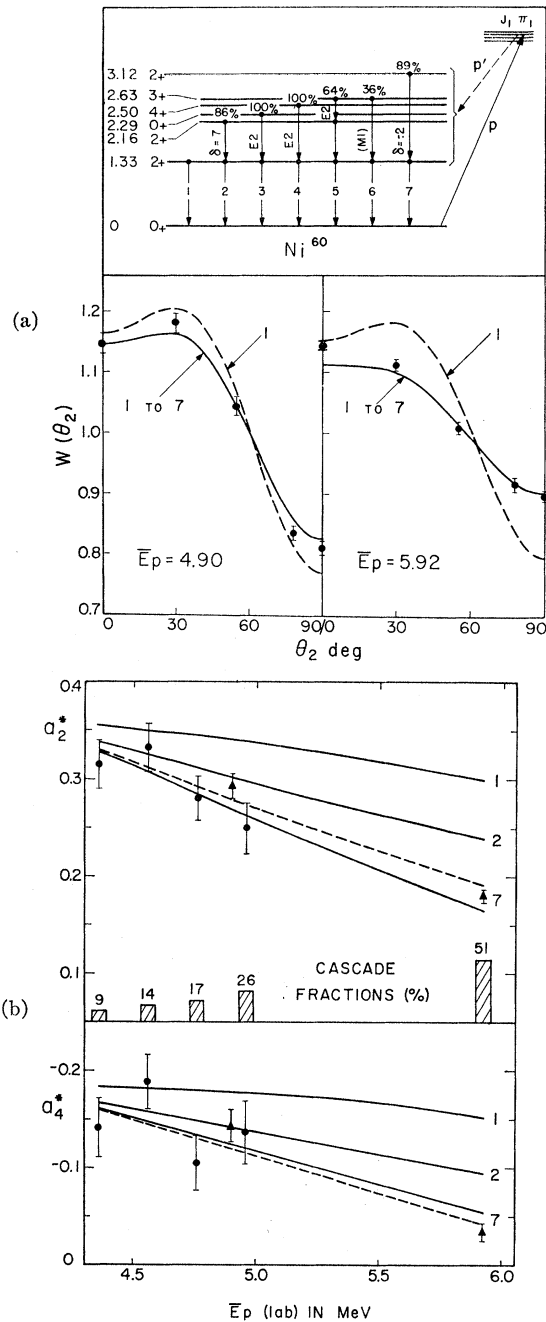
FIG. 20. (a) Experimental angular distributions (Ref. 29) for 1.33-MeV γ radiation from the $Ni^{60}(p, p'\gamma)$ reaction, compared with theoretical predictions for direct excitation [curve (1)], and for the sum of cascade radiations from the first six levels, using the nuclear spectroscopic information listed in the level diagram. (b) A comparison of the same results as in (a), but in more detail, with values of both $a_2{}^*$ and $a_4{}^*$ vs incident proton energy. For the upper two curves in each plot, γ rays from the first one and two levels have been taken into account. For the lower two curves, two different multipolarities have been assumed for the 2.63→1.33-MeV transition: $M1$ (solid line) and $E2$ (dashed line). Experimental data (Refs. 28 and 29) refer to two different targets with thicknesses of 120 keV (circles) and 260 keV (triangles) at $E_p = 5$ MeV.

TABLE III. Theoretical $(p, p'\gamma)$ angular distributions for cascade fractions of 1.33-MeV radiation originating from first six levels of Ni^{60}.

Cascade No.	Level of origin (MeV)	Transition type	$\bar{E}_p = 4.90$ MeV			$\bar{E}_p = 5.92$ MeV		
			$\% \sigma_{in}$	$a_2{}^*$	$a_4{}^*$	$\% \sigma_{in}$	$a_2{}^*$	$a_4{}^*$
(1)	1.33	$2^+(E2)0^+$	74.8	0.340	−0.178	46.2	0.300	−0.152
(2)	2.16	$2^+(M1+E2)2^+(E2)0^+$ $\delta = +0.75$	14.0	0.086	0.058	17.8	0.082	0.056
(3)	2.29	$0^+(E2)2^+(E2)0^+$	4.6	0	0	9.8	0	0
(4)	2.50	$4^+(E2)2^+(E2)0^+$	2.1	0.390	−0.153	4.6	0.366	−0.120
(5)	2.63	$3^+(E2)2^+(M1+E2)2^+(E2)0^+$ $\delta = +0.75$	1.7	−0.035	0.127	4.8	−0.034	0.113
(6)	2.63	$3^+(M1)2^+(E2)0^+$	1.2	−0.386	0.169	3.2	−0.367	0.150
(6a)	2.63	$3^+(M1)2^+$	1.2	−0.270	0	3.2	−0.257	0
(7)	3.12	$2^+(M1+E2)2^+(E2)0^+$ $\delta = +0.2$	0.4	0.167	0.104	3.6	0.167	0.111
	higher levels	not established	···	···	···	6.8	···	···

lying state is typical unless a correction for the effect of level-width fluctuations is included.[1] Only on reducing the number of partial waves and using Beyster penetrabilities is the numerical agreement sufficiently close. The structural fit is, however, very satisfactory in all instances, and illustrates the expected progressive diminution in anisotropy with increasing incident neutron energy (see also Fig. 16).

9. INFLUENCE OF CASCADES FROM HIGHER LEVELS

Cascade radiations from higher levels can exert a pronounced effect on an $(N, N'\gamma)$ angular distribution, particularly in the case of a $2_1{}^+(E2)0_1{}^+$ transition since many of the higher states in medium-weight even nuclei have substantial decays to the first 2^+ state. In most instances, the net effect of the cascading process is usually to diminish the anisotropy of the distribution corresponding to direct excitation of the first 2^+ state. An exception arises where the only cascade originates from a 4^+ state, as in the case of Fe^{56} at neutron bombarding energies between 2.1 and 2.6 MeV. The angular distributions of the two cascade γ rays in the $4^+(E2)2^+$-$(E2)0^+$ cascade process are identical (Sec. 3), and are more anisotropic than that for the direct $2^+(E2)0^+$ transition. Day and Walt[18] assumed isotropy when subtracting such a cascade contribution from their experimental angular distribution for 0.845-MeV γ radiation for the Fe^{56} $(n, n'\gamma)$ reaction at $\bar{E}_n = 2.56$ MeV. This correction affected its anisotropy in the wrong direction (0.08 of the $a_2{}^*$ value), but was of no consequence because of the limited accuracy of their angular distribution measurement.

A clear demonstration of the effect of cascade fractions is possible in the case of recent measurements[28,29] of

angular distributions of 1.33-MeV radiation from the Ni^{60} $(p, p'\gamma)$ reaction for bombarding energies ranging from 4.4 to 6.0 MeV. In the theoretical analysis, the angular distribution for direct excitation of the first 2^+ state as well as for cascade fractions from the next five states have been taken into account, as indicated in Fig. 20(a). Most of the nuclear spectroscopic information shown in the level diagram is now well established,[29] except for the multipolarity of the $2.63{\rightarrow}1.33$-MeV transition, which has been assumed to be $M1$. With this information, theoretical distributions for all seven transitions have been calculated. In order to obtain the final overall result, experimental information for relative (p, p') cross sections has been used, such as has been listed in Table III. As is shown in the lower half of this diagram, the inclusion of these cascade fractions reduces the anisotropy for direct excitation only slightly at $\bar{E}_p = 4.90$ MeV, but quite markedly at $\bar{E}_p = 5.92$ MeV.

This effect of cascades can be examined more closely in the plots of $a_2{}^*$ and $a_4{}^*$ versus proton energy of Fig. 20(b). Over the range covered by these experiments, the percentage of cascades included in the total yield of 1.33-MeV radiation increases from 9 to 51. The expected values for direct excitation of the first level are represented by the uppermost curves, while inclusion of the cascade from the second level causes a substantial reduction in the absolute $a_2{}^*$ and $a_4{}^*$ values. The assumption of $M1$ multipolarity for the $2.63{\rightarrow}1.33$ MeV transition does introduce some uncertainty, since a choice of $E2$ multipolarity for this radiation would alter the overall prediction perceptibly, as shown by the dashed curves. The influence of this transition is unfortunately enhanced because the upper cascade (1.29 MeV) was not resolved from 1.33-MeV radiation in

the scintillator spectrum,[29] and its effect had to be included.

It is evident that the influence of cascade radiations from the first six levels is quite substantial, and that the experimental results are in excellent agreement with these calculations using statistical reaction theory at least up to 6-MeV proton bombarding energy. The data points with smaller error bars were obtained using a thinner target (factor of 2), with consequently less averaging over compound states. The small fluctuations in $a_2{}^*$ and $a_4{}^*$ values (of the order of ± 0.04) could be caused by fluctuations in the density of levels with large $(p, p_1{}')$ reduced widths. Nevertheless, the agreement of these $(p, p'\gamma)$ angular distributions with the assumption of simple compound-nucleus formation is quite striking, once the contributions of cascade radiations have been taken into account.

10. SYSTEMATICS OF ANGULAR DISTRIBUTIONS

A. Introduction

In addition to evaluating numerical distributions for an extensive range of spin combinations encountered in practice, we have undertaken a survey of distribution

TABLE IV. Values of Perey–Buck transmission coefficients used for calculation of the systematics of angular distributions.

l	$T_l^{(-)}$	$T_l^{(+)}$	$T_l^{(-)\prime}$	$T_l^{(+)\prime}$
0	0.9239	0.9239	0.9442	0.9442
1	0.4979	0.5160	0.4400	0.4540
2	0.8925	0.7184	0.7852	0.6431
3	0.0984	0.1638	0.0423	0.0648
4	0.0328	0.0231	0.0092	0.0075

behavior for sequences involving stepwise variation in the various individual spins and parities, without regard to the question of the physical existence of appropriate nuclei. These *Spielrechnungen* shed considerable light on systematic trends in distribution behavior. In order to secure standardization of all input parameters except spins, parities and multipole mixtures, the orbital momenta were confined to $l \leqq 4$ and a single set of Perey–Buck generalized transmission coefficients $T_l^{(\pm)}$ was arbitrarily employed throughout. These are listed in Table IV. In point of fact, these correspond to penetrabilities for scattering of 3-MeV neutrons to the ground state and first level of Fe^{56}. In the calculations the "two-channel approximation" was used. In the case of nucleon distributions 138 different sequences were considered, as against 822 sequences (omitting forbidden $0 \rightarrow 0$ transitions) for γ distributions *without* intermediate unobserved transitions. For instance, the following spin combinations for J_0/J_2 were investigated with permutation of positive and negative parities: $0(1)5/0(1)5$,
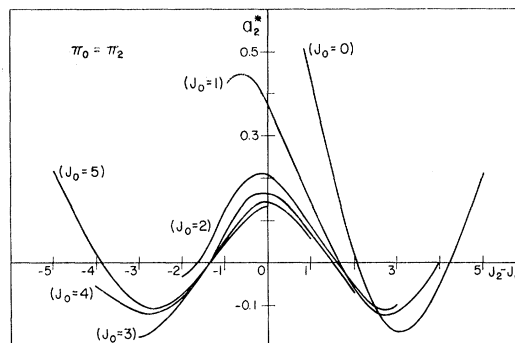
FIG. 21. Systematic variation of $a_2{}^*$ with the spin difference $J_2 - J_0$ for various integer spins J_0 in the case of inelastic nucleon scattering, when there is no change in parity from the initial to the final state ($\pi_0 = \pi_2$, whence $l_1 + l_2 =$ even). The curve for $J_0 = 0$ goes on to intercept the $a_2{}^*$ axis at $a_2{}^* = 0.853$, but this part has been left out for reasons of space. The data indicate that transitions with small angular momentum transfer evince large anisotropy in the nucleon distribution. The parameters underlying the calculation are given in the text.

$\frac{1}{2}(1)\frac{11}{2}/\frac{1}{2}(1)\frac{11}{2}$, wherein for computational reasons, the six cases involving 0^- levels had to be omitted.

B. Nucleon Distributions

A striking uniformity in trend was observed in the inelastic nucleon distributions. This can be rendered evident on plotting $a_2{}^*$ against $\Delta J \equiv J_2 - J_0$, since the distribution structure is essentially dictated by the value of $a_2{}^*$ (the very much smaller terms $a_4{}^*$, $a_6{}^*$, $\cdots$ simply effect a slight modification of the basic structure). Such plots for integer spins are depicted in Figs. 21 and 22 (which distinguish between instances for which the parities π_0 and π_2 are the same, and those in which they differ). The curves display vindication of Wolfenstein's expectation[2,34] that the distribution anisotropy (governed by $a_2{}^*$) should be large when the spins of the particles and of the target in initial and final states are small and the orbital momenta of the bombarding particles are unrestricted to the lowest values. Positive $a_2{}^*$ values represent distributions which dip at
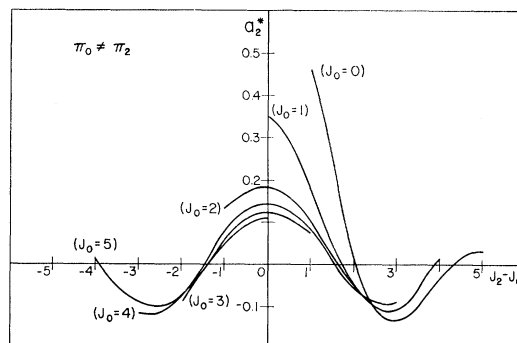
FIG. 22. As Fig. 21, but with a parity change ($\pi_0 \neq \pi_2$, whence $l_1 + l_2 =$ odd).
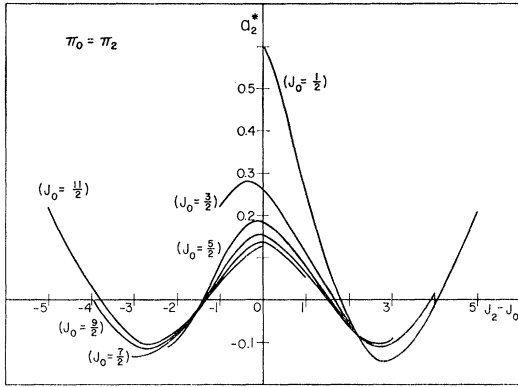
FIG. 23. As Fig. 21, but for half-integer spins, with no parity change.

90°, and negative a_2^* values, distributions which peak at 90°. The over-all trend toward reversal of behavior as ΔJ increases beyond 1 and again beyond 4 is paralleled by the corresponding curves for half-integer spins, Figs. 23 and 24. Isolated exceptions to this tendency occur when the influence of an exceptionally large a_4^* dominates over the a_2^*, as occurs for the sequences $0^+/2^\pm$, $2^+/0^+$, $\frac{1}{2}^+/\frac{5}{2}^+$.

In Fig. 18, the calculated variation of a_2^* with J_2 for inelastic proton distributions (corresponding to the 2.46-MeV level in Ni⁵⁸) has the same general trend for low nuclear spins as the $J_0=0$ curve of Fig. 21. However, the reversal in the sign of a_2^* for $\Delta J=5$ (Figs. 21–24) does not occur. The source of this difference could be the partial-wave cutoff $(l \leqq 4)$ taken for the systematic calculations shown in Figs. 21–24, although the a_2^* value for such a high spin does depend somewhat on the spin choices for other low-lying states. The (p, p') calculations were made using the ABACUS-2 Code[5] with orbital momenta of $l \leqq 10$ included, so that for these the predicted behavior for high nuclear spins should be more reliable. For levels with higher excitations, the magnitude of each a_2^* value diminishes slowly, but the large fore–aft anisotropies for low spins $(J_0=0, 1)$ still persist as a distinguishing feature.

C. Gamma Distributions

Of the ensemble of computed data, using the $T_l^{(\pm)}$ values from Table IV, we concentrate attention upon distributions of dipole and quadrupole γ radiation, represented by well over 1000 sets of results since most of the 822 sequences considered were such as to involve a γ transition of mixed multipolarity L, L'. By setting δ to the arbitrarily large input value 100 (or, better, 1000), the computation furnished separate results for pure $L(\delta=0$, evaluated automatically) and nearly pure L' (δ large) multipole radiation, thus delivering two sets of results per sequence. First we present some

theoretical considerations that have a bearing upon distribution characteristics.

We first consider dipole radiation (pure $M1$ or $E1$). The index ν is restricted to the values 0 and 2, and the distribution takes the form

$$W(\theta_2) = 1 + a_2^* P_2(y) = 1 + a_2^*(\tfrac{3}{2}y^2 - \tfrac{1}{2}), \quad (68)$$

with $y \equiv \cos \theta_2$. On differentiation one sees that the plot of $W(\theta_2)$ vs θ_2 has turning points at 0°, 90°, 180°, with the one at 90° corresponding to a *dip if* $a_2^*>0$ and a *peak if* $a_2^*<0$. Here and throughout, we note that $|a_\nu^*|<1$. The zero values of $P_2(y)$ at $\theta\approx55°$ and 125° cause W to be unity at these angles in this normalized representation. Similarly it follows that

$$a_2^* = W(0°) - 1 = \tfrac{2}{3}[W(0°) - W(90°)]. \quad (69)$$

Analogous considerations apply to quadrupole radiation (pure $M2$ or $E2$), for which ν takes the values 0, 2, 4 and the distribution assumes the form

$$W(\theta_2) = 1 + a_2^* P_2(y) + a_4^* P_4(y)$$
$$= 1 + a_2^*(\tfrac{3}{2}y^2 - \tfrac{1}{2}) + a_4^*(\tfrac{35}{8}y^4 - \tfrac{30}{8}y^2 + \tfrac{3}{8}). \quad (70)$$

Differentiation now indicates the presence of turning points not only at $\theta_2 = 0°$, 90°, 180° but also at the two intermediate angles given by the condition that

$$y \equiv \cos \theta_2 = \pm[(15a_4^* - 6a_2^*)/35a_4^*]^{\frac{1}{2}} \quad (71)$$

be real. This is satisfied (i) for *positive* a_4^* when $a_2^* < \tfrac{5}{2}a_4^*$ (including the entire negative region of a_2^*); (ii) for *negative* a_4^* when a_2^* is positive, or when a_2^* is negative but $|a_2^*| < \tfrac{5}{2}|a_4^*|$. Under these circumstances, subsidiary turning points modify the structure of the distribution (symmetrically about 90°) in a manner which will next be examined. We study the ratio

$$r = \frac{W(0°)}{W(90°)} - 1 = \frac{5a_4^* + 12a_2^*}{3a_4^* - 4a_2^* + 8} \quad (|a_2^*|, |a_4^*|<1).$$
$$(72)$$

Then (i) for *positive* a_4^* this is positive when a_2^* is
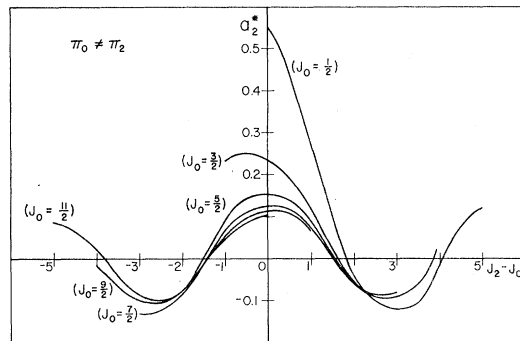
FIG. 24. As Fig. 23, but with a parity change.

positive, or when a_2^* is negative but $|\ a_2^*\ |<\frac{5}{12}\ |\ a_4^*\ |$: for numerically larger negative values of a_2^*, the ratio is negative, indicating that marked peaking occurs at 90°; (ii) for *negative* a_4^* the ratio r is positive for positive a_2^* which have a magnitude exceeding $\frac{5}{12}\ |\ a_4^*\ |$, whereas r is negative for all negative values of a_2^* and for those positive values below $\frac{5}{12}\ |\ a_4^*\ |$. From these results, a schematic of distribution structure from 0° to 180° has been drawn up which shows the changes in appearance as a_2^* is varied (Fig. 25).

In the case of sequences where $|\ a_2^*\ |$ happens to be vanishingly small compared with $|\ a_4^*\ |$ these γ distri-
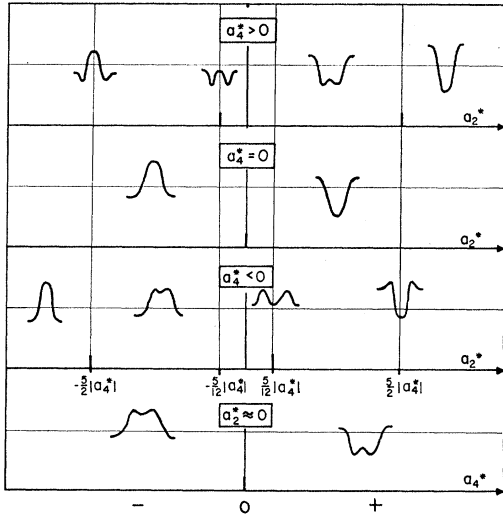
Fig. 25. Symbolic scheme depicting the change in distribution structure with change in a_2^* and a_4^*. Each curve is understood to represent the shape of the distribution from 0° to 180°, as given by the expression $W(\theta)=1+a_2^*\ P_2(\cos\theta)+a_4^*\ P_4(\cos\theta)$. When $a_4^*>0$, the peak at 90° diminishes as a_2^* becomes less negative, until $W(90°)=W(0°)$ at $a_2^*=-(5/12)a_4^*$; for increasing a_2^*, the 90° value lies below that for 0°, and when $a_2^*>\frac{5}{2}a_4^*$ the effect of a_4^* becomes imperceptible. When $a_4^*=0$, the curves are of pure **Λ** or **V** form according as $a_2^*<0$ or $a_2^*>0$. When $a_4^*<0$, the form is pure **Λ** for large negative values of a_2^*, whereas the dip at 90° becomes increasingly pronounced between $a_2^*=-\frac{5}{2}\ |\ a_4^*\ |$ and $a_2^*>0$; the 90° value equals that at 0° when $a_2^*=(5/12)\ |\ a_4^*\ |$, and thereafter falls below the 0° value. In the special case when $a_2^*\approx0$, the distributions take the form **M** or **W** according as $a_4^*<0$ or $a_4^*>0$.

butions take on the forms shown at the bottom of Fig. 25, corresponding to displaced P_4 curves. The normalized distributions have the value unity at the angles 31°, 70°, 120°, and 149° at which $P_4(y)$ vanishes, and have subsidiary maxima or minima at 49° and 131°, the angles at which the value of $[1\mp|\ a_4^*\ |\ P_4(y)]$ peaks or dips, respectively.

These overall predictions have been borne out by scrutiny of the structures of computed γ distributions. Since the basis of these predictions is furnished by values of a_2^* and a_4^* but not by the basic data, namely nuclear spins and γ multipolarities, their relevance to γ distribution systematics is only indirect. In an attempt
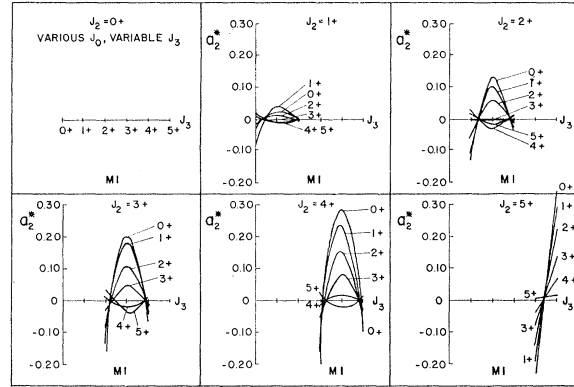
Fig. 26. Systematics of γ distributions. The curves show plots of a_2^* vs J_3 for $M1$ radiation in the transition sequence

$$J_0\longrightarrow J_1---\to J_2\underset{M1}{\longrightarrow}J_3.$$

In each case a set of curves for different values of J_0 is collated for a given value of J_2.

to link the a_2^* values systematically to spin sequences and multipolarities, the set of *Spielrechnung* computations embodying permutation of commonly-encountered nuclear spins was undertaken. The results are conveniently expressed in graphical form: we here confine ourselves to data for a_2^*, presented in Figs. 26–29, whereas systematic results for a_4^* are given in Table V.

Within the diversity of data, some overall features are apparent which may be regarded to have universal validity. The variation in values of a_2^*, and thus essentially of the distribution structure, for different nuclear spins depends sensitively upon the multipole order L (and hence upon $|\ J_2-J_3\ |$) but not markedly upon the multipole character (E or M) of the radiation effecting the observed transition (compare Figs. 26 and
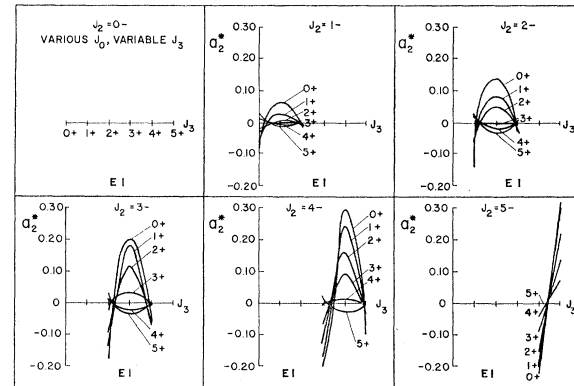
Fig. 27. As Fig. 26, but for $E1$ radiation effecting the observed transition $J_2\to J_3$. The distribution systematics are practically uninfluenced by the multipole character of the dipole radiation (M or E). A very similar systematic trend applies in the case of a transition sequence involving half-integer spins (results are not shown for reasons of space).
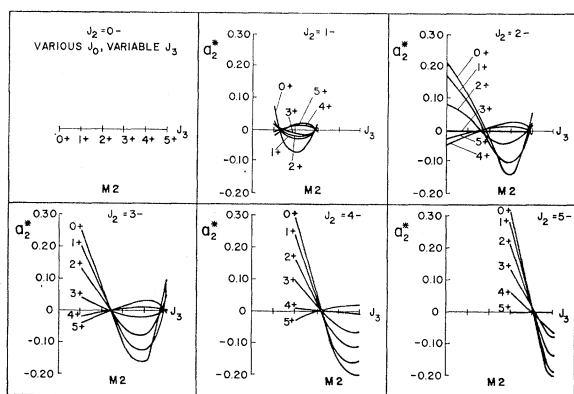
FIG. 28. As Fig. 26, but for $M2$ radiation. The systematic trend for quadrupole radiation may be seen to differ from that for dipole. Results for a half-integer spin sequence show the same behavior as those depicted here for an integer spin sequence.

27). In other words, the parities of the nuclear levels do not play a decisive role in determining the form of the distribution. This observation is significant in view of the fact that the momentum combinations l_1, l_2 are governed by the relative parity π_0/π_2. The result may, however, stem from choice of a set of transmission coefficients associated with a nucleus in the neighborhood of the s-wave neutron resonance of the optical model.

Another clearly apparent feature in each of Figs. 26–29 is the decrease in variation of the a_ν^* as the target spin J_0 becomes larger; in other words, the distributions have larger amplitude and are more acutely influenced by the residual nuclear spins J_2 and J_3 when the initial spin J_0 is low, as has long been known. In this sense, J_0 exerts a more crucial influence upon distribution structure than do J_2 or J_3.

We begin by discussing the results for *dipole radiation*. No disparity was found between the influences of J_2 and J_3 upon the form of the γ distribution. Furthermore, the a_2^* are in all cases numerically largest when $J_2 = J_3$.
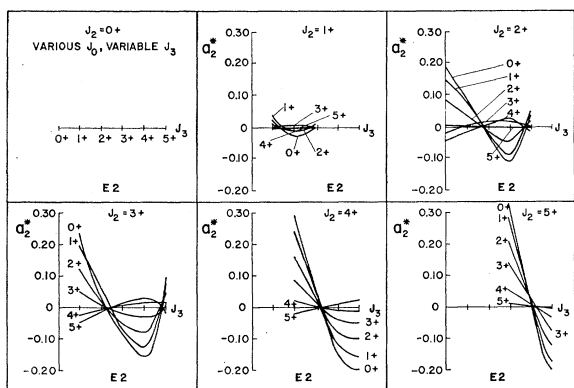
FIG. 29. As Fig. 28, but for $E2$ radiation. The similarity to the trends shown in Fig. 28 is evident. It exists also in the corresponding curves for a half-integer spin sequence.

and smallest when $| J_3 - J_2 | = 1$. It was found that a_2^* is predominantly negative when $| J_3 - J_2 | = 1 = L$ (distributions peak at 90°) and positive when $J_3 - J_2 = 0 = L - 1$ (distributions dip). To this rule of systematics, only the curves for large numerical values of $J_0 (\gtrsim 4)$ appear to constitute an exception—and this may be a specious deviation resulting from too low a limit upon the partial waves taken into consideration $(l \leq 4)$ when high nuclear spins are involved.

The character of the a_2^* curves for *quadrupole radiation*, Figs. 28 and 29, is altogether different from the preceding, and of rather more complicated structure. As a general rule applicable to quadrupole transitions when the spin of the final nuclear state is not too small $(J_3 \gtrsim \frac{3}{2})$, it was found that a_2^* tends to vanish for $J_2 = J_3 - 2$ and $J_2 = J_3 + 1$, and to reach a local maximum between $J_2 = J_3$ and $J_2 = J_3 - 1$. The over-all systematic features can be expressed in tabular form (Table V) listing the predominant sign of the a_ν^* and

TABLE V. a_ν^* characteristics and distributional structure for quadrupole radiation, in terms of the spin difference of transition levels.

$J_3 - J_2$	a_2^*	a_4^*	Form
-2	$+$ (large)	$-$	V
-1	$+$	$+$ (large)	W
0	$-$ (large)	$-$ (large)	M or Λ
$+1$	$-$ (large)	$+$ (small)	Λ
$+2$	$+$	$-$ (vanishing)	V

the resultant distribution structure (expressed in a self-evident symbolic form: Λ, M, W, V, corresponding to the distribution curves shown in Fig. 25).

11. ANALYSIS OF EXPERIMENTAL γ DISTRIBUTIONS FOR HEAVY NUCLEI

We here confine attention to a portion of the extensive set of measurements undertaken by the Texas group under I. L. Morgan, who determined γ distributions over a wide range of angles for $(n, G\gamma)$ processes on nuclei ranging from those of low mass[25] (C^{12}, N^{14}, O^{16}) and medium mass (see Refs. 24, 25, 33, 39–41) (Mg^{24}, Al^{27}, Si^{29}, Ca^{40}, Fe^{56}) to the heavy nuclei[25,37,42] $Pb^{206,207,208}$ and Bi^{209}. Absolute γ-distributions from inelastic scattering of 4.1- and 2.5-MeV neutrons on these latter heavy nuclei form the subject of analysis in this section, since they involve a large variety of spin sequences, satisfy the requirements of the statistical

[39] R. W. Benjamin, D. O. Nellis, and I. L. Morgan, Bull. Am. Phys. Soc. **8**, 478 (1963).

[40] R. W. Benjamin, D. O. Nellis, I. L. Morgan, and W. E. Tucker, Bull. Am. Phys. Soc. **9**, 153 (1964).

[41] I. L. Morgan, Bull. Am. Phys. Soc. **9**, 154 (1964).

[42] D. O. Nellis, I. L. Morgan, and R. W. Benjamin, Bull. Am. Phys. Soc. **8**, 478 (1963).

continuum assumption, and up to the present have only in part been compared with theoretical predictions.[43–49] The application of theory not only illustrates several of the facets covered in preceding sections and raises fresh points of interest, but in the case of Pb^{206} complements the discussion of inelastic neutron distributions presented in Sec. 8.

In each instance, we have employed the maximum number of partial waves for which Perey–Buck transmission coefficients $T_l^{(\pm)}$ have been listed ($l \leq 5$), and taken account of extra exit channels to states of known (or assigned) spin, of γ-cascade contributions and of mixed multipolarity in observed and unobserved γ transitions. The results are depicted in a representation similar to that adopted by the Texas group, who normalized all data to unity at $\theta_2 = 90°$ and cited numerical cross sections separately. We have used this normalization here (even though it can adversely affect the extent of over-all agreement if the point for 90° appears to be either flagrantly high or low with regard to the distribution of the remaining points) simply because the experimenters gave particular attention to the 90° measurement and because the present results can thereby more easily be compared directly with the original data (see also Ref. 50). The theoretical curves have been labeled according to the number of exit channels taken into consideration extra to those of the "two-channel approximation" and the number of cascades of given multipolarity whose contribution was added to the cross section for the observed transition. Since in the case of γ radiation in cascade transitions of

mixed multipolarity no information was available about the mixing ratios, separate cases had to be considered in each instance; the respective transitions were treated as if of pure magnetic or pure electric multipole character. The numerical result in either case was almost the same[50] at 90°, but the structure depended markedly upon the multipolarity. The 90° differential cross section was then derived by adding all the contributions from *pure* cascade transitions (irrespective of multipole character) to those from *mixed* transitions taken as of pure magnetic multipolarity (Cascade case M) or of pure electric multipolarity (Cascade case E) throughout. Hence, e.g., for the four cascades $E2$, $M1/E2$, $M1/E2$, $E1$ added to the observed $E2$ decay of the first excited state of Pb^{206} we depict the cross section for the combination $E2$, $M1$, $M1$, $E1$ as 4CaM and for the combination $E2$, $E2$, $E2$, $E1$ as 4CaE. In absence of detailed knowledge concerning the individual cascade fractions, the respective contributions have been summed directly without introducing the weighting factors employed in Sec. 9.

Results for Pb^{206} at $E_n = 4.1$ MeV are shown in Fig. 30, the upper portion of which refers to the decay of the first excited state and the lower portion to the $3^+ \rightarrow 2^+$ transition from the third to the first level. In both instances, not only the experimental magnitude but also the distribution amplitude exceed the theoretical values. The specious numerical agreement in the two-channel approximation is lost as soon as extra exit channels are taken into account, and only up to a point redeemed by the inclusion of cascade contributions. The situation is complicated by the fact that only 10 of the 18 extra levels shown in the level scheme in Fig. 30 have been observed by nuclear bombardment (these are depicted as full lines, whereas the others are shown dashed). This results in an ambiguity not only as to the number of extra channels which should be taken into consideration, but also as to the inclusion or exclusion of cascade contributions to the $3^+ \rightarrow 2^+$ differential cross section (energy-level compilations[51] show two cascades, depicted as dashed vertical lines in Fig. 30, from 4^+ states feeding the 3^+ level). Under the circumstances, results of computations for both of these possibilities have been given. It is more likely, though, that the results for 18 extra channels and 2 cascades represent the more meaningful choice of the two alternatives. In either case, the $M1$ component is preponderant in the observed transition.

The same procedure has been adopted in the case of the ground-state transition shown in the upper part of Fig. 30, where all four cascades, depicted as solid

[43] Beyster penetrabilities (Refs. 44, 45) for $l_1 \leq 4$, $l_2 \leq 3$ have been used by Nellis (Ref. 37 and private communication) to derive theoretical distribution curves for the $2^+ \rightarrow 0^+$ γ transition in Pb^{206}, using emended Hosoe–Suzuki formulae (Refs. 47, 48) and for the $3^- \rightarrow 0^+$ γ transition in Pb^{208}, using hand-calculated expressions (Ref. 37) which check against those furnished by the code "MANDY."

[44] R. G. Schrandt, J. R. Beyster, M. Walt, and E. W. Salmi, Los Alamos Report LA-2099 (1957) (unpublished).

[45] For a discussion concerning the present status of the transmission coefficients tabulated by R. G. Schrandt, J. R. Beyster, M. Walt, and E. W. Salmi (Ref. 44), see the comments of R. B. Day in Ref. 46.

[46] R. B. Day, in *Progress in Fast Neutron Physics*, edited by G. C. Phillips, J. B. Marion, and J. R. Risser (University of Chicago Press, Chicago, 1963), pp. 111 and 268.

[47] In the appendix to the paper of M. Hosoe and S. Suzuki (Ref. 48), the last three curly brackets of Eq. (8) should read, respectively, $\{3+1.714P_2(\cos\theta)\}$, $\{4-0.7143P_2(\cos\theta)\}$, $\{6+0.8571P_4(\cos\theta)\}$, and the second curly bracket of Eq. (9) should read $\{6+1.6837P_2(\cos\theta)\}$. The expression for the γ distribution given in the appendix to the paper of F. D. Seward (Ref. 49) has an error in the penultimate bracket, which should read $(10+4.762P_2-2.857P_4)$.

[48] M. Hosoe and S. Suzuki, J. Phys. Soc. Japan **14**, 699 (1959).

[49] F. D. Seward, Phys. Rev. **114**, 514 (1959).

[50] The differential cross section at 90° is given by the expression $d\sigma(90°) = a_0 - (1/2)a_2 + (3/8)a_4 - (5/16)a_6 + (35/128)a_8 - \cdots$, in which the δ-independent term a_0 is numerically predominant. Hence the influence of δ through the higher-order terms a_2, a_4, $\cdots$ is slight. We have already drawn attention to the vanishing of the δ-dependence at 55° and 125° when terms higher than a_0 and a_2 are vanishingly small. In the general case, the influence of the mixing ratio δ is most perceptible at 0°, where $d\sigma(0°) = \Sigma_\nu a_\nu$.

[51] K. Way, N. B. Gove, C. L. McGinnis, and R. Nakasima, in *Energy Levels of Nuclei* (Springer-Verlag, Berlin, 1961), Group I, Vol. 1 of Landolt-Börnstein, *Nuclear Physics and Technology*, New Series. See also, *Nuclear Data Sheets*, compiled by the Nuclear Data Group, under K. Way, at the Oak Ridge National Laboratory.
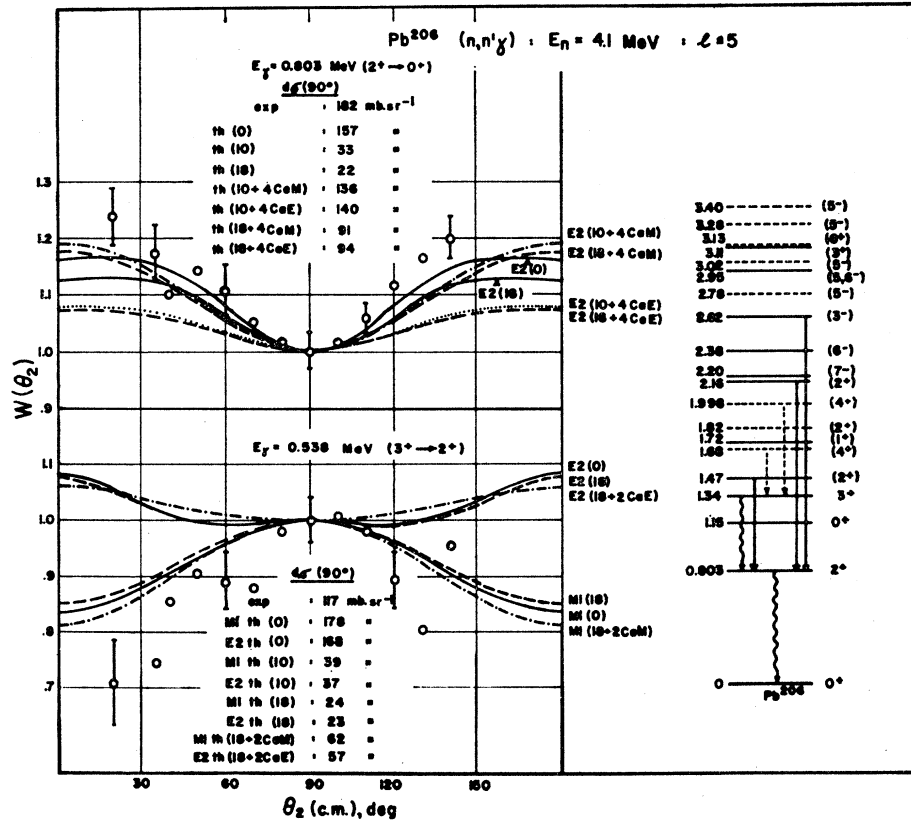
FIG. 30. Comparison of the experimental data of Morgan *et al.* (Refs. 25, 37, 42) with theoretical curves for two γ distributions following inelastic scattering of 4.1-MeV neutrons on Pb[206]. The theoretical functions have been calculated with Perey–Buck transmission coefficients $T_l^{(\pm)}$ up to $l_{max}=5$. The nomenclature and the level scheme (which differs very slightly from that adopted for Fig. 17, with which the present results should be compared) are explained in the text. The rather poor structural and numerical agreement may be a result of insufficient consideration of cascade contributions to the cross section for the observed radiation or, in the case of the 0.538-MeV $3^+\to2^+$ transition, to a consideration of pure radiation only, rather than an $M1+E2$ mixture with $0>\delta\gtrsim-0.5$.

vertical lines, stem from levels observed in nuclear bombardment.

The unacceptably poor agreement between theory and experiment can most likely be ascribed to inadequate recognition of additional cascade contributions, whose influence upon the magnitude and structure of the distributions would suffice to reduce the discrepancies very appreciably. Only those cascade contributions involving a single unobserved γ transition have been included in our calculations.

Note added in proof. On the other hand, some improvement in fit would, as in the cases to follow, result for the 0.538-MeV $(3^+\to2^+)$ γ distribution on admitting an $E2$ admixture with $0>\delta\gtrsim-0.5$ to the observed preponderantly $M1$ radiation.

We next discuss each of the results for Pb[207] at $E_n=4.1$ MeV, shown in Figs. 31 and 32. The experimental data in the upper part of Fig. 31 are distributed too discontinuously for any conclusion to be drawn as regards the multipole mixture from a comparison with the theoretical curves. Even though a *structural* comparison is precluded, the right numerical magnitudes are obtained when three extra exit channels are taken into account. The ground-state transition treated in the lower part of Fig. 31 has a more regular distribution, which in form and magnitude is well fitted by theoretical curves for predominantly $M1$ radiation when three extra exit channels are included in the calculation. The best fit

ensues when the de-excitation radiation is taken to contain a 25% admixture of $E2$ multipolarity $(\delta=-0.5)$. This is evident in the figure, and so is the fact that distribution curves for pure multipolarity do not represent bounds between which those for mixed multipolarity must invariably lie. In this instance, the $\delta=-0.5$ curve would roughly represent a lower bound, and a $\delta=+1.7$ curve an upper bound, as is explained later. If account is taken of a γ cascade from the $\frac{7}{2}^-$ level (pure $E2$ multipolarity), the structural agreement remains excellent, the best fit being attained with $\delta=0$ rather than $\delta=-0.5$ for the observed transition. The cascade, however, contributes a large cross section, which somewhat impairs the numerical agreement.

For the nucleus Pb[207] at $E_n=4.1$ MeV, the Texas group also measured the angular distribution of 2.64-MeV γ radiation which they tentatively attributed to de-excitation of a level at 2.635 MeV of unknown spin–parity recently observed by Cranberg[52] in the course of inelastic neutron scattering investigations. A least-squares-fit analysis to establish the values of the normalized Legendre weighting coefficients a_ν^* appropriate to this distribution gave the result $a_2^*=+0.188$, $a_4^*=-0.009$. The small value of a_4^* led the authors to suggest a dipole assignment to the radiation and thence a spin assignment of $\frac{3}{2}^\pm$ to the 2.635-MeV level. Of

---

[52] L. Cranberg (private communication).

these two possibilities, the present more detailed analysis rules out the spin $\frac{3}{2}^+$, and in its stead suggests the further alternatives $\frac{5}{2}^\pm$. A set of computations has been carried out with J_2 set to $\frac{3}{2}^\pm$, $\frac{5}{2}^\pm$, $\frac{7}{2}^\pm$, noting that the anisotropy of the observed distribution eliminates a $\frac{1}{2}^\pm$ spin assignment. Four extra exit channels were taken into consideration, leading to levels of Pb^{207} shown in Fig. 31, and the values of a_2^* and a_4^* so determined were compared with those established empirically. To this end, it was necessary to allow for multipole mixing in the case of $\frac{3}{2}^-$, $\frac{5}{2}^+$, and $\frac{7}{2}^-$ assignments and to plot the results in a form amenable to comparison with the experimental values. The δ ellipse representation which, in general, would be well suited to this purpose is in the present case precluded by the fact that the loci of points for different values of δ in δ-dependent distributions lie along straight lines of mutually differing slope in a plot of a_4^* vs a_2^*, and not

FIG. 31. Preliminary measurements by the Texas group of two γ-distributions following inelastic scattering of 4.1-MeV neutrons on Pb^{207}, compared with theoretical predictions based on Perey–Buck penetrabilities for $l \leqq 5$.

along ellipses. The extremum values of δ characterizing the ends of each of the lines can readily be derived from a knowledge of the multipole terms $M(L_2L_2)$, $M(L_2L_2')$, $M(L_2'L_2')$ [see Eq. (26)]. When the a_2^* for a given value of δ (for instance, $\delta=0$) is known, that for any other value of δ can be generated[53] from the expression

$$a_2^*(\delta) = a_2^*(0)[M(L_2L_2)+2\delta M(L_2L_2')+\delta^2 M(L_2'L_2')]$$
$$\times[(1+\delta^2)M(L_2L_2)]^{-1}. \quad (73)$$

In order that $a_2^*(\delta)$ be an extremum, its derivative with respect to δ must vanish. This provides the condition

$$\delta^2[M(L_2L_2')]-\delta[M(L_2'L_2')-M(L_2L_2)]$$
$$-M(L_2L_2')=0, \quad (74)$$
whence

$$\delta_{\lim} = \{M(L_2'L_2')-M(L_2L_2)\pm[M^2(L_2'L_2')$$
$$-2M(L_2L_2)M(L_2'L_2')+M^2(L_2L_2)$$
$$+4M^2(L_2L_2')]^{\frac{1}{2}}\}/[2M(L_2L_2')]. \quad (75)$$

Substitution of the numerical values of the M terms as listed in the computer output furnishes the limiting δ values. (E.g., the values $\delta=-0.577$ and $\delta=+1.732$ in the case of $M1+E2$ radiation effecting a $\frac{3}{2}^-\to\frac{1}{2}^-$ transition, already cited in connection with the lower part of Fig. 31. For $M2+E3$ radiation effecting a $\frac{5}{2}^+\to\frac{1}{2}^-$ transition, the limiting δ values are -0.707 and $+1.414$, and for $M3+E4$ radiation in the case of a $\frac{7}{2}^-\to\frac{1}{2}^-$ transition the limiting δ values are -0.775 and $+1.291$.) Thence the extremum values of a_2^* can easily be determined and bounds to the straight lines in the a_4^* vs a_2^* representation established.

Accordingly, the alternative representation of $|\delta|$ vs a_2^* was adopted for comparison with the experimental value; this is shown at the top of Fig. 32. Since calculations showed that for each of the possible spin assignments the value of a_4^* is so small compared with a_2^* that its influence upon the distribution structure is negligible, it suffices to compare the a_2^* values alone. Fig. 32 clearly indicates that a spin $\frac{3}{2}^+$ assignment is unacceptable, but that the data are compatible with the assignments $\frac{3}{2}^-$ (for $M1+E2$ mixed radiation with $\delta=\delta_{\lim}=+1.732$), $\frac{5}{2}^-$ (pure $E2$), or $\frac{5}{2}^+$ (for $M2+E3$ radiation with $\delta\approx0$ or $\delta\simeq-2.4$). For each of these possibilities, it was confirmed that not only the distribution structure, but also the absolute magnitudes agree well with the experimental data. A reduction of the error limits in the latter would assist in discriminating between the remaining alternatives.

In Fig. 33 are depicted results for the ground-state transition from the first level (3^-) of Pb^{208} at various incident neutron energies, when account is taken of
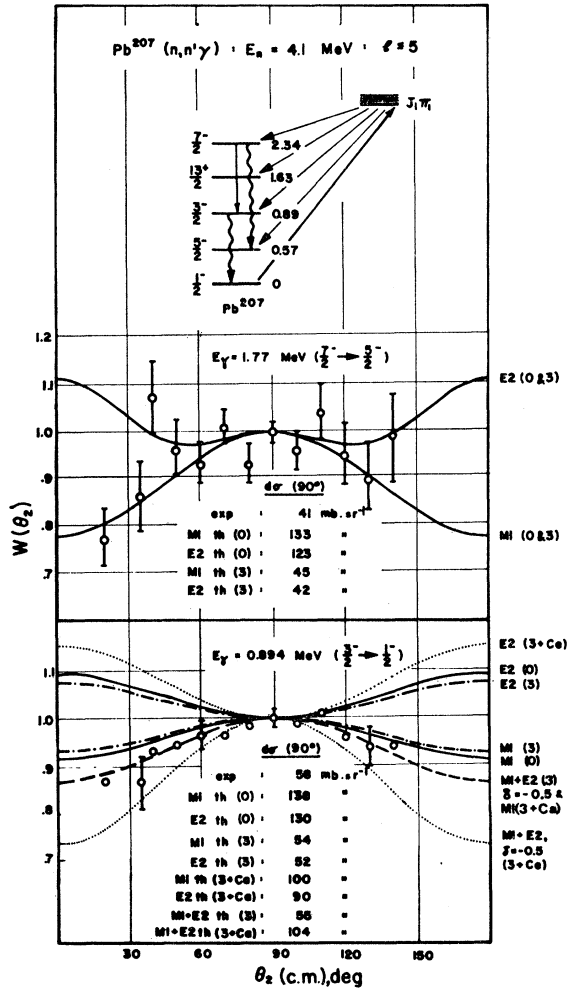
[53] For generating the $a_\nu^*(\delta)$ in general, it may be better to commence from those for $\delta=1$ or $\delta=\infty$ (pure L_2' radiation), since the range of ν for pure L_2 radiation may be lower than for L_2'.
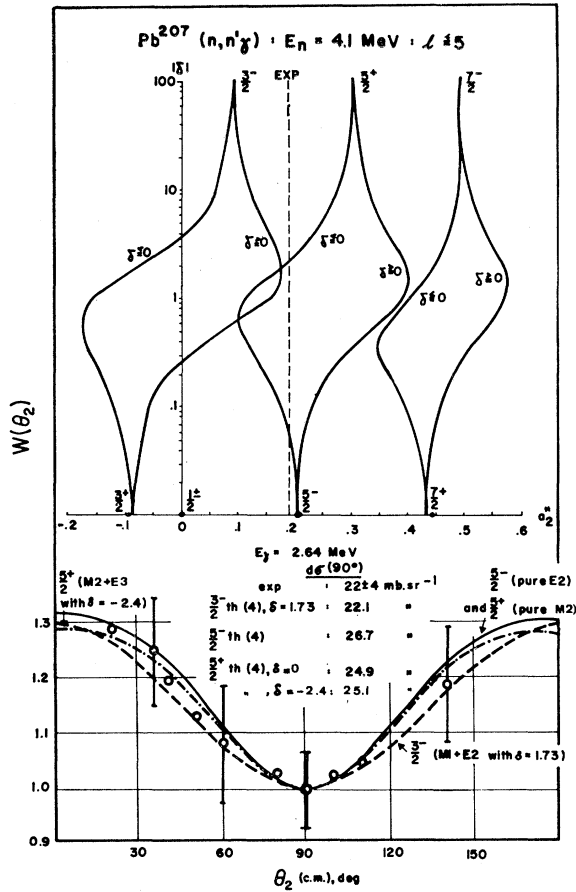
FIG. 32. Experimental distribution of a 2.64-MeV γ-ray transition observed by the Texas group and ascribed to de-excitation of a level at 2.635 MeV recently detected by Cranberg (Ref. 52), compared with theoretical predictions for various assignments of spin and parity for this level. The experimental data are commensurate with the possible assignments $\frac{3}{2}^{-}(M1+E2)$ radiation with $\delta=+1.73$, $\frac{5}{2}^{-}$(pure $E2$ radiation), or $\frac{5}{2}^{+}(M2+E3)$ radiation with $\delta\approx0$ or $\delta\cong-2.4$).

several extra exit channels and cascade contributions. As expected, the agreement in magnitude and structure improves with increasing energy (threshold effects clearly persist at 3 MeV), and at the highest energy may be regarded as satisfactory. Although only three cascade transitions to the 3^{-} level are shown in Nuclear Data Sheets,[51] the 1.36-MeV γ transition observed by Nellis[25,42] has tentatively been ascribed to γ decay from the 3.961-MeV (6^{-}) state to the 3^{-} level at 2.615 MeV, and its contribution to the de-excitation cross section of the 3^{-} state was therefore included in the calculation —it is in any case very small compared with the other three cascade contributions. Independent calculations by Nellis[54] using Beyster penetrabilities up to $l_{1}\leq4$, $l_{2}\leq3$ have yielded good fits to the distribution structure as well as good numerical agreement with the experimental results. At $E_{n}=4.1$ MeV, the value of $d\sigma(90°)$

[54] D. O. Nellis and I. L. Morgan (private communication).

was 84 mb sr^{-1} on considering only three extra exit channels (up to the 3.709-MeV level) and two cascades (from the 3.198-MeV and the 3.475-MeV levels), of which the second was taken to be of pure $M1$ multipolarity. At $E_{n}=3.5$ MeV, Nellis obtained the result $d\sigma(90°)=60$ mb sr^{-1} on including two extra channels (to the 3.198- and the 3.475-MeV levels) and one cascade (from the 3.198-MeV level), whereas at $E_{n}=3.0$ MeV, the cross section was determined as $d\sigma(90°)=34$ mb sr^{-1} on the basis of the two-channel approximation, which is valid in this latter case. The use of fewer partial waves and of Beyster penetrabilities is responsible for the cross sections being lower throughout than those given in the present paper, and hence in better agreement with the values established experimentally.

The data shown in Fig. 34 for two γ transitions going to the 3^{-} first level of Pb^{208} following inelastic scattering of 4.1-MeV neutrons represent preliminary measurements, which have rather large error limits. For this reason, it is not possible to elucidate the multipole character of the radiation from the data shown in the upper part of Fig. 34, and there is a discrepancy be-
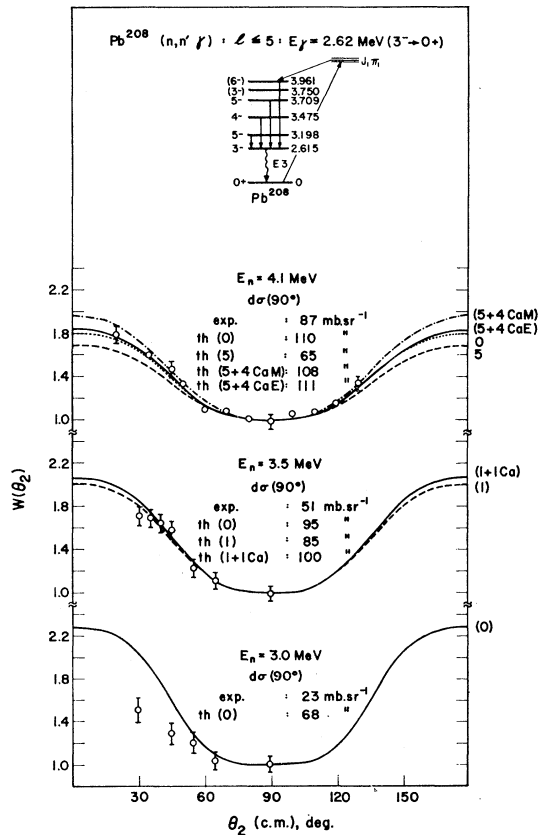
FIG. 33. Experimental and theoretical data for the ground-state decay of the first level (3^{-}) of Pb^{208}, excited by inelastic scattering of 3-, 3.5-, and 4.1-MeV neutrons. With increasing energy the degree of agreement improves, which could be an indication that threshold fluctuation effects are playing an ever diminishing role.

tween the rather small experimental cross section and those calculated theoretically. Since measurements of the K-conversion coefficient α_K yield a value consistent with $M1$ or $E3$ multipolarity, we infer that the $M1$ curve is more likely to apply to this situation.

The set of results in the lower part of Fig. 34 is not symmetrical about 90° and hence cannot be fitted adequately by any theoretical curve, but the numerical cross section at 90° agrees well with the calculated values when three cascades are taken into consideration. The cascades shown as dashed vertical lines in Fig. 34 have been taken over nuclear level schemes,[51] whereas those shown as full vertical lines correspond with those observed by Nellis et al.[37]

The results for the $\frac{13}{2}^+\rightarrow\frac{9}{2}^-$ γ transition in Bi^{209} at the two incident neutron energies $E_n = 2.55$ MeV and $E_n = 4.1$ MeV shown in Fig. 35 illustrate the almost isotropic distribution for a transition which takes place between levels of high spin (the vertical scale in the distribution function is therefore very extended). A noteworthy feature of the distributions is the fact that the structure for an $E3$ transition is practically the same as that for an $M2$ (both dip at 90° and have
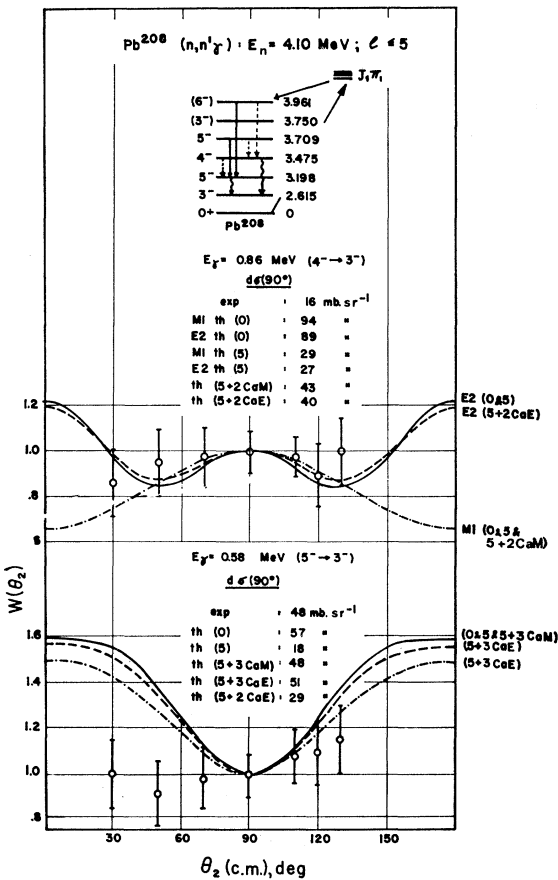
Fig. 34. Theoretical and preliminary experimental results for the Pb^{208} $(n, n'\gamma)$ reaction at $E_n = 4.1$ MeV, including the effect of extra exit channels and cascade contributions.
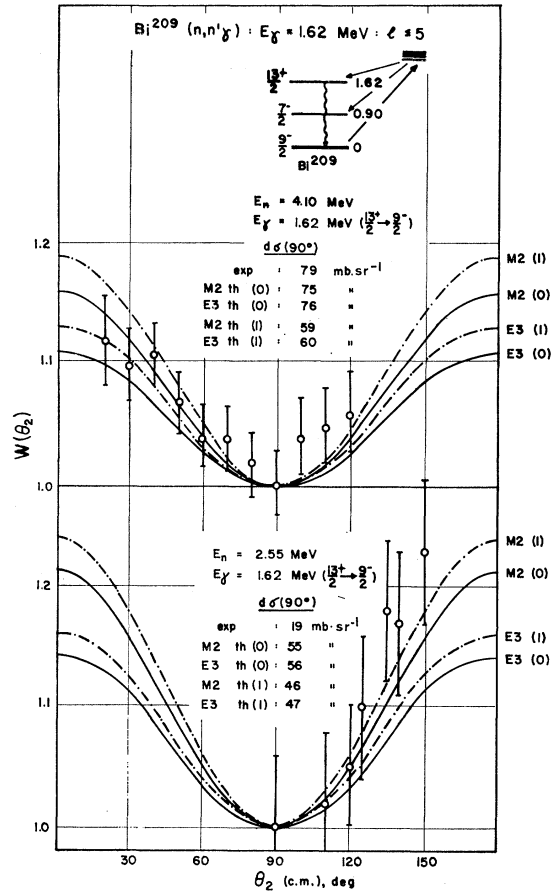
Fig. 35. Data for the 1.62-MeV γ-ray distribution in the transition $13/2^+\rightarrow9/2^-$ in Bi^{209}, initiated by inelastic neutron scattering at $E_n = 2.55$ MeV and $E_n = 4.1$ MeV. The distribution between levels of such high nuclear spin is almost isotropic, for which reason the vertical scale has been exaggerated.

roughly the same small amplitude), unlike results for other spin sequences, which displayed the tendency for curves of opposite multipole character to be roughly mutual inversions of one another. Comparatively little is known of the level scheme of Bi^{209}, and hence the calculations could take only one extra channel into account, namely that to the intermediate $\frac{7}{2}^-$ level at 0.90 MeV. The numerical agreement can accordingly be classed as but fair (at the lower energy, threshold effects play a decisive role), yet the structural agreement is good. Because of the special characteristics of the distribution functions, no conclusion as regards the multipole mixing in the observed radiation could be drawn. It might be mentioned in conclusion that the evaluation of the distribution for a high-spin sequence such as the above was made possible only through the existence of an automatic code for a high-speed computer, since the very large number of terms which figure in the tabulation preclude hand calculation (there are 800 terms to be built and summed over for $l \leq 5$). The results may therefore be considered to provide

particularly satisfactory evidence for the validity of the theoretical approach.

12. CONCLUDING REMARKS

A. General

Our main purpose has been to review the current theoretical and experimental status of angular distributions of both inelastic nucleons and succeeding γ radiations on the basis of compound-nucleus formation. Their systematic behavior has been examined, as well as some detailed aspects of comparisons of selected experimental data with such predictions. In these concluding remarks we attempt to review, at least briefly, some of the remaining experimental results, and to indicate possible lines of future development.

B. Inelastic Proton Distributions

One area of inelastic nucleon scattering that has been greatly neglected is the measurement of (p, p') angular distributions in medium and heavy nuclei under conditions where CN formation is the dominant reaction mode and sufficient energy averaging has been provided in order to satisfy the statistical requirements of this theory. Seward's early investigations[49] provided a pioneering contribution to this field. He deliberately used relatively thick (150-keV) targets, in order that many CN levels would contribute to the reaction being studied. His distributions of (p, p_1') groups for Ti^{48} ($E_p < 5.5$ MeV), Cr^{52} ($E_p = 5.4 - 7.0$ MeV) and Fe^{56} ($E_p = 5.5$ MeV) were nearly isotropic (10%), in essential agreement with the theoretical predictions for such 2^+ states. One exception was seen for Ti^{48} ($E_p = 7.02$ MeV), with a distinct forward peaking typical of a direct interaction contribution. His excitation curves ($E_p = 3.5 - 7$ MeV, $\theta_1 = 90°$) did reveal some "intermediate" structure, which he attributed to fluctuations in the number or properties of the several CN levels included in his energy spread of 150 keV. Since his angular distributions were taken at only a few scattered incident energies, any possible effect of this intermediate structure on such distributions was not investigated.

Recently, two more exhaustive investigations concerning the excitation curves[55] and angular distributions[56] of many Ni^{58} (p, p') groups have been initiated, the basic impetus being a search for possible intermediate resonances or at least structure. The excitation curves (taken in 25-keV steps from 8 to 11 MeV with a 25-keV target) show small fluctuations ($\pm 15\%$) as

well as some broader structure.[55] The angular distribution data (taken in 25-keV steps from 9.12 to 9.55 MeV with a 18-keV target) for most of the (p, p') groups reveal many rapid fluctuations. In addition, in the case of the (p, p_1') group some intermediate structure is also apparent.[56] These fluctuating distributions emphasize the importance of sufficient energy averaging if comparisons with CN theory are contemplated.

Energy averages of these data (corresponding to an energy spread of ≈ 300 keV) are shown in Fig. 36. Since the experimental points represent relative cross sections, they have been normalized [by the same factor for all (p, p') groups] for purposes of comparison with the theoretical differential cross sections. The forward peaking for the Ni^{58} (p, p_1') group (1.33-MeV first 2^+ state) reveals a substantial DI contribution; in addition, part of the $\theta_1 = 90°$ peaking for the 2.46-MeV (4^+) group could have a similar origin. The remaining (p, p') distributions of Fig. 36 are essentially symmetric about 90°, with only that for the 2.90-MeV state having any appreciable fore–aft asymmetry. In the latter case, the experimental distribution has an asymmetry closely resembling the prediction (dashed curve) for a 1^+ level, which includes a contribution for an unresolved 2.94-MeV state (assumed to be 6^+). It is quite possible that these experimental distributions for the higher levels may be dominated by the CN process, and that such data can be used for spin determinations. Unfortunately the spins of these higher states in Ni^{58} are not established with certainty, although preliminary $(p, p'\gamma)$ data[57] favors a spin-2 assignment for both the 3.04- and 3.26-MeV states of Ni^{58}. If any conclusions are to be drawn at this point from the comparisons shown in Fig. 36, a spin-0 possibility[57] for the 2.78-MeV state appears to be ruled out both on the basis of the observed (p, p') angular pattern as well as relative cross section.

At a bombarding energy as high as 9.5 MeV, one can expect DI contributions to complicate such comparisons, at least for the lowest-lying states. A much more favorable situation should be attainable at lower incident energies (say, 4–7 MeV), although possible contributions of intermediate resonances (including analog states) to the averaged angular patterns may have to be considered. An obvious first step would be the measurement of an energy-averaged (p, p') distribution for a known 0^+ level, in order to verify the large fore–aft asymmetry expected (Figs. 18, 36) as well as to provide a check that sufficient statistical averaging has been achieved. A search for previously unknown spin-0 and spin-1 levels would then be worthwhile.

C. Inelastic Neutron Distributions

The experimental situation regarding inelastic neutron distributions is much clearer than for inelastic

[55] J. E. Monahan, A. J. Elwyn, R. E. Segel, L. L. Lee, Jr., L. Meyer-Schützmeister, Z. Vager, and P. P. Singh, Bull. Am. Phys. Soc. **10**, 495 (1965); A. Elwyn, L. L. Lee, Jr., L. Meyer-Schützmeister, J. E. Monahan, R. E. Segel, P. P. Singh, and Z. Vager, *ibid.* **10**, 104 (1965).

[56] R. K. Mohindra and L. W. Swenson, Bull. Am. Phys. Soc. **10**, 496 (1965); L. W. Swenson, R. K. Mohindra, and D. M. Van Patter, *ibid.* **10**, 104 (1965).

[57] S. M. Shafroth, A. K. Sen Gupta, and G. T. Wood, Bull. Am. Phys. Soc. **9**, 93 (1964); and private communication.

FIG. 36. Comparison of the aver-
aged angular distribution results of
Mohindra and Swenson (Ref. 56) for
six $Ni^{58}(p, p')$ groups with theoretical
predictions for $E_p=9.35$ MeV based
on an optical model of the derivative
Woods–Saxon type (see Sec. 8). The
data represent the average of 16 dis-
tributions taken in the range $E_p=$
9.12–9.55 MeV, using a 18-keV tar-
get. They have been subjected to a
single over-all normalization in order
to fit them to the theoretical region
of values.
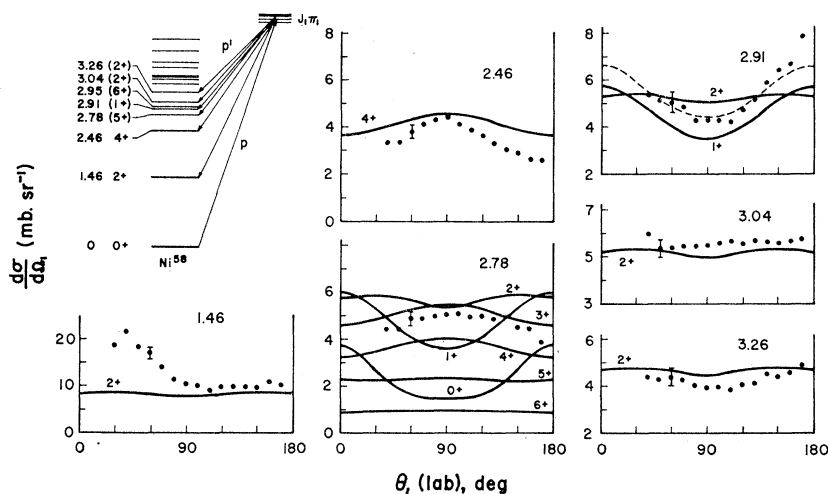
proton distributions as far as comparisons with CN theory are concerned. A key factor is the fact that substantial CN cross sections are attainable for most levels ($J_2<5$) for neutron energies not much (a few hundred keV) above threshold, irrespective of the nuclear mass. Auerbach and Moore[58] have recently reviewed the comparisons between theory and experiment for heavy nuclei (Ta^{181}, W^{184}, Th^{232}, Pb^{208}), while Cranberg included a discussion of his preliminary data for Pb^{206}, Pb^{207} and Bi^{209} in his earlier review.[34]

Angular distributions having large anisotropies typical of spin-0 states have thus far been reported only for 0^+ levels in Pb^{206} (1.19 MeV) and Ce^{140} (1.90 MeV).[34] The angular distributions for low-lying 2^+ states (W^{184}, Th^{232}, U^{238}) are nearly isotropic, and consistent with theoretical calculations,[58] which predict only a slight peaking (about 10%) at 90°. Cranberg's distribution for the 0.80-MeV 2^+ level of Pb^{206} ($E_n=2.50$ MeV) shows a distinct fore–aft asymmetry ($\approx 25\%$) which is considerably less than that predicted unless level-width fluctuations are taken into account.[36] For levels of higher spins (3^+, 4^+), the experimental distributions are typically nearly isotropic as expected, although recent data of Gilboy and Towle[59] for the 2.085-MeV 4^+ state in Fe^{56} indicate a slightly larger peaking at 90° than predicted for $E_n=3.99$ MeV. Another possible disagreement exists in the case of their data for the 2.62-MeV 3^- state of Pb^{208} for $E_n=3.96$ MeV, since the least-squares fit indicates a minimum (≈ 30 %) rather than the predicted peaking ($\approx 10\%$) at 90°. There is a puzzling discrepancy (see Fig. 33) in the Pb^{208} ($n, n'\gamma$) distribution results[54] for an incident energy of 3.0 MeV, which is closer to threshold, but there are satisfactory fits at $E_n=3.5$ and 4.1 MeV. It would be of interest to see if this possible discrepancy in the (n, n') distribution persists or perhaps increases for neutron energies closer to threshold.

The experimental (n, n') distributions for odd nuclei bear out the systematic predictions shown in Figs. 23 and 24. For example, the angular distributions for states in Pb^{207} ($J_0=\frac{1}{2}^-$) should be roughly comparable with the ($J_0=\frac{1}{2}$) curve of Fig. 23, i.e., one should expect low spin states to have the most asymmetric (n, n') distributions. Cranberg's angular distributions[34] for the 0.89-MeV ($\frac{3}{2}^-$) and 0.57-MeV ($\frac{5}{2}^-$) states have large asymmetries [$W(0°)/W(90°)$] decreasing from about 1.7 to 1.2 as (J_2-J_0) changes from 1 to 2, while that for the 1.63-MeV ($\frac{13}{2}^+$) state with (J_2-J_0)=6 is essentially isotropic. The systematic predictions of Figs. 23 and 24 also show that the distribution anisotropy for a given value of (J_2-J_0) should be reduced for a larger target spin J_0. This is borne out in Cranberg's data for Bi^{209} ($J_0=\frac{9}{2}^-$), since the observed asymmetry for the 0.90-MeV ($\frac{7}{2}^-$) state is much smaller (1.1–1.2) than that for the 0.89-MeV state in Pb^{207} which also has $| J_2-J_0 |=1$. Recently, Gilboy and Towle[60] have reported preliminary data for Y^{89} ($J_0=\frac{1}{2}^-$) that include some anisotropic as well as isotropic distributions for various levels, some of which appear to be in conflict with tentative spin assignments made earlier by Shafroth et al.,[61] provided that the systematic trends of Figs. 23 and 24 remain valid.

The effect of level-width fluctuations on the (n, n') *cross section* near threshold for low-lying states has been clearly demonstrated by the recent work of Tucker, Wells, and Meyerhof.[62] Similar detailed examinations of the effect near threshold on the inelastic neutron *distributions* should be of interest, particularly for low spin states with large predicted asymmetries at higher energies, such as is indicated by Cranberg's preliminary

[58] E. H. Auerbach and S. O. Moore, Phys. Rev. **135**, B895 (1964).
[59] W. B. Gilboy and J. H. Towle, Nucl. Phys. **64**, 130 (1965).

[60] W. B. Gilboy and J. H. Towle, *Comptes Rendus du Congrès International de Physique Nucléaire*, edited by P. Gugenberger (Centre National de la Recherche Scientifique, Paris, 1964), Vol. II, p. 690.
[61] S. M. Shafroth, P. N. Trehan, and D. M. Van Patter, Phys. Rev. **129**, 704 (1963).
[62] A. B. Tucker, J. T. Wells, and W. E. Meyerhof, Phys. Rev. **137**, B1181 (1965).

data[34] for the 1.19-MeV state of Pb[206]. In this connection, we note that under conditions where only s-wave outgoing neutrons contribute to the (n, n') cross section for a particular level (see Sec. 7), the limiting *neutron* distribution should be isotropic. Therefore, at energies sufficiently close to threshold, the large angular asymmetries typical (at higher incident energies) of states with small $(J_2 - J_0)$ values should vanish.

D. $(p, p'\gamma)$ Distributions

The early studies of $(p, p'\gamma)$ radiations from low-lying states in medium-weight even nuclei revealed the feasibility of angular distribution measurements.[63] An important question that needed to be settled was whether or not sufficient averaging over compound states could be achieved in order that representative angular distributions could be determined for comparison with statistical theory. An average over a rather large number of compound states is required, since it is not the total number which is of concern, but rather the number of states with a small range of J_1 values that have large reduced widths for the (p, p_1') channel of interest. For example, in the case of inelastic excitation of a first 2[+] state at a low bombarding energy, one is mainly concerned with the statistical average of $\frac{3}{2}^+$ and $\frac{5}{2}^+$ states with large (p, p_1') reduced widths. Therefore, the number of compound states (of all J, π) that need to be averaged may be of the order of 10[3] rather than 10[2]. For this reason, the first measurements of $(p, p'\gamma)$ distributions were carried out for a series of different bombarding energies to see if any large fluctuations were detected.[28] An example of such measurements is the series shown for Ni[60] in Fig. 20(b) for $\bar{E}_p = 4.36–4.96$ MeV (solid circles).[28] Since the theoretical predictions vary slowly within this energy interval, it is reasonable to average the four measurements together to improve the statistical averaging. In this example, the average extends over an energy spread of nearly 0.5 MeV and includes an estimated total number of compound states (all J, π) of approximately 2500. While some fluctuations in the individual measurements of $(p, p'\gamma)$ distributions were observed, particularly for the second 2[+] states, the results indicate that adequate statistical averaging was achieved if the energy average included at least 1000 compound states. Obviously, this could be done equally well by making only one distribution measurement with a sufficiently thick target.

The first measurements of such energy-averaged $(p, p'\gamma)$ distributions confirmed the expectation that transitions of the types $4^+(E2)2^+$, $2^+(M1, E2)2^+$ and $0^+(E2)2^+$ could be distinguished for sufficiently prominent γ radiations in the $(p, p'\gamma)$ spectra.[28] These measurements have provided the primary evidence for the identification of $(0^+, 2^+, 4^+)$ triplets for even

nuclei in the Ni, Zn region. Unfortunately, for the bombarding energies used (4.4–5.0 MeV), γ radiations from higher states above about 3 MeV are usually not sufficiently prominent to allow good angular distribution measurements. In order to study levels at higher excitations, more recent investigations have been made with incident energies up to 7 or 8 MeV.[29,57] The assumption that DI contributions can be neglected may no longer be valid. Nevertheless, these $(p, p'\gamma)$ distribution measurements have revealed no detectable discrepancy with CN theory to date. These measurements have been generally confined to incident energies below the (p, n) threshold in order to eliminate problems with γ radiations from induced activities as well as the $(p, n\gamma)$ reaction. It is just under these conditions that $(p'-\gamma)$ correlation measurements for such bombarding energies have shown the best agreement with CN theory.[17]

Use of these higher bombarding energies permits the investigation of the complicated nuclear structure typically lying above 3-MeV excitation in such medium-weight nuclei. An interesting problem would be the determination of the $(E1, M2)$ admixture in the decay of the collective 3[−] octupole levels, since the sensitivity of a $3^-(E1, M2)2^+$ distribution to the (D, Q) admixture is as large as shown in Fig. 13 for a $3^+(M1, E2)2^+$ transition.

While the use of incident energies in the range of about 5–7 MeV permits the study of higher level structure, it does have the major disadvantage that the $(p, p'\gamma)$ spectra observed with NaI scintillation detectors are typically quite complex.[29,57] With the advent of high-resolution Ge (Li-drifted) detectors, studies of such complicated $(p, p'\gamma)$ spectra have become much more attractive. Using these new detectors, the advantage of the simplicity of the energy-averaged angular distribution measurements will still be maintained, as compared with the more general approach[64] of angular correlation measurements to elucidate magnetic substate populations independently of reaction mechanism.

E. $(n, n'\gamma)$ Distributions

Early measurements of $(n, n'\gamma)$ angular distributions using sodium iodide detectors were subject to technical limitations, particularly low counting rates and large backgrounds. While most of these data were in reasonably good agreement with CN theory, unexplained discrepancies did remain, as pointed out by Van Patter et al.[65] in the case of the Fe[56] $(n, n_1'\gamma)$ reaction. In his recent review of $(n, n'\gamma)$ measurements, Day[46] noted that systematic errors may have been present in some of these earlier measurements. A major advance in this field has been accomplished by the Texas nuclear group who have carried out an extensive program using a total

[63] D. M. Van Patter, R. Rikmenspoel, and P. N. Trehan, Nucl. Phys. **27**, 467 (1961).

[64] A. E. Litherland and A. J. Ferguson, Can. J. Phys. **39**, 788 (1961).

[65] D. M. Van Patter, N. Nath, S. M. Shafroth, S. S. Malik, and M. A. Rothman, Phys. Rev. **128**, 1246 (1962).

absorption γ-spectrometer system for pulsed $(n, n'\gamma)$ measurements, eliminating many of the technical difficulties of previous investigations. From comparisons with theory such as are shown in Figs. 14, 19, 30–34, their results using this system appear to be quite reliable. For this reason, we have chosen samples of only their $(n, n'\gamma)$ distribution data for discussion. In their most recent report, Morgan *et al.*[25] give a detailed summary of their present results.

For target nuclei with $J_0 = 0^+$, the $(n, n'\gamma)$ angular patterns for levels with spins 1, 2, or 3 differ sufficiently to permit spin assignments if the ground-state γ transitions are prominent enough. For example, Mathur and Morgan[25] have found a $2(Q)0$ distribution for the ground-state decay of the 2.53-MeV state of Ar^{40}, and have clearly eliminated a possibility [66] of spin 1 for this level. They have also identified a $4^+(E2)2^+$ pattern for a $3.22 \rightarrow 1.45$ MeV transition, although it is not clear that a $2^+(M1, E2)2^+$ possibility has been eliminated. For transitions of mixed multipolarity, the present accuracy of $(n, n'\gamma)$ distribution measurements is usually only sufficient to identify the major multipole. Examples of such mixed transitions in heavy nuclei have been described in Sec. 11, and in some instances even the dominant multipole is uncertain due to the limited experimental accuracy. By way of contrast, the determination of multipole admixtures for $2^+(M1, E2)2^+$ and $3(D, Q)2$ transitions from $(p, p'\gamma)$ distributions (Figs. 6 and 13) reveal the present higher precision which can be achieved by this alternative approach.

Future developments in $(n, n'\gamma)$ distribution measurements will very likely involve the use of lithium-drifted germanium detectors. Chasman *et al.*[67] have examined the response of such a detector (3 cm³) bombarded with neutrons with energies of 1.2, 2.2, 4.7, and 16.3 MeV. They point out that background effects due to neutron activation should be less important (roughly an order of magnitude) than for NaI detectors, while background contributions from $(n, n'\gamma)$ and $(n,$ charged particle) reactions are comparable per unit volume. They were able to see an enhancement of $(n, n'\gamma)$ radiations from samples of aluminum and lead. While discrete background γ peaks were observed, particularly from $(n, n'\gamma)$ processes in the germanium isotopes, these detectors may well prove to be quite valuable for $(n, n'\gamma)$ distribution measurements, particularly if such prompt $(n, n'\gamma)$ background events can be removed using a sufficiently large detector in conjunction with a time-of-flight system.

Note added in proof. A recent investigation by J. M. Daniels and J. Felsteiner [Bull. Am. Phys. Soc. **10**, 1116 (1965)] of $(n, n'\gamma)$ spectra from Co^{59} and Cu^{63} using a Li–Ge detector has revealed new γ radiations.

They have not attempted any distribution measurements.

F. Other Reactions

The predictions for angular distributions which we have discussed should be equally applicable to other reactions involving spin-$\frac{1}{2}$ particles such as the (p, n), (n, p), (He^3, n) or (He^3, p) processes, provided that CN formation predominates. Johnson *et al.*[68] have compared their absolute (p, n) yields near threshold with Hauser–Feshbach calculations for many medium-weight nuclei with low thresholds, mainly in the range of 1–3 MeV. They have concluded that this CN theory works well for an interval of a few keV to 500 keV above threshold. At such low energies, we would also expect agreement with CN predictions for the angular patterns of both (p, n) and $(p, n\gamma)$ radiations; however, there appears to be very little experimental information of this type available.

At somewhat higher incident energies of 4.7–5.5 MeV, Lightbody *et al.*[69] have recently reported angular distributions for the (p, n_0) and (p, n_1) groups from Y^{89} $(J_0 = \frac{1}{2}^-)$, corresponding to excitation of states with $J_2 = \frac{9}{2}^+$ and $\frac{1}{2}^-$, respectively. On the basis of the systematics presented in Figs. 23 and 24, we would expect near isotropy for the n_0 group, and substantial fore–aft peaking for the n_1 group. Qualitatively, these predictions are borne out, although some fluctuations in the n_0 distributions are observed, which could result from insufficient statistical averaging $(\Delta E = 25$ keV$)$. The presence of CN analog states[70] in Zr^{90} complicates these results, and affects the angular distributions measured at $E_p = 4.68$ and 5.02 MeV.

Iyengar *et al.*[71] have measured distributions of the Cl^{37} (p, n_0) group at incident energies (5.1, 5.3, and 5.5 MeV) considerably above threshold (1.64 MeV) with a target thickness of 150 keV. Since their results appear to be inconsistent with CN predictions, they conclude that direct interactions are contributing to the reaction yield. We would recommend more extensive measurements of (p, n) and $(p, n\gamma)$ distributions at lower incident energies and for heavier nuclei. The relatively high yield of $(p, n\gamma)$ radiations and the typically complex low-energy spectrum favors the use of high-resolution germanium detectors, as illustrated by the recent investigation of the Ca^{48} $(p, n\gamma)$ reaction by Chasman *et al.*,[72] which included γ–γ coincidence measurements between the Li–Ge detector and a NaI counter.

[66] T. Wakatsuki, Y. Hirao, and I. Miura, Nucl. Phys. **39**, 335 (1962).

[67] C. Chasman, K. W. Jones, and R. A. Ristinen, Brookhaven National Laboratory Report 9157, April 1965 (unpublished); R. A. Ristinen, C. Chasman, and K. W. Jones, Bull. Am. Phys. Soc. **10**, 36 (1965).

[68] C. H. Johnson, C. C. Trail, and A. Galonsky, Phys. Rev. **136**, B1719 (1964); C. H. Johnson, A. Galonsky, and J. P. Ulrich, *ibid.* **109**, 1243 (1958).

[69] D. B. Lightbody, G. E. Mitchell, and A. Sayres, Phys. Letters **15**, 155 (1965).

[70] J. D. Fox, C. F. Moore, and D. Robson, Phys. Rev. Letters **12**, 198 (1964).

[71] K. V. K. Iyengar, S. K. Gupta, B. Lal, and D. Kondaiah (to be published).

[72] C. Chasman, K. W. Jones, and R. A. Ristinen, Bull. Am. Phys. Soc. **10**, 26 (1965).

While the number of experimentally favorable (n, p) reactions may be much more limited than that of (p, n) reactions, it is possible for the CN mechanism to predominate in some instances. The production cross section and angular distribution of a 0.767-MeV γ ray arising from a $0.797 \rightarrow 0.030$ MeV $(2^- \rightarrow 3^-)$ transition in the $Ca^{40}(n, p\gamma)K^{40}$ reaction has been found by Tucker[25,33] to be consistent with CN predictions for $E_n = 3.5$ to 5.0 MeV, although some systematic background problems were present. However, as also in the case of He^3-induced reactions, DI contributions may be more important for many (n, p) studies.

We conclude from this present survey of experimental information that there is a wide range of application of CN theory to energy-averaged distributions which merits attention, both now and in the future as improved experimental techniques become available.

APPENDIX A: TABULATION OF RESTRICTED LEGENDRE EXPANSION COEFFICIENTS $\alpha_{i\nu}$

The Tables (VI to X) which follow for various nuclear spin sequences list in each instance the momentum combination l_1, j_1, J_1, l_2, j_2, followed by the expansion coefficients $\alpha_{i\nu}$ for different radiations (see Secs. 4A and 4B). For each momentum ensemble the $\alpha_{i\nu}$ for outgoing nucleons and subsequent γ radiation [of pure multipolarity $L = |J_2 - J_3|$ (or $|J_2 - J_3| + 1$ when $J_2 - J_3 = 0$) and, when relevant, $L' = |J_2 - J_3| + 1$ (or $|J_2 - J_3| + 2$)] have been tabulated. The reason for listing coefficients for such multipole combinations as $E1$ or $M2$, and $E2$ or $M3$, although in practice the alternative multipolarity would be precluded by rules governing the transition probability, lies in the usefulness of such a full tabulation for hand conversion of the $\alpha_{i\nu}$ to those for other spin sequences.

TABLE VI. $0^+ \rightarrow J_1\pi_1 \rightarrow 2^+ \rightarrow 0^+$ transition sequence.

l_1	j_1	J_1	l_2	j_2	Rad.	α_{i0}	α_{i2}	α_{i4}	α_{i6}	α_{i8}
0	$\frac{1}{2}$	$\frac{1}{2}^+$	2	$\frac{3}{2}$	N'	2				
					$\gamma:E2$	2				
				$\frac{5}{2}$	N'	2				
					$\gamma:E2$	2				
1	$\frac{1}{2}$	$\frac{1}{2}^-$	1	$\frac{3}{2}$	N'	2				
					$\gamma:E2$	2				
			3	$\frac{5}{2}$	N'	2				
					$\gamma:E2$	2				
	$\frac{3}{2}$	$\frac{3}{2}^-$	1	$\frac{1}{2}$	N'	4				
					$\gamma:E2$	4	2			
				$\frac{3}{2}$	N'	4	-2.4			
					$\gamma:E2$	4				
			3	$\frac{5}{2}$	N'	4	-0.45714			
					$\gamma:E2$	4	-1.42857			
				$\frac{7}{2}$	N'	4	2.85714			
					$\gamma:E2$	4	0.57143			
2	$\frac{3}{2}$	$\frac{3}{2}^+$	0	$\frac{1}{2}$	N'	4				
					$\gamma:E2$	4	2			
			2	$\frac{3}{2}$	N'	4	-2.4			
					$\gamma:E2$	4				
				$\frac{5}{2}$	N'	4	-0.45714			
					$\gamma:E2$	4	-1.42857			
			4	$\frac{7}{2}$	N'	4	2.85714			
					$\gamma:E2$	4	0.57143			
	$\frac{5}{2}$	$\frac{5}{2}^+$	0	$\frac{1}{2}$	N'	6				
					$\gamma:E2$	6	3.42857	-3.42857		
			2	$\frac{3}{2}$	N'	6	-0.68571			
					$\gamma:E2$	6	1.22449	3.91837		
				$\frac{5}{2}$	N'	6	0.68571	-2.57143		
					$\gamma:E2$	6	-1.22449	-2.20408		
			4	$\frac{7}{2}$	N'	6	2.85714	-2.57143		
					$\gamma:E2$	6	-2.08163	0.65306		
				$\frac{9}{2}$	N'	6	5.71429	2.57143		
					$\gamma:E2$	6	1.22449	-0.08163		

TABLE VI. (*Continued*)

l_1	j_1	J_1	l_2	j_2	Rad.	α_{i0}	α_{i2}	α_{i4}	α_{i6}	α_{i8}
3	$\frac{5}{2}$	$\frac{5}{2}^-$	1	$\frac{1}{2}$	N'	6				
					$\gamma:E2$	6	3.42857	-3.42857		
				$\frac{3}{2}$	N'	6	-0.68571			
					$\gamma:E2$	6	1.22449	3.91837		
			3	$\frac{5}{2}$	N'	6	0.68571	-2.57143		
					$\gamma:E2$	6	-1.22449	-2.20408		
				$\frac{7}{2}$	N'	6	2.85714	-2.57143		
					$\gamma:E2$	6	-2.08163	0.65306		
	$\frac{7}{2}$	$\frac{7}{2}^-$	1	$\frac{3}{2}$	N'	8	5.71429			
					$\gamma:E2$	8	4.08163	-2.93878		
			3	$\frac{5}{2}$	N'	8	3.80952	-3.42857		
					$\gamma:E2$	8	0.68027	5.22449		
				$\frac{7}{2}$	N'	8	4.44444	-2.80520	-2.02020	
					$\gamma:E2$	8	-2.17687	-3.91837		
4	$\frac{7}{2}$	$\frac{7}{2}^+$	2	$\frac{3}{2}$	N'	8	5.71429			
					$\gamma:E2$	8	4.08163	-2.93878		
				$\frac{5}{2}$	N'	8	3.80952	-3.42857		
					$\gamma:E2$	8	0.68027	5.22449		
			4	$\frac{7}{2}$	N'	8	4.44444	-2.80520	-2.02020	
					$\gamma:E2$	8	-2.17687	-3.91837		
				$\frac{9}{2}$	N'	8	6.11833	-0.25502	-3.82002	
					$\gamma:E2$	8	-2.58503	1.42486		
	$\frac{9}{2}$	$\frac{9}{2}^+$	2	$\frac{5}{2}$	N'	10	9.52381	4.28571		
					$\gamma:E2$	10	4.76191	-2.85714		
			4	$\frac{7}{2}$	N'	10	7.64791	-0.31877	-4.77502	
					$\gamma:E2$	10	0.21645	6.23377		
				$\frac{9}{2}$	N'	10	7.89715	0.17165	-4.70156	-1.24603
					$\gamma:E2$	10	-3.03030	-5.45455		

TABLE VII. $0^+ \to J_{1\pi1} \to 2^+ \to 2^+$ transition sequence.

l_1	j_1	J_1	l_2	j_2	Rad.	α_{i0}	α_{i2}	α_{i4}	α_{i6}	α_{i8}
0	$\frac{1}{2}$	$\frac{1}{2}^+$	2	$\frac{3}{2}$	N'	2				
					$\gamma:M1$	2				
					$\gamma:E2$	2				
				$\frac{5}{2}$	N'	2				
					$\gamma:M1$	2				
					$\gamma:E2$	2				
1	$\frac{1}{2}$	$\frac{1}{2}^-$	1	$\frac{3}{2}$	N'	2				
					$\gamma:M1$	2				
					$\gamma:E2$	2				
			3	$\frac{5}{2}$	N'	2				
					$\gamma:M1$	2				
					$\gamma:E2$	2				
	$\frac{3}{2}$	$\frac{3}{2}^-$	1	$\frac{1}{2}$	N'	4				
					$\gamma:M1$	4	1.4			
					$\gamma:E2$	4	-0.42857			
				$\frac{3}{2}$	N'	4	-2.4			
					$\gamma:M1$	4				
					$\gamma:E2$	4				
			3	$\frac{5}{2}$	N'	4	-0.45714			
					$\gamma:M1$	4	-1			
					$\gamma:E2$	4	0.30612			
				$\frac{7}{2}$	N'	4	2.85714			
					$\gamma:M1$	4	0.4			
					$\gamma:E2$	4	-0.12245			

TABLE VII. (Continued)

l_1	j_1	J_1	l_2	j_2	Rad.	α_{i0}	α_{i2}	α_{i4}	α_{i6}	α_{i8}
2	$\frac{3}{2}$	$\frac{3}{2}+$	0	$\frac{1}{2}$	N'	4				
					$\gamma{:}M1$	4	1.4			
					$\gamma{:}E2$	4	-0.42857			
			2	$\frac{3}{2}$	N'	4	-2.4			
					$\gamma{:}M1$	4				
					$\gamma{:}E2$	4				
				$\frac{5}{2}$	N'	4	-0.45714			
					$\gamma{:}M1$	4	-1			
					$\gamma{:}E2$	4	0.30612			
			4	$\frac{7}{2}$	N'	4	2.85714			
					$\gamma{:}M1$	4	0.4			
					$\gamma{:}E2$	4	-0.12245			
	$\frac{5}{2}$	$\frac{5}{2}+$	0	$\frac{1}{2}$	N'	6				
					$\gamma{:}M1$	6	2.4			
					$\gamma{:}E2$	6	-0.73469	-0.97959		
			2	$\frac{3}{2}$	N'	6	-0.68571			
					$\gamma{:}M1$	6	0.85714			
					$\gamma{:}E2$	6	-0.26239	1.11953		
				$\frac{5}{2}$	N'	6	0.68571	-2.57143		
					$\gamma{:}M1$	6	-0.85714			
					$\gamma{:}E2$	6	0.26239	-0.62974		
			4	$\frac{7}{2}$	N'	6	2.85714	-2.57143		
					$\gamma{:}M1$	6	-1.45714			
					$\gamma{:}E2$	6	0.44606	0.18659		
				$\frac{9}{2}$	N'	6	5.71429	2.57143		
					$\gamma{:}M1$	6	0.85714			
					$\gamma{:}E2$	6	-0.26239	-0.02332		
3	$\frac{5}{2}$	$\frac{5}{2}-$	1	$\frac{1}{2}$	N'	6				
					$\gamma{:}M1$	6	2.4			
					$\gamma{:}E2$	6	-0.73469	-0.97959		
				$\frac{3}{2}$	N'	6	-0.68571			
					$\gamma{:}M1$	6	0.85714			
					$\gamma{:}E2$	6	-0.26239	1.11953		
			3	$\frac{5}{2}$	N'	6	0.68571	-2.57143		
					$\gamma{:}M1$	6	-0.85714			
					$\gamma{:}E2$	6	0.26239	-0.62974		
				$\frac{7}{2}$	N'	6	2.85714	-2.57143		
					$\gamma{:}M1$	6	-1.45714			
					$\gamma{:}E2$	6	0.44606	0.18659		
	$\frac{7}{2}$	$\frac{7}{2}-$	1	$\frac{3}{2}$	N'	8	5.71429			
					$\gamma{:}M1$	8	2.85714			
					$\gamma{:}E2$	8	-0.87464	-0.83965		
			3	$\frac{5}{2}$	N'	8	3.80952	-3.42857		
					$\gamma{:}M1$	8	0.47619			
					$\gamma{:}E2$	8	-0.14577	1.49271		
				$\frac{7}{2}$	N'	8	4.44444	-2.80520	-2.02020	
					$\gamma{:}M1$	8	-1.52381			
					$\gamma{:}E2$	8	0.46647	-1.11953		
4	$\frac{7}{2}$	$\frac{7}{2}+$	2	$\frac{3}{2}$	N'	8	5.71429			
					$\gamma{:}M1$	8	2.85714			
					$\gamma{:}E2$	8	-0.87464	-0.83965		
				$\frac{5}{2}$	N'	8	3.80952	-3.42857		
					$\gamma{:}M1$	8	0.47619			
					$\gamma{:}E2$	8	-0.14577	1.49271		
			4	$\frac{7}{2}$	N'	8	4.44444	-2.80520	-2.02020	
					$\gamma{:}M1$	8	-1.52381			
					$\gamma{:}E2$	8	0.46647	-1.11953		
				$\frac{9}{2}$	N'	8	6.11833	-0.25502	-3.82002	
					$\gamma{:}M1$	8	-1.80952			
					$\gamma{:}E2$	8	0.55394	0.40710		

Table VII. (*Continued*)

l_1	j_1	J_1	l_2	j_2	Rad.	α_{i0}	α_{i2}	α_{i4}	α_{i6}	α_{i8}
4	$\frac{9}{2}$	$\frac{9}{2}^+$	2	$\frac{5}{2}$	N'	10	9.52381	4.28571		
					$\gamma:M1$	10	3.33333			
					$\gamma:E2$	10	-1.02041	-0.81633		
			4	$\frac{7}{2}$	N'	10	7.64791	-0.31877	-4.77502	
					$\gamma:M1$	10	0.15152			
					$\gamma:E2$	10	-0.04638	1.78108		
				$\frac{9}{2}$	N'	10	7.89715	0.17165	-4.70156	-1.24603
					$\gamma:M1$	10	-2.12121			
					$\gamma:E2$	10	0.64935	-1.55844		

Table VIII. $0^+ \rightarrow J_1\pi_1 \rightarrow 3^- \rightarrow 2^+$ transition sequence.

l_1	j_1	J_1	l_2	j_2	Rad.	α_{i0}	α_{i2}	α_{i4}	α_{i6}
0	$\frac{1}{2}$	$\frac{1}{2}^+$	3	$\frac{5}{2}$	N'	2			
					$\gamma:E1$	2			
					$\gamma:M2$	2			
				$\frac{7}{2}$	N'	2			
					$\gamma:E1$	2			
					$\gamma:M2$	2			
1	$\frac{1}{2}$	$\frac{1}{2}^-$	2	$\frac{5}{2}$	N'	2			
					$\gamma:E1$	2			
					$\gamma:M2$	2			
			4	$\frac{7}{2}$	N'	2			
					$\gamma:E1$	2			
					$\gamma:M2$	2			
	$\frac{3}{2}$	$\frac{3}{2}^-$	2	$\frac{3}{2}$	N'	4	0.8		
					$\gamma:E1$	4	-0.96		
					$\gamma:M2$	4	0.34286		
				$\frac{5}{2}$	N'	4	-2.51429		
					$\gamma:E1$	4	0.24		
					$\gamma:M2$	4	-0.08571		
			4	$\frac{7}{2}$	N'	4	-0.95238		
					$\gamma:E1$	4	0.8		
					$\gamma:M2$	4	-0.28571		
				$\frac{9}{2}$	N'	4	2.66667		
					$\gamma:E1$	4	-0.4		
					$\gamma:M2$	4	0.14286		
2	$\frac{3}{2}$	$\frac{3}{2}^+$	1	$\frac{3}{2}$	N'	4	0.8		
					$\gamma:E1$	4	-0.96		
					$\gamma:M2$	4	0.34286		
			3	$\frac{5}{2}$	N'	4	-2.51429		
					$\gamma:E1$	4	0.24		
					$\gamma:M2$	4	-0.08571		
				$\frac{7}{2}$	N'	4	-0.95238		
					$\gamma:E1$	4	0.8		
					$\gamma:M2$	4	-0.28571		
	$\frac{5}{2}$	$\frac{5}{2}^+$	1	$\frac{1}{2}$	N'	6			
					$\gamma:E1$	6	-2.05714		
					$\gamma:M2$	6	0.73469	2.69388	
				$\frac{3}{2}$	N'	6	-3.77143		
					$\gamma:E1$	6	-1.13143		
					$\gamma:M2$	6	0.40408	-1.34694	
			3	$\frac{5}{2}$	N'	6	-2.84082		
					$\gamma:E1$	6	0.06857		
					$\gamma:M2$	6	-0.02449	-1.34694	
				$\frac{7}{2}$	N'	6	-0.81633	-1.46939	
					$\gamma:E1$	6	1.02857		
					$\gamma:M2$	6	-0.36735	1.79592	

TABLE VIII. (*Continued*)

l_1	j_1	J_1	l_2	j_2	Rad.	α_{i0}	α_{i2}	α_{i4}	α_{i6}
3	$\frac{5}{2}$	$\frac{5}{2}^-$	0	$\frac{1}{2}$	N'	6			
					$\gamma:E1$	6	-2.05714		
					$\gamma:M2$	6	0.73469	2.69388	
			2	$\frac{3}{2}$	N'	6	-3.77143		
					$\gamma:E1$	6	-1.13143		
					$\gamma:M2$	6	0.40408	-1.34694	
				$\frac{5}{2}$	N'	6	-2.84082	2.32653	
					$\gamma:E1$	6	0.06857		
					$\gamma:M2$	6	-0.02449	-1.34694	
			4	$\frac{7}{2}$	N'	6	-0.81633	-1.46939	
					$\gamma:E1$	6	1.02857		
					$\gamma:M2$	6	-0.36735	1.79592	
				$\frac{9}{2}$	N'	6	1.97403	-3.03869	
					$\gamma:E1$	6	1.02857		
					$\gamma:M2$	6	-0.36735	-0.77551	
	$\frac{7}{2}$	$\frac{7}{2}^-$	0	$\frac{1}{2}$	N'	8			
					$\gamma:E1$	8	-2.85714		
					$\gamma:M2$	8	1.02041	4.40816	
			2	$\frac{3}{2}$	N'	8	-1.90476		
					$\gamma:E1$	8	-1.90476		
					$\gamma:M2$	8	0.68027	-0.48980	
				$\frac{5}{2}$	N'	8	-1.08844	-1.95918	
					$\gamma:E1$	8	-0.57143		
					$\gamma:M2$	8	0.20408	-2.77551	
			4	$\frac{7}{2}$	N'	8	0.45352	-3.67954	3.12213
					$\gamma:E1$	8	0.76190		
					$\gamma:M2$	8	-0.27211	-0.17811	
				$\frac{9}{2}$	N'	8	2.53968	-4.08028	0.29385
					$\gamma:E1$	8	1.56190		
					$\gamma:M2$	8	-0.55782	2.62709	
4	$\frac{7}{2}$	$\frac{7}{2}^+$	1	$\frac{1}{2}$	N'	8			
					$\gamma:E1$	8	-2.85714		
					$\gamma:M2$	8	1.02041	4.40816	
				$\frac{3}{2}$	N'	8	-1.90476		
					$\gamma:E1$	8	-1.90476		
					$\gamma:M2$	8	0.68027	-0.48980	
			3	$\frac{5}{2}$	N'	8	-1.08844	-1.95918	
					$\gamma:E1$	8	-0.57143		
					$\gamma:M2$	8	0.20408	-2.77551	
				$\frac{7}{2}$	N'	8	0.45352	-3.67954	3.12213
					$\gamma:E1$	8	0.76190		
					$\gamma:M2$	8	-0.27211	-0.17811	
	$\frac{9}{2}$	$\frac{9}{2}^+$	1	$\frac{3}{2}$	N'	10	6.66667		
					$\gamma:E1$	10	-3.33333		
					$\gamma:M2$	10	1.19048	4.28571	
			3	$\frac{5}{2}$	N'	10	3.29004	-5.06494	
					$\gamma:E1$	10	-1.81818		
					$\gamma:M2$	10	0.64935	-2.20779	
				$\frac{7}{2}$	N'	10	3.17460	-5.10035	0.36731
					$\gamma:E1$	10	-0.12121		
					$\gamma:M2$	10	0.04329	-3.11688	

TABLE IX. $0^+ \to J_1\pi_1 \to 4^+ \to 2^+$ transition sequence.

l_1	j_1	J_1	l_2	j_2	Rad.	α_{i0}	α_{i2}	α_{i4}	α_{i6}	α_{i8}
0	$\frac{1}{2}$	$\frac{1}{2}^+$	4	$\frac{7}{2}$	N'	2				
					$\gamma:E2$	2				
					$\gamma:M3$	2				
				$\frac{9}{2}$	N'	2				
					$\gamma:E2$	2				
					$\gamma:M3$	2				
1	$\frac{1}{2}$	$\frac{1}{2}^-$	3	$\frac{7}{2}$	N'	2				
					$\gamma:E2$	2				
					$\gamma:M3$	2				
	$\frac{3}{2}$	$\frac{3}{2}^-$	3	$\frac{5}{2}$	N'	4	1.14286			
					$\gamma:E2$	4	1.12245			
					$\gamma:M3$	4	1.17857			
				$\frac{7}{2}$	N'	4	-2.47619			
					$\gamma:E2$	4	-0.44898			
					$\gamma:M3$	4	-0.47143			
2	$\frac{3}{2}$	$\frac{3}{2}^+$	2	$\frac{5}{2}$	N'	4	1.14286			
					$\gamma:E2$	4	1.12245			
					$\gamma:M3$	4	1.17857			
			4	$\frac{7}{2}$	N'	4	-2.47619			
					$\gamma:E2$	4	-0.44898			
					$\gamma:M3$	4	-0.47143			
				$\frac{9}{2}$	N'	4	-1.21212			
					$\gamma:E2$	4	-1			
					$\gamma:M3$	4	-1.05			
	$\frac{5}{2}$	$\frac{5}{2}^+$	2	$\frac{3}{2}$	N'	6	1.71429			
					$\gamma:E2$	6	2.40525	-0.83382		
					$\gamma:M3$	6	2.52551	-0.13265		
				$\frac{5}{2}$	N'	6	-3.42857	-0.85714		
					$\gamma:E2$	6	0.96210	0.83382		
					$\gamma:M3$	6	1.01020	0.13265		
			4	$\frac{7}{2}$	N'	6	-3.42857	2.80519		
					$\gamma:E2$	6	-0.50729	0.30321		
					$\gamma:M3$	6	-0.53265	0.04824		
				$\frac{9}{2}$	N'	6	-1.55844	-0.70130		
					$\gamma:E2$	6	-1.45190	-0.83382		
					$\gamma:M3$	6	-1.52449	-0.13265		
3	$\frac{5}{2}$	$\frac{5}{2}^-$	1	$\frac{3}{2}$	N'	6	1.71429			
					$\gamma:E2$	6	2.40525	-0.83382		
					$\gamma:M3$	6	2.52551	-0.13265		
			3	$\frac{5}{2}$	N'	6	-3.42857	-0.85714		
					$\gamma:E2$	6	0.96210	0.83382		
					$\gamma:M3$	6	1.01020	0.13265		
				$\frac{7}{2}$	N'	6	-3.42857	2.80519		
					$\gamma:E2$	6	-0.50729	0.30321		
					$\gamma:M3$	6	-0.53265	0.04824		
	$\frac{7}{2}$	$\frac{7}{2}^-$	1	$\frac{1}{2}$	N'	8				
					$\gamma:E2$	8	3.74150	-2.12245		
					$\gamma:M3$	8	3.92857	-0.33766	3.40909	
				$\frac{3}{2}$	N'	8	-4.95238			
					$\gamma:E2$	8	2.77940	-0.30321		
					$\gamma:M3$	8	2.91837	-0.04824	-2.72727	
			3	$\frac{5}{2}$	N'	8	-4.57143	3.74026		
					$\gamma:E2$	8	1.37026	1.07501		
					$\gamma:M3$	8	1.43878	0.17102	-0.55785	
				$\frac{7}{2}$	N'	8	-3.17460	0.93506	-2.02020	
					$\gamma:E2$	8	-0.19436	0.88206		
					$\gamma:M3$	8	-0.20408	0.14033	2.47934	

TABLE IX. (*Continued*)

l_1	j_1	J_1	l_2	j_2	Rad.	α_{i0}	α_{i2}	α_{i4}	α_{i6}	α_{i8}
4	$\frac{7}{2}$	$\frac{7}{2}^+$	0	$\frac{1}{2}$	N'	8				
					$\gamma:E2$	8	3.74150	-2.12245		
					$\gamma:M3$	8	3.92857	-0.33766	3.40909	
			2	$\frac{3}{2}$	N'	8	-4.95238			
					$\gamma:E2$	8	2.77940	-0.30321		
					$\gamma:M3$	8	2.91837	-0.04824	-2.72727	
			2	$\frac{5}{2}$	N'	8	-4.57143	3.74026		
					$\gamma:E2$	8	1.37026	1.07501		
					$\gamma:M3$	8	1.43878	0.17102	-0.55785	
			4	$\frac{7}{2}$	N'	8	-3.17460	0.93506	-2.02020	
					$\gamma:E2$	8	-0.19436	0.88206		
					$\gamma:M3$	8	-0.20408	0.14033	2.47934	
				$\frac{9}{2}$	N'	8	-1.15440	-2.40632	2.82546	
					$\gamma:E2$	8	-1.50632	-0.51100		
					$\gamma:M3$	8	-1.58163	-0.08130	-2.02638	
	$\frac{9}{2}$	$\frac{9}{2}^+$	0	$\frac{1}{2}$	N'	10				
					$\gamma:E2$	10	4.76190	-2.85714		
					$\gamma:M3$	10	5	-0.45455	5.45455	
			2	$\frac{3}{2}$	N'	10	-3.03030			
					$\gamma:E2$	10	3.78788	-0.90909		
					$\gamma:M3$	10	3.97727	-0.14463	-2.35537	
				$\frac{5}{2}$	N'	10	-2.59740	-1.16883		
					$\gamma:E2$	10	2.31911	0.94620		
					$\gamma:M3$	10	2.43506	0.15053	-2.97521	
			4	$\frac{7}{2}$	N'	10	-1.44300	-3.00790	3.53182	
					$\gamma:E2$	10	0.58751	1.49565		
					$\gamma:M3$	10	0.61688	0.23794	2.16465	
				$\frac{9}{2}$	N'	10	0.18365	-4.62565	3.70700	-2.97129
					$\gamma:E2$	10	-1.08225	0.42957		
					$\gamma:M3$	10	-1.13636	0.06834	1.90718	

TABLE X. $\frac{1}{2}^+ \rightarrow J_1\pi_1 \rightarrow \frac{3}{2}^+ \rightarrow \frac{1}{2}^+$ transition sequence. *Note*: For brevity, the $\alpha_{i\nu}$ for $E2$ radiation have not been listed, since numerically they are identical to those for $M1$ radiation. The sign of the α_{i0} is, of course, the same, but that for the α_{i2} is opposite (higher values of ν than $\nu=2$ are excluded by the Racah rule $\nu \leq 2J_2$). As discussed in Sec. 4C, the conversion factors from $M1$ to $E2$ radiation for this spin sequence are $C_0 = c_{i0} = +1$, $C_2 = c_{i2} = -1$.

l_1	j_1	J_1	l_2	j_2	Rad.	α_{i0}	α_{i2}	α_{i4}	α_{i6}	α_{i8}
0	$\frac{1}{2}$	0^+	2	$\frac{3}{2}$	N'	0.5				
					$\gamma:M1$	0.5				
		1^+	0	$\frac{1}{2}$	N'	1.5				
					$\gamma:M1$	1.5				
			2	$\frac{3}{2}$	N'	1.5				
					$\gamma\ M1$	1.5				
				$\frac{5}{2}$	N'	1.5				
					$\gamma:M1$	1.5				
1	$\frac{1}{2}$	0^-	1	$\frac{3}{2}$	N'	0.5				
					$\gamma:M1$	0.5				
		1^-	1	$\frac{1}{2}$	N'	1.5				
					$\gamma:M1$	1.5				
				$\frac{3}{2}$	N'	1.5				
					$\gamma:M1$	1.5				
			3	$\frac{5}{2}$	N'	1.5				
					$\gamma:M1$	1.5				

Table X. (Continued)

l_1	j_1	J_1	l_2	j_2	Rad.	α_{i0}	α_{i2}	α_{i4}	α_{i6}	α_{i8}
1	$\frac{3}{2}$	1^-	1	$\frac{1}{2}$	N'	1.5				
					$\gamma:M1$	1.5	−0.375			
				$\frac{3}{2}$	N'	1.5	−0.6			
					$\gamma:M1$	1.5	0.3			
			3	$\frac{5}{2}$	N'	1.5	0.6			
					$\gamma:M1$	1.5	−0.075			
		2^-	1	$\frac{1}{2}$	N'	2.5				
					$\gamma:M1$	2.5	−0.875			
				$\frac{3}{2}$	N'	2.5				
					$\gamma:M1$	2.5				
			3	$\frac{5}{2}$	N'	2.5	0.71429			
					$\gamma:M1$	2.5	0.625			
				$\frac{7}{2}$	N'	2.5	1.78571			
					$\gamma:M1$	2.5	−0.25			
2	$\frac{3}{2}$	1^+	0	$\frac{1}{2}$	N'	1.5				
					$\gamma:M1$	1.5	−0.375			
			2	$\frac{3}{2}$	N'	1.5	−0.6			
					$\gamma:M1$	1.5	0.3			
				$\frac{5}{2}$	N'	1.5	0.6			
					$\gamma:M1$	1.5	−0.075			
		2^+	0	$\frac{1}{2}$	N'	2.5				
					$\gamma:M1$	2.5	−0.875			
			2	$\frac{3}{2}$	N'	2.5				
					$\gamma:M1$	2.5				
				$\frac{5}{2}$	N'	2.5	0.71429			
					$\gamma:M1$	2.5	0.625			
			4	$\frac{7}{2}$	N'	2.5	1.78571			
					$\gamma:M1$	2.5	−0.25			
	$\frac{5}{2}$	2^+	0	$\frac{1}{2}$	N'	2.5				
					$\gamma:M1$	2.5	−1			
			2	$\frac{3}{2}$	N'	2.5				
					$\gamma:M1$	2.5				
				$\frac{5}{2}$	N'	2.5	0.81633			
					$\gamma:M1$	2.5	0.71429			
			4	$\frac{7}{2}$	N'	2.5	2.04082	0.45918		
					$\gamma:M1$	2.5	−0.28571			
		3^+	2	$\frac{3}{2}$	N'	3.5	2.4			
					$\gamma:M1$	3.5	−1.2			
				$\frac{5}{2}$	N'	3.5	1.88571	−0.78571		
					$\gamma:M1$	3.5	0.3			
			4	$\frac{7}{2}$	N'	3.5	2.38095	−0.21429		
					$\gamma:M1$	3.5	1			
				$\frac{9}{2}$	N'	3.5	3.33333	1.5		
					$\gamma:M1$	3.5	−0.5			
3	$\frac{5}{2}$	2^-	1	$\frac{1}{2}$	N'	2.5				
					$\gamma:M1$	2.5	−1			
				$\frac{3}{2}$	N'	2.5				
					$\gamma:M1$	2.5				
			3	$\frac{5}{2}$	N'	2.5	0.81633	−0.81633		
					$\gamma:M1$	2.5	0.71429			
				$\frac{7}{2}$	N'	2.5	2.04082	0.45918		
					$\gamma:M1$	2.5	−0.28571			

TABLE X. (Continued)

l_1	j_1	J_1	l_2	j_2	Rad.	α_{i0}	α_{i2}	α_{i4}	α_{i6}	α_{i8}
3		3^-	1	$\frac{3}{2}$	N'	3.5	2.4			
					$\gamma:M1$	3.5	−1.2			
			3	$\frac{5}{2}$	N'	3.5	1.88571	−0.78571		
					$\gamma:M1$	3.5	0.3			
				$\frac{7}{2}$	N'	3.5	2.38095	−0.21429		
					$\gamma:M1$	3.5	1			
	$\frac{7}{2}$	3^-	1	$\frac{3}{2}$	N'	3.5	2.5			
					$\gamma:M1$	3.5	−1.25			
			3	$\frac{5}{2}$	N'	3.5	1.96429	−0.96429		
					$\gamma:M1$	3.5	0.3125			
				$\frac{7}{2}$	N'	3.5	2.48016	−0.26299	−0.88384	
					$\gamma:M1$	3.5	1.04167			
		4^-	3	$\frac{5}{2}$	N'	4.5	4.20918	1.79082		
					$\gamma:M1$	4.5	−1.47321			
				$\frac{7}{2}$	N'	4.5	3.64796	0.48840	−1.13636	
					$\gamma:M1$	4.5	0.58929			
4	$\frac{7}{2}$	3^+	2	$\frac{3}{2}$	N'	3.5	2.5			
					$\gamma:M1$	3.5	−1.25			
				$\frac{5}{2}$	N'	3.5	1.96429	−0.96429		
					$\gamma:M1$	3.5	0.3125			
			4	$\frac{7}{2}$	N'	3.5	2.48016	−0.26299	−0.88384	
					$\gamma:M1$	3.5	1.04167			
				$\frac{9}{2}$	N'	3.5	3.47222	1.84091	0.35354	
					$\gamma:M1$	3.5	−0.52083			
		4^+	2	$\frac{5}{2}$	N'	4.5	4.20918	1.79081		
					$\gamma:M1$	4.5	−1.47321			
			4	$\frac{7}{2}$	N'	4.5	3.64796	0.48840	−1.13636	
					$\gamma:M1$	4.5	0.58929			
				$\frac{9}{2}$	N'	4.5	3.97727	1.17149	−0.78512	
					$\gamma:M1$	4.5	1.31250			
	$\frac{9}{2}$	4^+	2	$\frac{5}{2}$	N'	4.5	4.28571	1.92857		
					$\gamma:M1$	4.5	−1.5			
			4	$\frac{7}{2}$	N'	4.5	3.71429	0.52597	−1.45455	
					$\gamma:M1$	4.5	0.6			
				$\frac{9}{2}$	N'	4.5	4.04959	1.26160	−1.00496	−0.89714
					$\gamma:M1$	4.5	1.33636			
		5^+	4	$\frac{7}{2}$	N'	5.5	5.77778	3.68182	1.37374	
					$\gamma:M1$	5.5	−1.73333			
				$\frac{9}{2}$	N'	5.5	5.25253	2.26573	−0.54949	−1.30210
					$\gamma:M1$	5.5	0.86667			

APPENDIX B: DISTRIBUTION SYMMETRY ABOUT 90°

As has been shown by Blatt and Weisskopf,[73] and discussed by Sheldon,[74] angular distributions of nuclear reaction products are symmetric about 90° if (i) parity is conserved in the reaction, (ii) the measurement of the distribution is effected in a system which makes no distinctions between right- and left-hand coordinate systems, and (iii) the parity of the wave function describing the reaction (hence, essentially, the parity of the intermediate state) is definite. Before going on to comment upon these requirements in turn, we recall the Blatt–Weisskopf derivation of distribution symmetry about 90° when the above conditions are fulfilled.

The differential cross section for a reaction $A(a, b)B$ may be expressed as

$$d\sigma = (\hat{s}_a)^{-2}(\hat{s}_A)^{-2}\sum_s |\, q_s(\theta, \phi)\,|^2 \, d\Omega \qquad (76)$$

in terms of reaction amplitudes q which depend not only upon the angle θ of emergence of b but, in the general case, also upon the azimuthal angle ϕ referred

[73] J. M. Blatt and V. F. Weisskopf, *Theoretical Nuclear Physics* (John Wiley & Sons, Inc., New York, and Chapman & Hall, Ltd., London, 1952), 1st ed., Chap. X.3, pp. 533–535.

[74] E. Sheldon, in *Les Mécanismes des Réactions Nucléaires* VIe Cours de Perfectionnement de l'Association des Chercheurs en Physique, Grächen/Saint-Nicolas, April 1964 (Bureau d'impression MRP, Rue de Bourg 11, Lousanne, 1965), p. 155 (especially p. 164).

to a plane defined by the quantization axis and a spin axis. The individual amplitudes q_s additionally depend upon the spin states of the reaction partners in the initial and final systems, viz., s_A, s_a, s_b, s_B, collectively described by the single index s. In the outgoing channel the parity operation corresponds to the transformation

$$\theta \to \pi - \theta, \qquad \phi \to \pi + \phi, \tag{77}$$

and hence, on the assumption of definite, conserved parity [conditions (i) and (iii)], since then

$$q_s(\pi - \theta, \pi + \phi) = \pm q_s(\theta, \phi), \tag{78}$$

it follows that

$$\frac{d\sigma}{d\Omega}(\pi - \theta, \pi + \phi) = \frac{d\sigma}{d\Omega}(\theta, \phi). \tag{79}$$

Now, condition (ii) is tantamount to averaging over spins, as in the case of unaligned targets or polarization-insensitive radiation detectors, which restores symmetry about the quantization axis and removes the ϕ dependence. In consequence,

$$\frac{d\sigma}{d\Omega}(\pi - \theta) = \frac{d\sigma}{d\Omega}(\theta), \tag{80}$$

and the distribution is, in the center-of-mass system, symmetric about 90°.

Conversely, it is evident on the one hand that under conditions that satisfy requirement (ii), the distribution of γ radiation depends on the multipolarity L (and on the mixing ratio δ for multipolarities L, L') but *not* upon the parity of the radiation and hence *not* upon the multipole character (E or M), so that it cannot of itself yield information on the parities of the nuclear states between which the γ transition takes place. On the other hand, it follows that distributions from aligned nuclei, or distributions measured by counters sensitive to polarization (e.g., to linear polarization in the case of fermions, or to circular polarization in the case of γ rays), cease to display symmetry about 90°. This feature, dealt with in earlier reviews[11,12,75] and discussed in detail by a number of authors,[76–80] provides the underlying reason for CN angular *correlations* to be devoid of precise symmetry about 90°, since they essentially correspond to a determination of distributions from nuclei aligned in a selected direction (for a discussion of correlation symmetries, see Ref. 81).

Whereas under the experimental conditions examined in this paper, the requirements (i) and (ii) are satisfied irrespective of whether we deal with a CN or a DI mechanism, the circumstances under which (iii) is satisfied have no such independence, and merit further consideration.

The condition (iii) is clearly not satisfied in the case of DI processes, since these do not involve an explicit intermediate state associated with incoming and outgoing reaction channels, and hence cannot entail a definite parity. Accordingly, DI particle distributions lack precise symmetry about 90°, and can, especially in the case of elastic nucleon scattering, evince strong forward peaking (backward peaking has also been discerned in heavy-ion reactions). To a lesser extent, this is featured also in inelastic nucleon distributions but, as has already been stressed in Sec. 2, exceptions to such behavior exist, in that the DI distributions can in certain instances take on a form which is almost perfectly symmetrical about 90° and closely resembles the type of structure characteristic of a CN mechanism, albeit with a much larger peak-to-valley ratio and a totally different order of absolute magnitude. An example of such a situation has been given by Satchler et al.[82] for the $\mathrm{Cr}^{52}(p, p')_{1.43\ \mathrm{MeV}}$ reaction at $E_p = 5.54$ MeV. The DI distribution dips smoothly from 2.6 mb sr^{-1} at $\theta_{p'} = 0°$ to 0.9 mb sr^{-1} at 90° and rises symmetrically to 2.7 mb sr^{-1} at 180°. It thus has a fore–aft asymmetry of only 3.6% and a peak-to-valley ratio of 2.9. The CN distribution evaluated in the two-channel approximation with $l \leq 2$ rises from 17.0 mb sr^{-1} at 0° to 19.6 mb sr^{-1} at 90°, and accordingly has opposite structure, with the much smaller ratio $d\sigma(0°)/d\sigma(90°)$ of 0.9. Another such case has been found for the $\mathrm{Fe}^{56}(p, p')_{0.845\ \mathrm{MeV}}$ distribution at $E_p = 4.3$ MeV, where the inelastic proton differential cross section for a DI (CN) mechanism changes from 0.26 (1.50) mb sr^{-1} at 0° to 0.06 (1.61) mb sr^{-1} at 90° and thence to 0.22 (1.50) mb sr^{-1} at 180°, corresponding to a fore–aft asymmetry of 16% (0%) and a ratio $d\sigma(0°)/d\sigma(90°)$ of 4.18 (0.93). For comparison, it may be mentioned that the fore–aft asymmetry for the DI *elastic* distribution in the above case was computed to be

$$\frac{d\sigma(4°)}{d\sigma(176°)} = \frac{3.31 \times 10^7 \ \mathrm{mb\ sr}^{-1}}{42.67 \ \mathrm{mb\ sr}^{-1}} = 7.76 \times 10^5.$$

The CN distribution symmetry about 90° which ensues when (iii) is satisfied breaks down in the case of nonresonant processes or interferences between nuclear levels. It may accordingly be deemed to apply exactly only for the case of a resonance reaction involving but a single intermediate state, or, at the opposite extreme, for a reaction involving a statistically distributed continuum of states in the compound nu-

[75] H. Feshbach, in *Nuclear Spectroscopy*, edited by F. Ajzenberg-Selove (Academic Press Inc., New York, 1960), Part B, p. 625.

[76] G. R. Satchler, Proc. Phys. Soc. (London) **68A**, 1041 (1955); Nucl. Phys. **8**, 65 (1958).

[77] E. G. Beltrametti, Nucl. Phys. **8**, 445 (1958).

[78] L. W. Fagg and S. S. Hanna, Rev. Mod. Phys. **31**, 711 (1959).

[79] L. J. B. Goldfarb and R. C. Johnson, Nucl. Phys. **18**, 353 (1960).

[80] T. A. Welton, in *Fast Neutron Physics*, edited by J. B. Marion and J. L. Fowler (Interscience Publishers, Inc., New York, 1963), Part II, Chap. V.F., p. 1317.

[81] E. Sheldon, Phys. Letters **2**, 178 (1962).

[82] G. R. Satchler, R. M. Drisko, and R. H. Bassel, Bull. Am. Phys. Soc. **6**, 66 (1961) and preprint; E. Sheldon (unpublished).

cleus. Although general group-theoretical methods[83] (see also Ref. 73) suffice to show that symmetry must invariably result under these conditions, the departure from symmetry is not always to be taken as indicative of the intrusion of a non-CN mechanism, but rather as a disturbance of the above conditions, such as might arise when there is an incomplete statistical mixture of states in the compound nucleus. In such a situation, one would expect to observe fluctuations in the total reaction cross section. Only if the asymmetry does not fluctuate with incident energy, but remains a smooth and persistent function of energy does this constitute evidence for the intrusion of a foreign mechanism.

It remains but to mention that the isotropic emission of reaction products from a compound nucleus as given by statistical reaction theory is bound up with two further requirements, namely, (a) that the transmission coefficients are not spin-dependent, and (b) that the nuclear spin dependence of the level density is of the form

$$\rho(E, J) = (2J+1)\rho(E, 0). \tag{81}$$

Clearly, this is inapplicable to states of high nuclear spin; on replacing this by the more valid relationship[84,85]

$$\rho(E, J) = (2J+1) \exp\left[-J(J+1)/2\sigma^2\right]\rho(E, 0), \tag{82}$$

the distributions become anisotropic, while remaining

symmetric about 90°. A more detailed discussion of this has been given by Feshbach[75] and Goldstein.[86]

ACKNOWLEDGMENTS

[83] C. N. Yang, Phys. Rev. **74**, 764 (1948).
[84] H. A. Bethe, Rev. Mod. Phys. **50**, 332 (1936); **9**, 69 (1937).
[85] T. Ericson, Phil. Mag. Suppl. **9**, No. 36, 425 (1960).

[86] H. Goldstein, in *Fast Neutron Physics*, edited by J. B. Marion and J. L. Fowler (Interscience Publishers, Inc., New York, 1963), Part II, Chap. V.J., p. 1525.